2018

ANALYSIS OF ATP-DEPENDENT CHAPERONE PROTEIN INTERACTIONS WITH MISFOLDED PROTEINS, AMYLOIDS, AND AGGREGATED PROTEINS

Shannon May
University of Rhode Island, shannon_may@uri.edu

ANALYSIS OF ATP-DEPENDENT CHAPERONE PROTEIN INTERACTIONS WITH MISFOLDED PROTEINS, AMYLOIDS, AND AGGREGATED PROTEINS

BY

SHANNON E. MAY

A DISSERTATION SUBMITTED IN PARTIAL FULLFILLMENT OF THE REQUIREMENTS FOR THE DEGREE OF DOCTOR OF PHILOSOPHY IN NEUROSCIENCE WITH A SPECIALIZATION IN BIOCHEMISTRY

UNIVERSITY OF RHODE ISLAND

2018

DOCTOR OF PHILOSOPHY DISSERTATION

OF

SHANNON E. MAY

APPROVED:

Dissertation Committee:

Major Professor	Jodi L. Camberg
Co-major Professor	Nasser H. Zawia
	Alycia Mosley Austin
	Niall Howlett
	Andrea Rusnock
	ASSOCIATE DEAN OF THE GRADUATE SCHOOL

UNIVERSITY OF RHODE ISLAND

2018

ABSTRACT

Protein aggregation occurs when proteins adopt non-native conformations, exposing hydrophobic surfaces due to misfolding. The exposed regions of two or more proteins associate to form amorphous deposits or highly ordered, stable fibrillar structures called amyloid aggregates. Within the cell, a robust network of proteins safeguard against protein misfolding and aggregation. This network is referred to as the proteostasis network and includes molecular chaperone proteins, co-chaperone proteins, and the ubiquitin proteasome system. Molecular chaperone proteins function in various cellular processes including intracellular transport, oligomeric assembly, and efficient protein folding. Moreover, molecular chaperones are required for folding denatured, misfolded, and de novo proteins into their native conformation. It is thought that neurodegenerative diseases may be the result of a derailed proteostasis network in response to aging, mutations, and environmental stress, among other factors that contribute to protein aggregation.

The neurodegenerative diseases Alzheimer's disease, Huntington's disease, and Parkinson's disease are characterized by protein misfolding and accumulation into aggregates composed of amyloid fibrils. In each of these protein misfolding diseases, the roles of chaperone proteins are complex and not well understood. Given that these diseases share a common theme of protein misfolding and aggregation, researchers have questioned whether molecular chaperone proteins are involved in disease pathology, which has led to investigations into the possible use of chaperone-based strategies as treatment options. It is thought that protein aggregation in neurodegenerative diseases results from disturbances in pathways that regulate protein quality control. This thesis investigates the role of ATP-dependent chaperone proteins in

disaggregating and resolubilizing protein aggregates, including model aggregates, amyloids of Sup35 in yeast and hyperphosphorylated tau in human cells. Here, we investigated the biochemical properties of the Hsp100/Clp chaperone protein family, which couples ATP binding and hydrolysis to unfold and reactivate aggregated and misfolded polypeptides. We studied the role of molecular chaperone proteins in the progression of protein aggregation in a model of Alzheimer's disease and developed novel chaperone tools for targeting amyloid proteins for protein clearance. Furthermore, we investigated the mechanism of substrate recognition and amyloid disassembly by Hsp104 in a yeast [PSI^+] prion model of amyloid assembly. Moreover, we identified a novel function of the chaperone protein ClpX in protein disaggregation in vitro and in vivo. We observed that ClpX can bind and reactivate native and engineered protein aggregates in the absence of ATP. Lastly, in an Alzheimer's disease model of hyperphosphorylated tau, we monitored changes in chaperone protein levels in response to inhibition of protein phosphatases. Research from this dissertation will contribute to further understanding Alzheimer's disease pathogenesis, and, more broadly, the breakdown of protein homeostasis in neurodegenerative disease, and roles for chaperone proteins in managing proteotoxic aggregates in possible future therapies.

ACKNOWLEDGEMENTS

I thank my doctoral committee for their guidance, support, insight, and feedback that allowed me to conduct, interpret, and communicate my research findings. I am grateful to my major professor, Dr. Jodi Camberg, and my co-major professor, Dr. Nasser Zawia, for their mentorship throughout my graduate career. Dr. Jodi Camberg taught me techniques in microbiology and biochemistry and provided me with feedback about experimental design, data analysis, and effective science communication. I am grateful to Dr. Nasswer Zawia for helpful discussions about neuroscience, mechanisms of pathology, and toxicological research experimental design. Dr. Alycia Mosley Austin has served as a faculty member on my doctoral committee and has also been a valuable resource and mentor to me in the Interdisciplinary Neuroscience Program. Dr. Niall Howlett served as a faculty member on my core doctoral committee and provided me with valuable feedback about cell culture experimental design and techniques. I thank Cathy Trebino, Kim Andrews, and Janet Atoyan for their technical assistance. Lastly, I am grateful to the generous support and encouragement from my parents, James May and Rania May, and my sister, Meghan May.

PREFACE

This doctoral dissertation has been prepared in Manuscript Format under the guidelines of the University of Rhode Island Graduate School. Manuscript I is titled “In Vitro Approaches for Studying Amyloids and Neurotoxicity” and is formatted as a book chapter. Manuscript I is published in the textbook *Methods in Pharmacology and Neurotoxicology*, © Springer Science+Business Media, New York, 2018. Manuscript II is titled “Site-specific mutations in the Hsp104 N-domain impair [PSI^{+}] prion curing in Saccharomyces cerevisiae” and is formatted as a research article intended for submission to *Prion*. Manuscript III is formatted as a research article and is titled “The protein chaperone ClpX targets native and non-native aggregated substrates for remodeling, disassembly and degradation with ClpP.” Manuscript III was published in *Frontiers in Molecular Biosciences* in 2017. Lastly, Manuscript IV is titled “ATP-dependent chaperone protein expression in an Alzheimer’s disease model of tau hyperphosphorylation” and is formatted as a research article intended for submission to *Neurotoxicology*.

TABLE OF CONTENTS

LIST OF TABLES

LIST OF FIGURES

MANUSCRIPT IV

APPENDIX

Manuscript I

Publication Status: Published book chapter in the textbook *Methods in Pharmacology and Neurotoxicology,* © Springer Science+Business Media, New York, 2018

Title: In Vitro Approaches for Studying Amyloids and Neurotoxicity

Authors: Shannon May[1,2#], Aseel Eid[1,3#], Nasser Zawia[1,3], Jodi Camberg[1,2*]

Author Affiliations:

[1]Interdisciplinary Neuroscience Program, University of Rhode Island

[2] Biochemistry Laboratory, Department of Cell and Molecular and Biology, University of Rhode Island

[3]Neurodegeneration Laboratory, Department of Biomedical and Pharmaceutical Sciences, College of Pharmacy, University of Rhode Island

#Authors contributed equally to the development of the chapter.

*Corresponding author: Email: cambergj@uri.edu; Tel: 401-874-4961

1. Introduction to Protein Conformational Disorders and Neurodegeneration

Alzheimer's disease (AD), Parkinson's disease (PD), Huntington's disease (HD), and transmissible spongiform encephalopathies such as Creutzfeldt-Jakob disease are a group of progressive, fatal neurodegenerative diseases that share the common pathological feature of protein aggregation and amyloid deposits [1]. Amyloid deposits are composed of protein aggregates that result from proteins that adopt an aberrant, non-native conformation through a misfolding event [2]. Neurodegenerative diseases that share the common feature of protein misfolding are also referred to as protein conformational disorders [3].

Neurodegenerative diseases have a devastating impact on family members, caregivers, and society. Most diseases involve processes that impact the quality of life of an individual, from classic involuntary muscle movements witnessed in both PD and HD, to cognitive decline that occurs in individuals with AD. Neurodegenerative diseases also have a major impact on the economy and caregivers. In the case of AD, in 2015, American caregivers are estimated to have contributed over 18.2 billion hours of unpaid assistance to people with Alzheimer's dementia and other dementias, which amounts to approximately $230.1 billion in unpaid care [4]. Incidence rates of these age-related neurodegenerative diseases are expected to rise as the population ages. As of 2017, the Alzheimer's Association reports that an estimated 5.5 million people in the United States have Alzheimer's disease and by 2050, this number may increase to 16 million [4]. Understanding the biochemical, molecular, and cellular pathways and mechanisms involved in Alzheimer's disease pathology and progression is important for developing more efficient disease-modifying therapeutic strategies. This chapter will discuss *in vitro* technologies commonly used to isolate, visualize, and characterize amyloidogenic protein aggregates and in vivo methods of identifying protein aggregates in the brains of

patients with Alzheimer's disease. We will also provide examples of agents that have been shown to promote aggregation, and discuss different approaches that may inhibit or stall amyloid formation.

2. Proteostasis, Protein Misfolding and Aggregation

2.1 Protein Quality Control

Protein function is dependent on proper folding of a protein into a native, thermodynamically stable and biologically active conformation, with a three-dimensional structure. To ensure that proteins fold correctly there is a protein quality control network in cells, which consists of a group of molecular chaperone proteins and proteases. Stress and subsequent damage to functional, folded proteins may be caused by environmental changes (for example, shifts in temperature or hydration), free radicals, heavy metals, or tissue injury. These stresses can also modify the expression levels of components of the protein quality control machinery within the cell to manage the disruption to protein homeostasis [5,6] [7]. Thermotolerance studies in cells have led to the identification of many proteins that are highly expressed during exposure to heat stress. Therefore, these proteins were given the name "heat shock proteins". In eukaryotes, the heat shock response, which includes the increased expression of heat shock proteins in response to physiological stressors, is stimulated by activation of heat shock transcription factor (HSF-1) and transcription of chaperone genes, such as genes encoding chaperone proteins Hsp70 and Hsp40 [8-10]

Heat shock proteins are highly conserved and ubiquitous proteins that represent a component of the cellular protein quality control network. Heat shock proteins, or molecular chaperone proteins, are essential for managing protein folding and maintaining protein homeostasis in both normal conditions and conditions of

physiological cell stress [11]. Misfolded proteins pose a threat to cell viability by interfering with protein-protein interactions, protein-membrane interactions, promoting aberrant protein interactions and inducing aggregation. Protein misfolding also increases the demands on the protein quality control network, which is thought to lead to further misfolding and aggregation events [12,13]. During aging, the cell's ability to mount a heat shock response in response to stress conditions decreases [14] . Expression of ATP-dependent chaperone proteins, such as Hsp90 and Hsp70, declines with age and this decrease in expression levels is even greater in Alzheimer's disease and Huntington's disease [15].

Another component of the quality control network within the cell is the 26S proteasome, a large protein degradation machine that promotes the clearance of misfolded proteins and proteins with an ubiquitin tag. In some cases, misfolded and dysfunctional proteins are tagged with multiple ubiquitin domains by ubiquitin ligases and directed to the 26S proteasome for degradation. Protein degradation may also play a role in age-associated neurodegenerative diseases, including AD and PD, where protein aggregates have been shown to contain high levels of ubiquitin, which may contribute to neurodegeneration and neuronal cell death [16] . Research suggests that proteasome activity declines and may be impaired in the aging brain [17,18]. Together, the molecular chaperones and the 26S proteasome maintain steady-state levels of healthy proteins within the cell, creating a balance of active and degraded proteins, which becomes more fragile as the proteostasis network weakens or is overburdened.

2.2 Protein aggregation and amyloids

When proteostasis is disrupted due to protein folding inefficiency or instability, proteins become insoluble and aggregate. Several neurodegenerative diseases contain a highly specialized and thermodynamically stable aggregate, called an amyloid.

Amyloid deposits are composed of bundled fibrillar aggregates rich in stacked beta-sheets that are oriented perpendicular to the long axis of the amyloid fiber [19,20]. A network of hydrogen bonding interactions within and between beta sheets stabilize the highly ordered beta-rich structure of amyloids [21]. Amyloid fibrils have common beta-rich structures, fibril morphologies, and chemical properties. Generally, the mature amyloid fibril is approximately 100 Angstroms in diameter, twisted, and unbranched [22]. Amyloids are insoluble and resistant to detergents and many other chemicals known to disrupt protein folding and proteolysis [23,24]. A unifying feature of amyloids is their distinctive cross-beta pattern observed in X-ray diffraction studies. The amyloid fibril structure is characterized by stacked beta-sheets that have an approximate intersheet distance of 11 Angtstroms and interstrand distances of 4.8 Angstroms [22] .

It is thought that amyloids arise from a nucleation-dependent polymerization event called fibrillization (Figure 1). By contrast, intermediates in the amyloid assembly pathway, such as pre-amyloid oligomers, are soluble in solution and have diverse sets of conformational states [25]. How proteins progress through conformational stages of the amyloid assembly pathway(s) from oligomers to protofibrils and finally, to amyloid fibrils, is not well understood, but novel methods using molecular probes and optical spectroscopy may provide important information about these intermediate oligomeric species [26]. Although the precise molecular events of amyloid assembly are not known, *in vitro* experiments suggest that small oligomers assemble and polymerize to form an intermediate protofilament, which further aggregates to become a mature fibril [25]. The fibrillar aggregates accumulate into a deposit called an amyloid plaque, which is thought to be irreversible. In vivo preformed amyloids can act as “seeds” to promote mature amyloid formation in mouse models of amyloid assembly [27]. Although it is unknown how amyloids propagate, a prion-like mechanism has been suggested, where a

misfolded protein (i.e., an amyloid) induces conformational changes in folded protein by templated conformational conversion [28] . In this model, the amyloid acts as a seed or template to spread the beta-rich structure to other proteins, promoting fibrillization and thus seeding aggregation.

The pathogenesis of several neurodegenerative diseases is linked to the formation of amyloids that accumulate within specific tissue regions. In AD, amyloid beta plaques are formed from the misprocessing and overproduction of the amyloid precursor protein (APP), and plaques are typically found extracellular to neurons in the frontal cortex and hippocampus of patients (Figure 1B). A second hallmark of AD pathology is known as the tau tangle. Tau tangles, or neurofibrillary tangles (NFTs) are intracellular aggregates formed by the polymerization of paired helical filaments (Figure 1B) [29-31] [32]. In PD, misfolded, aggregated alpha-synuclein (α-synuclein) has been shown to be the major constituent of both Lewy bodies and Lewy neurite pathology in the brains of patients with PD patients [33]. HD is predominantly genetic, and involves duplications in the Huntingtin gene (Htt). Individuals with *htt* mutations develop aggregates of Htt in amyloid-containing inclusion bodies, which are typically found in the striatum, cortex, and the spinal cord [34]. Although these neurodegenerative diseases share the common feature of amyloids deposits, they also exhibit differences. The neuronal cell populations that are lost in each of the diseases varies, the disease symptoms are heterogeneous, and the pathological proteins that misfold into amyloid in each disease share few similarities in sequence and structure. In addition, amyloid load is poorly correlated to cognitive decline in neurodegenerative diseases and accumulating research points to prefibrillar oligomers as the toxic species responsible for neurodegeneration and behavioral symptoms [35].

Besides age-related neurodegenerative diseases, transmissible spongiform encephalopathies, also referred to as prion disorders, provide further examples of pathological alterations in protein conformation that are associated with neurodegeneration and lead to death in humans [1]. In these disorders, a soluble prion protein (PrP) adopts a new conformation, or protein fold. This new conformer of the prion protein is an amyloid and it has self-templating and infectious properties. In the prion conformation, the protein can then bind to another native protein and cause it to adopt the aberrant, alternative conformation. In this way, the abnormal conformer can self-template and propagate the disease-associated protein conformation [36]. Diseases that fall within the TSE category include scrapie in sheep, bovine spongiform encephalopathy ("mad cow" disease), chronic wasting disease in deer and elk, and Creutzfeldt-Jakob disease in humans [37] [38].

3. Detecting Amyloids and Monitoring Fibrillization

3.1 Monitoring the Kinetics of Amyloid Formation in vitro and Quantifying Aggregation

It is hypothesized that the mechanism of amyloid assembly is a nucleation-dependent fibrillization characterized by a rate-limiting, slow lag phase required to form a critical nucleus followed by the polymerization of fibrils at an exponential rate [39,40]. For a nucleus to form (termed "nucleation"), a set of high-energy oligomeric intermediates must be stabilized by a molecular event, such as a protein conformational change. The factors that drive nucleation and the structures of the high-energy conformational states that compose the nucleus are not well understood [41]. Although amyloids are stable structures in general, the fibrils can break into smaller fragments that may seed additional amyloids. Multiple detection and quantification methods for amyloids rely on the optical qualities of amyloids and the kinetics of amyloidogenesis. Congo Red and Thioflavin T (ThT) are small molecules that bind selectively to amyloids, inducing

changes in optical features such as fluorescence quantum efficiency [26]. Light scattering or fluorescence assays are used to monitor the kinetics of amyloid fibril assembly over time [38]. Traditional methods for screening amyloid aggregates include biophysical, optical, and microscopic techniques that visualize small molecule binding to amyloids, such as Congo red (CR) and ThioflavinT (ThT) dye binding [42]. The most commonly used techniques for reporting and quantifying amyloids, in addition to novel methods for identifying different conformational states of amyloids, are explained below.

3.2 Detection of Amyloids by Molecular Probes and Fluorescence Spectroscopy

Fluorescence spectroscopy is used to identify and characterize protein conformations of amyloids in vitro under both steady state and kinetic conditions, allowing researchers to investigate amyloid assembly and visualize amyloid fibrils. The most commonly used fluorescent dyes that bind selectively to amyloid are Congo Red [43] and ThioflavinT [44]. ThT is a benzothiazole-based fluorescent dye that specifically binds to the surface of cross-β sheets of amyloid fibrils[45]. Vassar and Culling demonstrated that ThT showed highly specific binding to amyloid deposits in tissue sections and this binding was associated with an enhanced fluorescence signal from ThT [23]. When ThT binds amyloid fibril in vitro or in situ, it shows enhanced fluorescence that can be monitored by fluorescent spectroscopy [46]. In vitro binding of amyloid fibrils to ThT was first described by Naiki and coworkers[44]. When ThT was added to samples containing up to 2.0 μg/mL of amyloid fibrils, researchers observed an intense fluorescence at an excitation maximum of 450 nm and an emission maximum of 482 nm [44]. The molecular probe ThT has also been used to monitor amyloid fibril assembly in real-time [47,48].

There are limitations and caveats to quantifying amyloid fibrils based on ThT fluorescence assays. The selectivity of ThT binding to amyloid fibrils is unclear. ThT

fluorescence emission can be affected by different amyloid fibril morphologies and pH; at a basic pH, the ThT molecule becomes hydroxylated [22]. ThT can also bind to other fibrils besides amyloids, such as keratin and elastin [49] . Moreover, research shows that ThT can bind to nucleic acids of DNA and this binding is associated with enhanced ThT fluorescence;[50] however, reducing the pH lowers the affinity of ThT for nucleic acids [51]. The presence of polyphenols such as curcumin, quercetin, and resveratrol in samples containing fibrillar amyloid-beta interferes with ThT fluorescence readings in both in situ ThT assays and single time-point ThT assays [52]. Considering that factors such as ionic strength, pH, fibril morphology, and concentration of both ThT and protein fibril can modify the fluorescence emission of ThT, it may be more useful to combine other methods of measuring amyloid fibril kinetics with ThT fluorescence assays [53].

Congo Red is a crimson-hued, lipophilic diazo dye that selectively binds with high specificity to amyloid fibrils in vitro, in situ, and ex vivo [46]. . The Congo Red birefringence assay can be used to identify amyloid fibrils. Using a polarized light microscope, the presence of amyloid can be investigated by determining if the sample stained with Congo Red shows apple-green birefringence under crossed polarizers; if no birefringence is observed, then it can be concluded that no amyloid is present [46]. The characteristic apple-green birefringence can be difficult to detect and other problems with this technique include high levels of background staining and challenges to reproducibility [53,46]. Research supports that Congo red does not bind to different amyloid fibrillar deposits by the same mechanism and may have relatively low sensitivity [54-56]

A spectroscopic assay that examined Congo Red dye binding to fibrillar beta-pleated sheet insulin, a representative amyloid, showed that the absorbance spectrum of Congo Red changes upon binding to amyloid [43]. Klunk and coworkers further

developed and extended the Congo Red-insulin fibril spectroscopic assay to quantify amyloid fibrils by examining amyloid-beta aggregation with Congo Red. Briefly, the absorbance of amyloid samples stained Congo Red and amyloid samples alone must be measured at the wavelengths 403 nm and 541 nm before performing necessary calculations to quantify the aggregated amyloid beta concentration in the samples [57]. When Congo Red binds to amyloid fibrils, it exhibits a red shift in absorbance maxima from 490 nm to 540 nm [58]. Congo red dye binding to amyloid fibrils causes Congo red to change in color from orange-red to rose and because of this, a spectral shift in the absorbance spectrum of Congo Red can be measured using a UV-Vis spectrophotometer [59].

Congo Red and Thioflavin T dyes do not bind to pre-amyloid conformations in the amyloid assembly pathway. The development and use of fluorescent dyes 1-anilinonapthalene-8-sulfonate (ANS), 4-4-bis-1-phenylamine-8-napthalene sulfonate (Bis_ANS), and 4-(dicyanovinyl)-julolidine (DCVJ) allows for identification and monitoring of early amyloid protein conformations [60]. Bis-ANS has been shown to bind to prefibrillar protein conformations associated with the early stages of the amyloid assembly pathway. When Bis-ANS binds to the hydrophobic residues on the surface of proteins and is excited at 360 nm, it emits a 530 nm wavelength [48]. DCVJ was shown to bind selectively to prefibrillar oligomers, making it a useful tool for studying the early stages of amyloid assembly [60].

Moreover, A drawback of Congo Red and Thioflavin T dyes is that they cannot be used *in vivo.* The development of BoDipy-Oligomer (BD-Oligo) by the research group of Teoh et al. may have bridged this gap in the field. BD-Oligo is a fluorescent probe selective for oligomeric intermediates in amyloid formation [61]. BoDipy-Oligomer can cross the blood brain barrier and can label disease-associated oligomers in real-time

without using radiation, making it an attractive candidate for clinical screens of presymptomatic patients of AD [61] [62]. A novel stain that has recently begun to be employed for the detection of Aβ plaques is Amylo-Glo. While this has recently been shown to bind to Aβ plaques in 11 month APP/PS1 transgenic mice, the specificity of the marker for Aβ as opposed to other aggregated proteins has not been predetermined [63]. Unlike Congo Red and Thioflavin T, Amylo-glo has a blue UV excitable stain, making it ideal for co-labeling and staining studies, it is also much brighter than these traditional dyes and appears more sensitive [64].

3.3 Seeding and Amplification Assays

3.3.1. Protein Misfolding Cyclic Amplification

Protein Misfolding Cyclic Amplification (PMCA) is a technique that was developed in 2001 for the detection and amplification of prion proteins [65]. The first phase of PMCA involves utilizing a trace amount of infectious prion purified from either brain homogenates or cell lysates to induce the conversion of the normal protein into the misfolded infectious aggregate. In the second phase, the sample is sonicated, which fragments the aggregate and therefore frees up the template to polymerize again. Therefore, by PMCA the fibril concentration increases exponentially [66]. A concern of the PMCA reaction and technique is its ability to detect low levels of prion protein in a sample, as well as the efficiency of the reaction. PMCA may vary depending on experimental conditions, such as the reaction components and sonication. A modification of the experimental design to include Teflon beads (PMCAb) increased the efficiency of the PMCA reaction and the sensitivity of prion detection [67].

Quantitative ‘qPMCA’ was developed to quantify the prion concentration in a sample since the amount of cycles of PMCA needed to detect the prion is directly related

to the amount present in the original sample [68,69]. Briefly, the procedure involves the purification of prion from the original lysate, followed by PMCA reactions containing multiple dilutions of prion. Then the number of rounds of PMCA required to produce a detectable signal are determined by Western blot analysis. From this, a curve is generated of prion concentration versus PMCA detection round. Extrapolating from this curve would provide the original prion levels in the sample [68,69]. Although developed for prions associated with TSEs, PCMA has recently been applied to the detection of Aβ oligomers in cerebrospinal fluid of patients with AD [70].

3.4 Inducing Amyloid Formation and Seeding

3.4.1 Quaking Induced Conversion Assay and the Amyloid Seeding Assay (ASA)

The amyloid seeding assay (ASA) is a method in which rapid amyloid formation or seeding occurs when amyloid fibrils are added to a fresh pool of soluble proteins. The ASA is useful tool to screen for agents that may be aggregation inhibitors, and for detecting prions in biological samples. The formation of these aggregates can be observed by monitoring Thioflavin T (ThT) binding to amyloid fibers over time [71].

Similar to PMCA, the Quaking Induced Conversion Assay (QuIC) was developed to address technical difficulties associated with PMCA. In QuIC automated orbital shaking is utilized instead of sonication, which is used in PMCA. Both the ASA and QuIC assays are limited in their ability to accurately quantify protein aggregates and are considered less reliable than the new real-time quaking induced conversion assay (RT-QuICK) [72]. RT-QuICK utilizes some components of the QuIC assay, such as intermittent shaking but also incorporates ThT to monitor the formation of fibrils, as seen in ASA's [73].Furthermore, prion and fibril concentration is accurately determined by using RT-QuICK if it is coupled with end-point dilution analysis. In this method,

homogenates are serially diluted. Then the samples are analyzed by RT-Quick for each dilution, and then ThT fluorescence levels are measured to establish a baseline. The advantage of utilizing RT-QuICK is that it is a rapid, sensitive, cost-effective assay as compared to alternative techniques [72].

3.4.2 Monitoring Amyloids in vivo

The ability to develop *in vivo* detection and monitoring methods for amyloid assembly remains difficult for most of the amyloidogenic diseases, especially in HD and PD. In HD, researchers have had success utilizing positron emission topography (PET) to monitor disease progression in individuals diagnosed with the disease relative to healthy individuals. However, in both PD and HD there is still no tracer that can both bind to aggregates and be simultaneously monitored by PET scans. In contrast, there have been more successful developments of radioligands selective for beta-amyloid and paired helical filament tau protein that enable *in vivo* monitoring and visualization of AD-related amyloid plaque and neurofibrillary tau protein aggregate accumulation.

The PET imaging agents that are selective for fibrillar amyloid-beta plaques include 11-C-labeled Pittsburgh compound B and florbetapir-F18 [74]. The first PET imaging probe developed that could bind to amyloid beta aggregates was Pittsburgh Compound B (PiB-C11) [75]. PiB-C11 effectively binds to amyloid plaques in brain regions of people with Alzheimer's disease that correlate with the same brain regions showing amyloid accumulation from post-mortem histopathological analysis of brain tissue [76]. However, PiB-C11 has a short half-life of approximately 20 minutes, which limits its efficiency [77]. The first FDA-approved PET tracer for clinical imaging of amyloid-beta deposits is florbetapir-F18 (Amyvid^{TM}) [76]. The PET ligand florbetapir-F18 (^{18}F-AV-45) binds to amyloid beta plaques with similar specificity and regional uptake as PiB-C11 and has a half-life of approximately 110 minutes [77]. Recent studies have

shown that florbetapir-F18 is both sensitive and specific to the detection of Aβ and can be used to clinically distinguish individuals [78]. Moreover, in vitro analysis of the of florbetapir-F18 binding in human postmortem brain tissue sections confirmed that the labeling intensity of florbetapir-F18 correlates with amyloid plaque density and the PET tracer did not bind to neurofibrillary tangles [74].

Research findings from postmortem brain analyses show that neurofibrillary tangles correlate with cognitive decline and neuronal death whereas amyloid plaques do not strongly correlate with dementia severity [79,80]. Therefore, there development of PET tracers that bind to paired helical filaments, which are composed of pathologically hyperphosphorylated tau, could be used to diagnose and monitor treatment outcomes in vivo [81]. The PET ligand ^{18}F-AV-1451 binds selectively and with high affinity to hyperphosphorylated tau in paired helical filaments [82,83]. A study that investigated ^{18}F-AV-1451 binding in healthy elderly people found that uptake and retention of AV-1451 correlated with age and amyloid plaque accumulation [84]. AV-451 uptake in the medial temporal lobe was also found to be significantly associated with cognitive decline and impaired episodic memory [84]. The development of amyloid beta and tau PET-imaging probes provide a new tool for measuring pathological amyloid beta and neurofibrillary tangle deposits in vivo, which could be useful in the clinic for diagnosis of Alzheimer's disease.

4.0 Cytotoxicity assays

Amyloid assembly intermediates are widely considered to be more toxic species in the amyloidogenesis pathway, rather than the mature amyloid fiber present in plaques, yet there is still ambiguity about whether protofibrils, oligomer species, or a combination of both causes toxicity. Research shows that oligomers from the self-assembly of amyloid beta peptide are 10-fold more toxic to neuronal cell cultures than

fibrillar amyloid-beta (1-42) peptide. Amyloid-beta peptide (1-42) is toxic to cells at micromolar concentrations whereas oligomeric species are toxic at nanomolar concentrations [85]. Reliable cytotoxicity assays provide important information about cellular health and viability following exposure to a toxic substance and are useful for investigating the correlation between protein aggregation and cytotoxicity, which may provide information important for understanding the pathogenesis of protein conformational diseases.

In vitro cytotoxicity assays are used to determine the viability of a cell following exposure to a toxic substance, such as a misfolded protein conformer or mature amyloid. The *in vitro* assays rely on the markers of cell death, whether that is the compromised integrity of the cell membrane, the release of enzymes into the extracellular space that are normally compartmentalized, etc., as direct and indirect measurements of cell viability. However, assays to monitor long-term cytotoxicity are lacking. Colorimetric *in vitro* assays are widely used pharmacology and ecotoxicology studies to determine cell death following exposure to a toxicant or a suspected toxic species [86]. Often several cytotoxicity assays are employed to accurately determine cell fitness and survival. Cytotoxicity assays have also shown the correlation that as the order of oligomer species increases, the degree of toxicity of the oligomer also increases providing valuable information about the identity of most toxic soluble oligomer species, which has implications for drug target research [87].

Below are examples of commonly used and robust assays for measuring the number of living cells (cell viability) and determining the number of dead cells (cytotoxicity). The LDH assay and MTT assay are spectrophotometry-based assays for measuring cytotoxicity in vitro. Despite the ease of use of these inexpensive assays and their ability to be used in high-throughput screening, there are several limitations

associated with their use. Notably, spectrophometric assays that indirectly measure plasma membrane breakdown do not distinguish among different cell death modalities [88]. Vital dye assays represent another method for measuring cell viability in response to cytotoxic agents in vitro. However, vital dyes are also limited by their inability to distinguish different modes of cell death [89].

4.1 LDH Leakage Assay for Compromised Membrane Integrity

Lactate dehydrogenase (LDH) is a cytosolic enzyme that can be used as a biomarker of cell death and cell lysis [90]. The lactate dehydrogenase assay is an example of an intracellular protein release assay. After cell death, the cell membrane loses its structural integrity, which results in the release of normally intracellular enzymes into the cell culture medium [91]. Colorimetric and fluorometric detection of LDH using commercially available kits allows researchers to monitor cytotoxicity in vitro [88] . LDH is catalyzes the oxidization of lactate to pyruvate and generates NADH; NADH strongly absorbs 340 nm light. Monitoring absorbance values using a 96-well plate provides an estimation of cytotoxicity [90]. The LDH assay is widely used to investigate cytotoxic affects and was recently applied to detect cytotoxicity of amyloids in rat embryonic neuronal cell culture [92,93]. However, disadvantages of the LDH assay include low sensitivity and a high degree of variability [86]. Moreover, LDH enzymatic activity can be affected by cell culture medium, such as pH and components within the medium, leading to an underestimation of cell death [88] .

4.2 MTT Assay

The 3-(4,5-dimethylthiazol-2-yl)-2,5-diphenyltetrazolium bromide (MTT) reduction inhibition assay, commonly referred to as the MTT assay, is a robust colorimetric assay for assessing cell viability in a variety of cultured cell types [90]. The MTT assay of cell

viability was first described by Mosmann [94]. MTT is a water-soluble tetrazolium salt that converts toformazan, which is purple and water insoluble, by reduction of the tetrazolium ring mediated by mitochondrial dehydrogenase enzymatic activity [95]. Only viable, metabolically active cells will convert MTT to formazan. Thus, formazen will accumulate as as a precipitate in viable, healthy cells. Spectrophotometric quantification of relative levels of formazan allows researchers to measure MTT conversion and overall cell viability [90]. The MTT assay is versatile and linear over a broad range of densities. However, the MTT assay may be more useful in cells with high metabolic activity [86].

4.3 Vital Dyes

Besides the LDH and MTT assay, vital dyes are frequently used by researchers to distinguish between living and dead cells *in vitro*. Vital dyes are fluorescent or colored molecules that can be used in membrane permeability assays to measure cell death [89] . Exclusion dyes, such as Trypan blue, cannot cross plasma membranes of healthy cells, and can be used to measure cell viability. Other commonly used exclusion dyes include propidium iodide and 4',6-diamidino-2-phenylindole, which label dead cells that no longer have intact plasma membranes [96]. Researchers determine the percentage of viable cells in response to a cytotoxic agent by staining the cells with an exclusion dye and counting the number of viable cells using a light microscope and a cell counting instrument, such as a hemocytometer. The percentage of viable cells is the ratio of viable cells to the total number of cells [89] .

Dyes can also be used to label living cells, such as calcein acetoxymethyl ester (calcein-AM). The vital dye calcein-AM has been used effectively in cytotoxicity assays [97,98]). Calcein-AM is lipid soluble and easily crosses cell membranes. Inside the cell, is hydrolyzed by cytosolic esterases to yield calcein, a fluorescent and membrane

impermeable product [89] . Cells with intact plasma membranes will retain fluorescent calcein. Dying or dead cells with damaged plasma membranes release calcein, which has a strong green fluorescence signal at 530 nm [99]. Therefore, cytotoxicity can be determined by measuring the release of calcein from lysed cells using a fluorimeter. A drawback of calcein-AM is that esterase enzymatic activity may be affected by events not related to cell death, which may lead the researcher to underestimate levels of cytotoxicity [89].

5. Pharmacological Agents and Drug Therapies for Protein Misfolding Diseases

Aggregation can be promoted by intrinsic and extrinsic factors, including the amino acid sequence of a polypeptide, pH, temperature, chaperone protein levels, and protein concentration [38]. Aggregation can be inhibited *in vitro* by different classes of compounds, notably anthracycline, anionic sulphonates, Congo red, and rifampicin, which prevent the formation of oligomers, as well as by other proteins. Prefibrillar oligomers are the most toxic protein conformation, not the mature amyloid fibril [100], therefore many pharmacological studies have explored different avenues for abrogating protein aggregation and its associated toxicity. Strategies explored so far include increasing the activity of the protein quality control network, stabilizing the soluble disease-associated protein, destabilizing the insoluble misfolded protein, preventing aggregation at the early stages of amyloid formation, and changing the protein folding landscape to favor native protein folding.

5.1 Metals

It has been shown that metals may have a role in inducing protein aggregation. Specifically, divalent $Cd^{2+,}$ but not Mn^{2+} impairs proteosomal activity in mouse neuronal cells expressing prion protein. This impaired proteasome system lead to an

accumulation of high molecular weight ubiquitinated proteins in the cell, and ultimately cell toxicity and death [101]. These observations were also replicated in yeast [102]. Arsenite, As (III) was also found to interfere with chaperone activity and with the folding of peptides in yeast. As (III) exposure was shown to induce the formation of over 140 protein aggregates, which can further induce misfolding and aggregation of other proteins [102]. A number of other metals have also been identified as promoting protein aggregation, and inhibiting of protein refolding both *in vivo* and *in vitro*, including Hg^{2+} and Pb^{2+} [103,104].

5.2 Therapeutic Intervention Methods Targeting Aggregates

A number of therapeutic strategies have been implemented as a means to target amyloid and aggregate formation due to the inherent toxicity of both the fibrils and aggregates [105,106]. Some techniques include inhibiting the formation of the β-sheet secondary structure by using short peptides, or small inhibitory molecules. Others include bolstering the natural defense towards aggregates, such as heat shock proteins, or agents that induce chaperone activity, to enhance clearance mechanisms.

5.2.1 β-sheet Breakers

β-sheet breakers are short peptides that recognize and inhibit the amyloid conformation. Specifically, this is commonly done using short peptides, that recognize the hydrophobic or “central core” of the beta amyloid (Aβ) peptide [100]. This class of peptides can bind to oligomers and fibrils to destabilize the β-sheet structure that is a common trait of amyloids. The unique property of these peptides is their specificity for abnormally folded proteins; they destabilize only non-native protein conformers without affecting the soluble protein conformer [100]. Thus, this class of drugs can deter amyloid fibrillogenesis and downstream aggregation [107].Two β-sheet breaker peptides, KLVFF

and LPFFD , have been shown to prevent the oligomerization of oligomers into amyloid fibrils, thus preventing the formation of amyloid plaques [108,109]. Research shows that the LPFFD peptide can better halt amyloid fibrillogenesis than KLVFF due to its lower hydrophobicity [110].

5.2.2 Antibodies

Several monoclonal antibodies have been developed that specifically target amyloid-beta monomers and oligomers, as well as some polyglutamine aggregates [105]. Two antibodies have been specifically examined for their role in mitigating Aβ pathology: bapineuzumab and solanezumab. Bapineuzumab targets the N-terminus of amyloid-beta whereas solanezumab binds to the central region. Both monoclonal antibodies have been tested in clinical trials in patients diagnosed with mild to moderate AD. However, despite success in the laboratory, monoclonal antibodies have not yet shown significant clinical changes or altered disease endpoints in patients [111].

A conformation specific peptide, which mimics a pathological conformation of amyloids, was developed using polymerized British amyloidosis (pABri) peptide. Although the peptide does not have sequence homology to amyloid-beta or any other human protein, pABri is synthesized in the beta-sheet form and elicits an immune response against the pABri peptide, as well as other amyloids. This technique been used successfully in APP transgenic mice to direct the immune system against amyloid formation, which led to a reduction in amyloid plaque burden and improved cognition [112].

5.2.3 Natural Products as Putative Therapeutic Agents

Pharmacological studies have identified many diverse compounds associated with increasing molecular chaperone expression, restoring proper protein folding,

decreasing the levels of pathologic misfolded proteins and inhibiting amyloid formation. For example, polyphenols have strong anti-amyloidogenic activity and act by promoting clearance of amyloid from the system. Most polyphenols have been shown to disrupt aggregation of α-synuclein [106]. A polyphenol that is commonly found in green tea, (−)-epigallocatechin-gallate has been shown to inhibit Huntington aggregation [113]. Other polyphenols such as curcumin have also been shown to aid in reducing protein aggregation through the induction of heat shock proteins [114]. Other examples include natural products that may interrupt or modulate the processing of amyloid in the brain, specifically pomegranate extract has been shown to disrupt Aβ in transgenic mice favoring the Aβ40 species over Aβ42 [115].

Drugs that inhibit amyloid fibrillization are also under investigation as potential therapies for protein conformational disorders. For example, cyclohexanehexol stereoisomers exhibit anti Aβ aggregation activity and are naturally occurring compounds with high absorption levels and no reported adverse side effects [100]. Additional research is focused on applications of chemical chaperones, ligands that bind to native proteins and osmolytes to stabilize the native protein state and destabilize the non-native, aberrantly folded state [38].

5.2.4 Molecular Chaperones

Molecular chaperone proteins, also referred to as heat shock proteins, are activated during cellular stress, and recognize and bind to surfaces of non-native or misfolded proteins to prevent or alleviate protein aggregation [116]. Biochemical assays have shown that several classes of molecular chaperones can modulate amyloid levels and inhibit amyloid fibrillization. Hsp70 and the co-chaperone Hsp40 were reported to block the self-assembly of polyglutamine [117]. Therefore, heat shock proteins represent

a potential therapeutic avenue for future development of drugs to alleviate amyloid burden.

Another class of possible therapeutic agents that may be effective against neurodegeneration includes small molecules that target the heat shock response or selectively alter the activity of chaperone proteins. Hsp90 has emerged as a possible target for neurodegeneration and cancer therapy because of its role as a robust protein chaperone that assists in stabilizing and activating several disease-related proteins. Geldanamycin is a potent inhibitor of the chaperone protein [118]. . Inhibiting Hsp90 activates the heat shock response of the cell by de-repressing expression of the global chaperone transcription factor HSF-1 [119] Preclinical studies for geldanamycin showed that the small molecule causes hepatotoxicity [120]. The quinone 19-position of geldanamycin is reactive with biological nucleophiles, such as glutathione [121]. Geldanamycin analogues with substitutions at the C19 position block nucleophilic substitution, thereby reducing unwanted reactions with biological molecules. Isomerization change from *trans* to *cis*-amide conformation of these geldanamycin analogues allowed for strong protein binding. Importantly, the analogues had reduced toxicity in epithelial and endothelial cells. The study provided strong evidence that these C19 substituents of geldanamycin did inhibit Hsp90 in dopaminergic neural cells and human cancer cells without incurring toxicity in cell lines, suggesting that these substituents may be promising agents for modulating protein folding in protein conformational disorders [121]. Inhibition of Hsp90 also activates Hsp70. Both chaperones recognize different sets of client proteins, and a reduction in Hsp90 function could promote Hsp70 function, leading to enhanced protein stabilization, degradation, or refolding [121]. Geldanamycin has also been shown to decrease cellular levels of hyperphosphorylated tau, which is stabilized by Hsp90 [122].

Chaperones, including the Hsp70/Hsp40 system of co-chaperones increase the degradation of protein aggregates and clearance of misfolded polyQ proteins by targeting the abnormal proteins to the proteasome, as observed by decreased half-life of the misfolded polyQ protein [123]. Therefore, overexpression of Hsp70/40 proteins is a therapeutic option to enhance clearance of aggregates; overexpression of Hsp70/40 can prevent amyloid formation, as well as rescue cells with amyloid accumulation [100]. It is known that molecular chaperones can bind unfolded polypeptides and prevent protein aggregation *in vitro* by solublizing and reactivating protein aggregates. The Hsp100 family of chaperones are composed of ATP-dependent disaggregases which unfold and reactivate proteins. Studies by Schirmer et al. showed that Hsp100 chaperones can work in synergy with Hsp70 to reactivate protein aggregate [124]. Yeast protein Hsp104 works with Hsp70/40 system to disassemble and rescue aggregated proteins has also been shown to disassemble amyloid fibers *in vitro* [125] . Overexpression of Hsp70 in a *Drosophila* model of Huntington's Disease mitigated neurodegeneration and increased the lifespan of the fly [126].

5.2.5 Chemical chaperones

Chemical chaperones are a unique class of drugs that can alter the balance of folded and misfolded proteins within the cell. Chemical chaperones are low molecular mass and can stabilize proteins against misfolding and aggregation, caused by thermal and chemical denaturing events. Some promising groups of compounds that target prion diseases include the anthracyclines, porphyrins, and diazo dyes. Chemical chaperones can alter protein conformation by blocking the conversion of soluble, biologically active prion protein to the insoluble, transmissible prion conformer [127,128]. The clinically approved anti-malarial compound quinacrine, binds specifically to the C-terminal helix of the normal isoform of the prion protein and stabilizes the normal protein conformation

[129]. By stabilizing the normal, cellular non-prion protein, whose function is not known, conversion to the misfolded, transmissible prion isoform is blocked. However, quinacrine cannot pass through the blood-brain barrier so it has limited therapeutic applications in animal models [49]. Therapeutic research for prion diseases now includes an array of compounds such as the polycationic compounds (i.e., dendritic polyamines), polysulphate polyanions/glycosaminoglycans, tetracyclic compounds, and tetrapyrrolic compounds that have anti-prion activities [130].

6. Conclusion

Much progress has been made in characterizing and understanding the structure and assembly of amyloid. The most toxic species in amyloid disorders are widely considered to be the oligomers preceding the formation of mature amyloid fibrils and plaque deposits. In addition, the conformational conversion process itself may cause downstream events that contribute to neurodegeneration. There are many pressing questions left to address in the field of amyloid proteins and neurodegenerative disease. It has been challenging to determine the structural identity and associated toxicity of various oligomers. However, the heterogeneous nature of oligomers and amyloids could explain the diverse phenotypes and clinical symptoms associated with different neurodegenerative diseases. Additionally, it is unknown when the soluble oligomers cause toxicity during the course of a disease and what molecular events trigger an initial misfolding event, which leads to amyloid generation. Is the initiating molecular event gradual, stochastic, spontaneous, or cumulative? Moreover, what is the time course of protein aggregation, and how does the cellular protein quality control system contribute to the development of plaques and the onset disease? Early intervention will most likely provide the best therapeutic advantage to mitigating these diseases. Research that examines the molecular mechanisms of amyloid assembly and accumulation and

investigates the conformations of cytotoxic pre-amyloid oligomers will provide valuable information that could be applied to the development of disease-modifying therapies.

References

1. Selkoe DJ (2003) Folding proteins in fatal ways. Nature 426 (6968):900-904. doi:10.1038/nature02264

2. Taylor JP, Hardy J, Fischbeck KH (2002) Toxic proteins in neurodegenerative disease. Science 296 (5575):1991-1995. doi:10.1126/science.1067122

3. Cerasoli E, Ryadnov MG, Austen BM (2015) The elusive nature and diagnostics of misfolded Abeta oligomers. Frontiers in chemistry 3:17. doi:10.3389/fchem.2015.00017

4. Alzheimer's A (2017) 2017 Alzheimer's disease facts and figures. Alzheimers Dement 13:325-373

5. Morimoto RI, Kline MP, Bimston DN, Cotto JJ (1997) The heat-shock response: regulation and function of heat-shock proteins and molecular chaperones. Essays Biochem 32:17-29

6. Balch WE, Morimoto RI, Dillin A, Kelly JW (2008) Adapting proteostasis for disease intervention. Science 319 (5865):916-919. doi:10.1126/science.1141448

7. Chaudhuri TK, Paul S (2006) Protein-misfolding diseases and chaperone-based therapeutic approaches. The FEBS journal 273 (7):1331-1349. doi:10.1111/j.1742-4658.2006.05181.x

8. Sarge KD, Murphy SP, Morimoto RI (1993) Activation of heat shock gene transcription by heat shock factor 1 involves oligomerization, acquisition of DNA-binding activity, and nuclear localization and can occur in the absence of stress. Mol Cell Biol 13 (3):1392-1407

9. Sorger PK (1991) Heat shock factor and the heat shock response. Cell 65 (3):363-366

10. Richard I Morimoto DJ, P Kroeger, S Mathur, S Murphy, A Nakai, K Sarge, K Abravaya, L Sistonen (1994) Regulation of Heat Shock Gene Transcription by a Family of Heat Shock Transcription Factors. The Biology of Heat Shock Proteins and Molecular Chaperones:417-455

11. Lindquist S, Craig EA (1988) The heat-shock proteins. Annu Rev Genet 22:631-677. doi:10.1146/annurev.ge.22.120188.003215

12. Gidalevitz T, Ben-Zvi A, Ho KH, Brignull HR, Morimoto RI (2006) Progressive disruption of cellular protein folding in models of polyglutamine diseases. Science 311 (5766):1471-1474. doi:10.1126/science.1124514

13. Gidalevitz T, Krupinski T, Garcia S, Morimoto RI (2009) Destabilizing protein polymorphisms in the genetic background direct phenotypic expression of mutant SOD1 toxicity. PLoS Genet 5 (3):e1000399. doi:10.1371/journal.pgen.1000399

14. Ben-Zvi A, Miller EA, Morimoto RI (2009) Collapse of proteostasis represents an early molecular event in Caenorhabditis elegans aging. Proc Natl Acad Sci U S A 106 (35):14914-14919. doi:10.1073/pnas.0902882106

15. Brehme M, Voisine C, Rolland T, Wachi S, Soper JH, Zhu Y, Orton K, Villella A, Garza D, Vidal M, Ge H, Morimoto RI (2014) A chaperome subnetwork safeguards proteostasis in aging and neurodegenerative disease. Cell Rep 9 (3):1135-1150. doi:10.1016/j.celrep.2014.09.042

16. Tanaka K, Matsuda N (2014) Proteostasis and neurodegeneration: the roles of proteasomal degradation and autophagy. Biochimica et biophysica acta 1843 (1):197-204. doi:10.1016/j.bbamcr.2013.03.012

17. Gray DA, Tsirigotis M, Woulfe J (2003) Ubiquitin, proteasomes, and the aging brain. Science of aging knowledge environment : SAGE KE 2003 (34):RE6. doi:10.1126/sageke.2003.34.re6

18. Carrard G, Bulteau AL, Petropoulos I, Friguet B (2002) Impairment of proteasome structure and function in aging. The international journal of biochemistry & cell biology 34 (11):1461-1474

19. Tycko R (2004) Progress towards a molecular-level structural understanding of amyloid fibrils. Curr Opin Struct Biol 14 (1):96-103. doi:10.1016/j.sbi.2003.12.002

20. Golde TE, Miller VM (2009) Proteinopathy-induced neuronal senescence: a hypothesis for brain failure in Alzheimer's and other neurodegenerative diseases. Alzheimers Res Ther 1 (2):5. doi:10.1186/alzrt5

21. Petkova AT, Yau WM, Tycko R (2006) Experimental constraints on quaternary structure in Alzheimer's beta-amyloid fibrils. Biochemistry 45 (2):498-512. doi:10.1021/bi051952q

22. Groenning M (2010) Binding mode of Thioflavin T and other molecular probes in the context of amyloid fibrils-current status. J Chem Biol 3 (1):1-18. doi:10.1007/s12154-009-0027-5

23. Nelson R, Eisenberg D (2006) Recent atomic models of amyloid fibril structure. Current opinion in structural biology 16 (2):260-265. doi:10.1016/j.sbi.2006.03.007

24. Greenwald J, Riek R (2010) Biology of amyloid: structure, function, and regulation. Structure 18 (10):1244-1260. doi:10.1016/j.str.2010.08.009

25. Zerovnik E (2002) Amyloid-fibril formation. Proposed mechanisms and relevance to conformational disease. European journal of biochemistry / FEBS 269 (14):3362-3371

26. Lindgren M, Hammarstrom P (2010) Amyloid oligomers: spectroscopic characterization of amyloidogenic protein states. FEBS J 277 (6):1380-1388. doi:10.1111/j.1742-4658.2010.07571.x

27. Holmes BB, Diamond MI (2012) Cellular mechanisms of protein aggregate propagation. Current opinion in neurology 25 (6):721-726. doi:10.1097/WCO.0b013e32835a3ee0

28. Brettschneider J, Del Tredici K, Lee VM, Trojanowski JQ (2015) Spreading of pathology in neurodegenerative diseases: a focus on human studies. Nat Rev Neurosci 16 (2):109-120. doi:10.1038/nrn3887

29. Grundke-Iqbal I, Iqbal K, Tung YC, Quinlan M, Wisniewski HM, Binder LI (1986) Abnormal phosphorylation of the microtubule-associated protein tau (tau) in Alzheimer cytoskeletal pathology. Proc Natl Acad Sci U S A 83 (13):4913-4917

30. Kosik KS, Joachim CL, Selkoe DJ (1986) Microtubule-associated protein tau (tau) is a major antigenic component of paired helical filaments in Alzheimer disease. Proc Natl Acad Sci U S A 83 (11):4044-4048

31. Ihara Y, Nukina N, Miura R, Ogawara M (1986) Phosphorylated tau protein is integrated into paired helical filaments in Alzheimer's disease. J Biochem 99 (6):1807-1810

32. Perl DP (2010) Neuropathology of Alzheimer's disease. The Mount Sinai journal of medicine, New York 77 (1):32-42. doi:10.1002/msj.20157

33. Breydo L, Wu JW, Uversky VN (2012) Alpha-synuclein misfolding and Parkinson's disease. Biochimica et biophysica acta 1822 (2):261-285. doi:10.1016/j.bbadis.2011.10.002

34. Arrasate M, Finkbeiner S (2012) Protein aggregates in Huntington's disease. Experimental neurology 238 (1):1-11. doi:10.1016/j.expneurol.2011.12.013

35. Cleary JP, Walsh DM, Hofmeister JJ, Shankar GM, Kuskowski MA, Selkoe DJ, Ashe KH (2005) Natural oligomers of the amyloid-beta protein specifically disrupt cognitive function. Nature neuroscience 8 (1):79-84. doi:10.1038/nn1372

36. Prusiner SB (1982) Novel proteinaceous infectious particles cause scrapie. Science 216 (4542):136-144

37. Moore RA, Taubner LM, Priola SA (2009) Prion protein misfolding and disease. Current opinion in structural biology 19 (1):14-22. doi:10.1016/j.sbi.2008.12.007

38. Fink AL (1998) Protein aggregation: folding aggregates, inclusion bodies and amyloid. Folding & design 3 (1):R9-23. doi:10.1016/S1359-0278(98)00002-9

39. Murphy RM (2007) Kinetics of amyloid formation and membrane interaction with amyloidogenic proteins. Biochimica et biophysica acta 1768 (8):1923-1934. doi:10.1016/j.bbamem.2006.12.014

40. Koo EH, Lansbury PT, Jr., Kelly JW (1999) Amyloid diseases: abnormal protein aggregation in neurodegeneration. Proceedings of the National Academy of Sciences of the United States of America 96 (18):9989-9990

41. Ruschak AM, Miranker AD (2009) The role of prefibrillar structures in the assembly of a peptide amyloid. J Mol Biol 393 (1):214-226. doi:10.1016/j.jmb.2009.06.026

42. Guijarro JI, Sunde M, Jones JA, Campbell ID, Dobson CM (1998) Amyloid fibril formation by an SH3 domain. Proceedings of the National Academy of Sciences of the United States of America 95 (8):4224-4228

43. Klunk WE, Pettegrew JW, Abraham DJ (1989) Quantitative evaluation of congo red binding to amyloid-like proteins with a beta-pleated sheet conformation. J Histochem Cytochem 37 (8):1273-1281. doi:10.1177/37.8.2666510

44. Naiki H, Higuchi K, Hosokawa M, Takeda T (1989) Fluorometric determination of amyloid fibrils in vitro using the fluorescent dye, thioflavin T1. Anal Biochem 177 (2):244-249

45. Reinke AA, Gestwicki JE (2011) Insight into amyloid structure using chemical probes. Chemical biology & drug design 77 (6):399-411. doi:10.1111/j.1747-0285.2011.01110.x

46. Nilsson MR (2004) Techniques to study amyloid fibril formation in vitro. Methods 34 (1):151-160. doi:10.1016/j.ymeth.2004.03.012

47. Bolder SG, Sagis LM, Venema P, van der Linden E (2007) Thioflavin T and birefringence assays to determine the conversion of proteins into fibrils. Langmuir 23 (8):4144-4147. doi:10.1021/la063048k

48. Hawe A, Sutter M, Jiskoot W (2008) Extrinsic fluorescent dyes as tools for protein characterization. Pharm Res 25 (7):1487-1499. doi:10.1007/s11095-007-9516-9

49. Khurana R, Coleman C, Ionescu-Zanetti C, Carter SA, Krishna V, Grover RK, Roy R, Singh S (2005) Mechanism of thioflavin T binding to amyloid fibrils. J Struct Biol 151 (3):229-238. doi:10.1016/j.jsb.2005.06.006

50. Canete M, Villanueva A, Juarranz A, Stockert JC (1987) A study of interaction of thioflavine T with DNA: evidence for intercalation. Cell Mol Biol 33 (2):191-199

51. Kelenyi G (1967) On the histochemistry of azo group-free thiazole dyes. J Histochem Cytochem 15 (3):172-180. doi:10.1177/15.3.172

52. Hudson SA, Ecroyd H, Kee TW, Carver JA (2009) The thioflavin T fluorescence assay for amyloid fibril detection can be biased by the presence of exogenous compounds. FEBS J 276 (20):5960-5972. doi:10.1111/j.1742-4658.2009.07307.x

53. Biancalana M, Koide S (2010) Molecular mechanism of Thioflavin-T binding to amyloid fibrils. Biochimica et biophysica acta 1804 (7):1405-1412. doi:10.1016/j.bbapap.2010.04.001

54. Ratnaswamy G, Koepf E, Bekele H, Yin H, Kelly JW (1999) The amyloidogenicity of gelsolin is controlled by proteolysis and pH. Chem Biol 6 (5):293-304. doi:10.1016/S1074-5521(99)80075-1

55. Jarrett JT, Lansbury PT, Jr. (1992) Amyloid fibril formation requires a chemically discriminating nucleation event: studies of an amyloidogenic sequence from the bacterial protein OsmB. Biochemistry 31 (49):12345-12352

56. Chen S, Berthelier V, Hamilton JB, O'Nuallain B, Wetzel R (2002) Amyloid-like features of polyglutamine aggregates and their assembly kinetics. Biochemistry 41 (23):7391-7399

57. Klunk WE, Jacob RF, Mason RP (1999) Quantifying amyloid beta-peptide (Abeta) aggregation using the Congo red-Abeta (CR-abeta) spectrophotometric assay. Anal Biochem 266 (1):66-76. doi:10.1006/abio.1998.2933

58. Miura T, Thomas GJ, Jr. (1995) Raman spectroscopy of proteins and their assemblies. Subcell Biochem 24:55-99

59. Klunk WE, Jacob RF, Mason RP (1999) Quantifying amyloid by congo red spectral shift assay. Methods Enzymol 309:285-305

60. Lindgren M, Sorgjerd K, Hammarstrom P (2005) Detection and characterization of aggregates, prefibrillar amyloidogenic oligomers, and protofibrils using fluorescence spectroscopy. Biophys J 88 (6):4200-4212. doi:10.1529/biophysj.104.049700

61. Teoh CL, Su D, Sahu S, Yun SW, Drummond E, Prelli F, Lim S, Cho S, Ham S, Wisniewski T, Chang YT (2015) Chemical Fluorescent Probe for Detection of Abeta Oligomers. Journal of the American Chemical Society. doi:10.1021/jacs.5b06190

62. Ono M, Watanabe H, Kimura H, Saji H (2012) BODIPY-based molecular probe for imaging of cerebral beta-amyloid plaques. ACS chemical neuroscience 3 (4):319-324. doi:10.1021/cn3000058

63. Schmued L, Raymick J, Tolleson W, Sarkar S, Zhang YH, Bell-Cohn A (2012) Introducing Amylo-Glo, a novel fluorescent amyloid specific histochemical tracer especially suited for multiple labeling and large scale quantification studies. J Neurosci Methods 209 (1):120-126. doi:10.1016/j.jneumeth.2012.05.019

64. Sarkar S, Raymick J, Schmued LC (2014) The use of recently developed histochemical markers for localizing neurotoxicant induced regional brain pathologies. Toxins (Basel) 6 (4):1453-1470. doi:10.3390/toxins6041453

65. Saborio GP, Permanne B, Soto C (2001) Sensitive detection of pathological prion protein by cyclic amplification of protein misfolding. Nature 411 (6839):810-813. doi:10.1038/35081095

66. Barria MA, Gonzalez-Romero D, Soto C (2012) Cyclic amplification of prion protein misfolding. Methods in molecular biology 849:199-212. doi:10.1007/978-1-61779-551-0_14

67. Gonzalez-Montalban N, Makarava N, Ostapchenko VG, Savtchenk R, Alexeeva I, Rohwer RG, Baskakov IV (2011) Highly efficient protein misfolding cyclic amplification. PLoS pathogens 7 (2):e1001277. doi:10.1371/journal.ppat.1001277

68. Atarashi R, Wilham JM, Christensen L, Hughson AG, Moore RA, Johnson LM, Onwubiko HA, Priola SA, Caughey B (2008) Simplified ultrasensitive prion detection by recombinant PrP conversion with shaking. Nature methods 5 (3):211-212. doi:10.1038/nmeth0308-211

69. Chen B, Morales R, Barria MA, Soto C (2010) Estimating prion concentration in fluids and tissues by quantitative PMCA. Nature methods 7 (7):519-520. doi:10.1038/nmeth.1465

70. Salvadores N, Shahnawaz M, Scarpini E, Tagliavini F, Soto C (2014) Detection of misfolded Abeta oligomers for sensitive biochemical diagnosis of Alzheimer's disease. Cell reports 7 (1):261-268. doi:10.1016/j.celrep.2014.02.031

71. Colby DW, Zhang Q, Wang S, Groth D, Legname G, Riesner D, Prusiner SB (2007) Prion detection by an amyloid seeding assay. Proceedings of the National Academy of Sciences of the United States of America 104 (52):20914-20919. doi:10.1073/pnas.0710152105

72. Wilham JM, Orru CD, Bessen RA, Atarashi R, Sano K, Race B, Meade-White KD, Taubner LM, Timmes A, Caughey B (2010) Rapid end-point quantitation of prion

seeding activity with sensitivity comparable to bioassays. PLoS pathogens 6 (12):e1001217. doi:10.1371/journal.ppat.1001217

73. Atarashi R, Sano K, Satoh K, Nishida N (2011) Real-time quaking-induced conversion: a highly sensitive assay for prion detection. Prion 5 (3):150-153. doi:10.4161/pri.5.3.16893

74. Choi SR, Schneider JA, Bennett DA, Beach TG, Bedell BJ, Zehntner SP, Krautkramer MJ, Kung HF, Skovronsky DM, Hefti F, Clark CM (2012) Correlation of amyloid PET ligand florbetapir F 18 binding with Abeta aggregation and neuritic plaque deposition in postmortem brain tissue. Alzheimer Dis Assoc Disord 26 (1):8-16. doi:10.1097/WAD.0b013e31821300bc

75. Price JC, Klunk WE, Lopresti BJ, Lu X, Hoge JA, Ziolko SK, Holt DP, Meltzer CC, DeKosky ST, Mathis CA (2005) Kinetic modeling of amyloid binding in humans using PET imaging and Pittsburgh Compound-B. J Cereb Blood Flow Metab 25 (11):1528-1547. doi:10.1038/sj.jcbfm.9600146

76. Koo J, Byun Y (2013) Current status of PET-imaging probes of beta-amyloid plaques. Arch Pharm Res 36 (10):1178-1184. doi:10.1007/s12272-013-0193-4

77. Wolk DA, Zhang Z, Boudhar S, Clark CM, Pontecorvo MJ, Arnold SE (2012) Amyloid imaging in Alzheimer's disease: comparison of florbetapir and Pittsburgh compound-B positron emission tomography. J Neurol Neurosurg Psychiatry 83 (9):923-926. doi:10.1136/jnnp-2012-302548

78. Clark CM, Pontecorvo MJ, Beach TG, Bedell BJ, Coleman RE, Doraiswamy PM, Fleisher AS, Reiman EM, Sabbagh MN, Sadowsky CH, Schneider JA, Arora A, Carpenter AP, Flitter ML, Joshi AD, Krautkramer MJ, Lu M, Mintun MA, Skovronsky DM, Group A-AS (2012) Cerebral PET with florbetapir compared with neuropathology at autopsy for detection of neuritic amyloid-beta plaques: a prospective cohort study. The Lancet Neurology 11 (8):669-678. doi:10.1016/S1474-4422(12)70142-4

79. Bierer LM, Hof PR, Purohit DP, Carlin L, Schmeidler J, Davis KL, Perl DP (1995) Neocortical neurofibrillary tangles correlate with dementia severity in Alzheimer's disease. Arch Neurol 52 (1):81-88

80. Arriagada PV, Growdon JH, Hedley-Whyte ET, Hyman BT (1992) Neurofibrillary tangles but not senile plaques parallel duration and severity of Alzheimer's disease. Neurology 42 (3 Pt 1):631-639

81. Okamura N, Harada R, Furumoto S, Arai H, Yanai K, Kudo Y (2014) Tau PET imaging in Alzheimer's disease. Curr Neurol Neurosci Rep 14 (11):500. doi:10.1007/s11910-014-0500-6

82. Marquie M, Normandin MD, Vanderburg CR, Costantino IM, Bien EA, Rycyna LG, Klunk WE, Mathis CA, Ikonomovic MD, Debnath ML, Vasdev N, Dickerson BC, Gomperts SN, Growdon JH, Johnson KA, Frosch MP, Hyman BT, Gomez-Isla T (2015) Validating novel tau positron emission tomography tracer [F-18]-AV-1451 (T807) on postmortem brain tissue. Ann Neurol 78 (5):787-800. doi:10.1002/ana.24517

83. Xia Y, Nivet E, Sancho-Martinez I, Gallegos T, Suzuki K, Okamura D, Wu MZ, Dubova I, Esteban CR, Montserrat N, Campistol JM, Izpisua Belmonte JC (2013) Directed differentiation of human pluripotent cells to ureteric bud kidney progenitor-like cells. Nat Cell Biol 15 (12):1507-1515. doi:10.1038/ncb2872

84. Scholl M, Lockhart SN, Schonhaut DR, O'Neil JP, Janabi M, Ossenkoppele R, Baker SL, Vogel JW, Faria J, Schwimmer HD, Rabinovici GD, Jagust WJ (2016) PET Imaging of Tau Deposition in the Aging Human Brain. Neuron 89 (5):971-982. doi:10.1016/j.neuron.2016.01.028

85. Dahlgren KN, Manelli AM, Stine WB, Jr., Baker LK, Krafft GA, LaDu MJ (2002) Oligomeric and fibrillar species of amyloid-beta peptides differentially affect neuronal viability. The Journal of biological chemistry 277 (35):32046-32053. doi:10.1074/jbc.M201750200

86. Bopp SK, Lettieri T (2008) Comparison of four different colorimetric and fluorometric cytotoxicity assays in a zebrafish liver cell line. BMC pharmacology 8:8. doi:10.1186/1471-2210-8-8

87. Ono K, Condron MM, Teplow DB (2009) Structure-neurotoxicity relationships of amyloid beta-protein oligomers. Proceedings of the National Academy of Sciences of the United States of America 106 (35):14745-14750. doi:10.1073/pnas.0905127106

88. Kroemer G, Galluzzi L, Vandenabeele P, Abrams J, Alnemri ES, Baehrecke EH, Blagosklonny MV, El-Deiry WS, Golstein P, Green DR, Hengartner M, Knight RA, Kumar S, Lipton SA, Malorni W, Nunez G, Peter ME, Tschopp J, Yuan J, Piacentini M, Zhivotovsky B, Melino G, Nomenclature Committee on Cell D (2009) Classification of cell death: recommendations of the Nomenclature Committee on Cell Death 2009. Cell Death Differ 16 (1):3-11. doi:10.1038/cdd.2008.150

89. Mery B, Guy JB, Vallard A, Espenel S, Ardail D, Rodriguez-Lafrasse C, Rancoule C, Magne N (2017) In Vitro Cell Death Determination for Drug Discovery: A Landscape Review of Real Issues. J Cell Death 10:1179670717691251. doi:10.1177/1179670717691251

90. Fotakis G, Timbrell JA (2006) In vitro cytotoxicity assays: comparison of LDH, neutral red, MTT and protein assay in hepatoma cell lines following exposure to cadmium chloride. Toxicology letters 160 (2):171-177. doi:10.1016/j.toxlet.2005.07.001

91. Decker T, Lohmann-Matthes ML (1988) A quick and simple method for the quantitation of lactate dehydrogenase release in measurements of cellular cytotoxicity and tumor necrosis factor (TNF) activity. J Immunol Methods 115 (1):61-69

92. Simmons LK, May PC, Tomaselli KJ, Rydel RE, Fuson KS, Brigham EF, Wright S, Lieberburg I, Becker GW, Brems DN, et al. (1994) Secondary structure of amyloid beta peptide correlates with neurotoxic activity in vitro. Molecular pharmacology 45 (3):373-379

93. Kayed R, Head E, Thompson JL, McIntire TM, Milton SC, Cotman CW, Glabe CG (2003) Common structure of soluble amyloid oligomers implies common mechanism of pathogenesis. Science 300 (5618):486-489. doi:10.1126/science.1079469
94. Mosmann T (1983) Rapid colorimetric assay for cellular growth and survival: application to proliferation and cytotoxicity assays. J Immunol Methods 65 (1-2):55-63
95. Carmichael J, DeGraff WG, Gazdar AF, Minna JD, Mitchell JB (1987) Evaluation of a tetrazolium-based semiautomated colorimetric assay: assessment of chemosensitivity testing. Cancer Res 47 (4):936-942
96. Crissman HA, Orlicky DJ, Kissane RJ (1979) Fluorescent DNA probes for flow cytometry. Considerations and prospects. J Histochem Cytochem 27 (12):1652-1654. doi:10.1177/27.12.391999
97. Roden MM, Lee KH, Panelli MC, Marincola FM (1999) A novel cytolysis assay using fluorescent labeling and quantitative fluorescent scanning technology. J Immunol Methods 226 (1-2):29-41
98. Papadopoulos NG, Dedoussis GV, Spanakos G, Gritzapis AD, Baxevanis CN, Papamichail M (1994) An improved fluorescence assay for the determination of lymphocyte-mediated cytotoxicity using flow cytometry. J Immunol Methods 177 (1-2):101-111
99. Weston SA, Parish CR (1990) New fluorescent dyes for lymphocyte migration studies. Analysis by flow cytometry and fluorescence microscopy. J Immunol Methods 133 (1):87-97
100. Wisniewski T, Sadowski M (2008) Preventing beta-amyloid fibrillization and deposition: beta-sheet breakers and pathological chaperone inhibitors. BMC neuroscience 9 Suppl 2:S5. doi:10.1186/1471-2202-9-S2-S5
101. Kanthasamy AG, Choi C, Jin H, Harischandra DS, Anantharam V, Kanthasamy A (2012) Effect of divalent metals on the neuronal proteasomal system, prion protein

ubiquitination and aggregation. Toxicology letters 214 (3):288-295. doi:10.1016/j.toxlet.2012.09.008

102. Jacobson T, Navarrete C, Sharma SK, Sideri TC, Ibstedt S, Priya S, Grant CM, Christen P, Goloubinoff P, Tamas MJ (2012) Arsenite interferes with protein folding and triggers formation of protein aggregates in yeast. Journal of cell science 125 (Pt 21):5073-5083. doi:10.1242/jcs.107029

103. Tamas MJ, Sharma SK, Ibstedt S, Jacobson T, Christen P (2014) Heavy metals and metalloids as a cause for protein misfolding and aggregation. Biomolecules 4 (1):252-267. doi:10.3390/biom4010252

104. Basha MR, Murali M, Siddiqi HK, Ghosal K, Siddiqi OK, Lashuel HA, Ge YW, Lahiri DK, Zawia NH (2005) Lead (Pb) exposure and its effect on APP proteolysis and Abeta aggregation. FASEB J 19 (14):2083-2084. doi:10.1096/fj.05-4375fje

105. Cheng B, Gong H, Xiao H, Petersen RB, Zheng L, Huang K (2013) Inhibiting toxic aggregation of amyloidogenic proteins: a therapeutic strategy for protein misfolding diseases. Biochimica et biophysica acta 1830 (10):4860-4871. doi:10.1016/j.bbagen.2013.06.029

106. Hard T, Lendel C (2012) Inhibition of amyloid formation. Journal of molecular biology 421 (4-5):441-465. doi:10.1016/j.jmb.2011.12.062

107. Francioso A, Punzi P, Boffi A, Lori C, Martire S, Giordano C, D'Erme M, Mosca L (2015) beta-sheet interfering molecules acting against beta-amyloid aggregation and fibrillogenesis. Bioorganic & medicinal chemistry 23 (8):1671-1683. doi:10.1016/j.bmc.2015.02.041

108. Soto C, Sigurdsson EM, Morelli L, Kumar RA, Castano EM, Frangione B (1998) Beta-sheet breaker peptides inhibit fibrillogenesis in a rat brain model of amyloidosis: implications for Alzheimer's therapy. Nature medicine 4 (7):822-826

109. Soto C, Kindy MS, Baumann M, Frangione B (1996) Inhibition of Alzheimer's amyloidosis by peptides that prevent beta-sheet conformation. Biochemical and biophysical research communications 226 (3):672-680. doi:10.1006/bbrc.1996.1413

110. Viet MH, Ngo ST, Lam NS, Li MS (2011) Inhibition of aggregation of amyloid peptides by beta-sheet breaker peptides and their binding affinity. The journal of physical chemistry B 115 (22):7433-7446. doi:10.1021/jp1116728

111. Panza F, Solfrizzi V, Imbimbo BP, Logroscino G (2014) Amyloid-directed monoclonal antibodies for the treatment of Alzheimer's disease: the point of no return? Expert opinion on biological therapy 14 (10):1465-1476. doi:10.1517/14712598.2014.935332

112. Goni F, Prelli F, Ji Y, Scholtzova H, Yang J, Sun Y, Liang FX, Kascsak R, Kascsak R, Mehta P, Wisniewski T (2010) Immunomodulation targeting abnormal protein conformation reduces pathology in a mouse model of Alzheimer's disease. PloS one 5 (10):e13391. doi:10.1371/journal.pone.0013391

113. Ehrnhoefer DE, Duennwald M, Markovic P, Wacker JL, Engemann S, Roark M, Legleiter J, Marsh JL, Thompson LM, Lindquist S, Muchowski PJ, Wanker EE (2006) Green tea (-)-epigallocatechin-gallate modulates early events in huntingtin misfolding and reduces toxicity in Huntington's disease models. Human molecular genetics 15 (18):2743-2751. doi:10.1093/hmg/ddl210

114. Maiti P, Manna J, Veleri S, Frautschy S (2014) Molecular chaperone dysfunction in neurodegenerative diseases and effects of curcumin. BioMed research international 2014:495091. doi:10.1155/2014/495091

115. Ahmed AH, Subaiea GM, Eid A, Li L, Seeram NP, Zawia NH (2014) Pomegranate extract modulates processing of amyloid-beta precursor protein in an aged Alzheimer's disease animal model. Curr Alzheimer Res 11 (9):834-843

116. Dobson CM (2004) Principles of protein folding, misfolding and aggregation. Seminars in cell & developmental biology 15 (1):3-16. doi:10.1016/j.semcdb.2003.12.008

117. Muchowski PJ, Schaffar G, Sittler A, Wanker EE, Hayer-Hartl MK, Hartl FU (2000) Hsp70 and hsp40 chaperones can inhibit self-assembly of polyglutamine proteins into amyloid-like fibrils. Proceedings of the National Academy of Sciences of the United States of America 97 (14):7841-7846. doi:10.1073/pnas.140202897

118. Whitesell L, Mimnaugh EG, De Costa B, Myers CE, Neckers LM (1994) Inhibition of heat shock protein HSP90-pp60v-src heteroprotein complex formation by benzoquinone ansamycins: essential role for stress proteins in oncogenic transformation. Proc Natl Acad Sci U S A 91 (18):8324-8328

119. Westerheide SD, Morimoto RI (2005) Heat shock response modulators as therapeutic tools for diseases of protein conformation. The Journal of biological chemistry 280 (39):33097-33100. doi:10.1074/jbc.R500010200

120. Supko JG, Hickman RL, Grever MR, Malspeis L (1995) Preclinical pharmacologic evaluation of geldanamycin as an antitumor agent. Cancer chemotherapy and pharmacology 36 (4):305-315. doi:10.1007/BF00689048

121. Kitson RR, Chang CH, Xiong R, Williams HE, Davis AL, Lewis W, Dehn DL, Siegel D, Roe SM, Prodromou C, Ross D, Moody CJ (2013) Synthesis of 19-substituted geldanamycins with altered conformations and their binding to heat shock protein Hsp90. Nature chemistry 5 (4):307-314. doi:10.1038/nchem.1596

122. Dickey CA, Kamal A, Lundgren K, Klosak N, Bailey RM, Dunmore J, Ash P, Shoraka S, Zlatkovic J, Eckman CB, Patterson C, Dickson DW, Nahman NS, Jr., Hutton M, Burrows F, Petrucelli L (2007) The high-affinity HSP90-CHIP complex recognizes and selectively degrades phosphorylated tau client proteins. The Journal of clinical investigation 117 (3):648-658. doi:10.1172/JCI29715

123. Bailey CK, Andriola IF, Kampinga HH, Merry DE (2002) Molecular chaperones enhance the degradation of expanded polyglutamine repeat androgen receptor in a cellular model of spinal and bulbar muscular atrophy. Human molecular genetics 11 (5):515-523

124. Schirmer EC, Glover JR, Singer MA, Lindquist S (1996) HSP100/Clp proteins: a common mechanism explains diverse functions. Trends in biochemical sciences 21 (8):289-296

125. Shorter J, Lindquist S (2008) Hsp104, Hsp70 and Hsp40 interplay regulates formation, growth and elimination of Sup35 prions. The EMBO journal 27 (20):2712-2724. doi:10.1038/emboj.2008.194

126. Muchowski PJ (2002) Protein misfolding, amyloid formation, and neurodegeneration: a critical role for molecular chaperones? Neuron 35 (1):9-12

127. Korth C, May BC, Cohen FE, Prusiner SB (2001) Acridine and phenothiazine derivatives as pharmacotherapeutics for prion disease. Proceedings of the National Academy of Sciences of the United States of America 98 (17):9836-9841. doi:10.1073/pnas.161274798

128. May BC, Fafarman AT, Hong SB, Rogers M, Deady LW, Prusiner SB, Cohen FE (2003) Potent inhibition of scrapie prion replication in cultured cells by bis-acridines. Proceedings of the National Academy of Sciences of the United States of America 100 (6):3416-3421. doi:10.1073/pnas.2627988100

129. Vogtherr M, Grimme S, Elshorst B, Jacobs DM, Fiebig K, Griesinger C, Zahn R (2003) Antimalarial drug quinacrine binds to C-terminal helix of cellular prion protein. Journal of medicinal chemistry 46 (17):3563-3564. doi:10.1021/jm034093h

130. Trevitt CR, Collinge J (2006) A systematic review of prion therapeutics in experimental models. Brain : a journal of neurology 129 (Pt 9):2241-2265. doi:10.1093/brain/awl150

Figure 1. A.) Amyloid assembly cascade. Natively folded proteins that are amyloidogenic may misfold into a non-native conformation, which can then self-associate and undergo nucleation to form fibrils. Additional elongation and condensation events enable further accumulation into amyloid containing aggregates. In vitro seeding and amplification assays such as PMCA, ASA, and RT-QuiCK can detect and quantitate pre-amyloid intermediates. Amyloid specific dyes ThioflavinT and Congo Red bind to amyloid-containing aggregates and can be used to monitor amyloid assembly kinetics in vitro.

B.) Protein aggregates of Alzheimer's Disease. Alzheimer's disease (AD) is characterized by the histopathological hallmarks of extracellular amyloid plaques and intracellular neurofibrillary tangles (NFT's). Amyloid plaques are largely composed of amyloid-beta peptide, which is a product of cleavage of amyloid precursor protein (APP). Phosphorylated tau (p-Tau) is a microtubule-associated protein associated with AD that accumulates intracellularly to form neurofibrillary tangles.

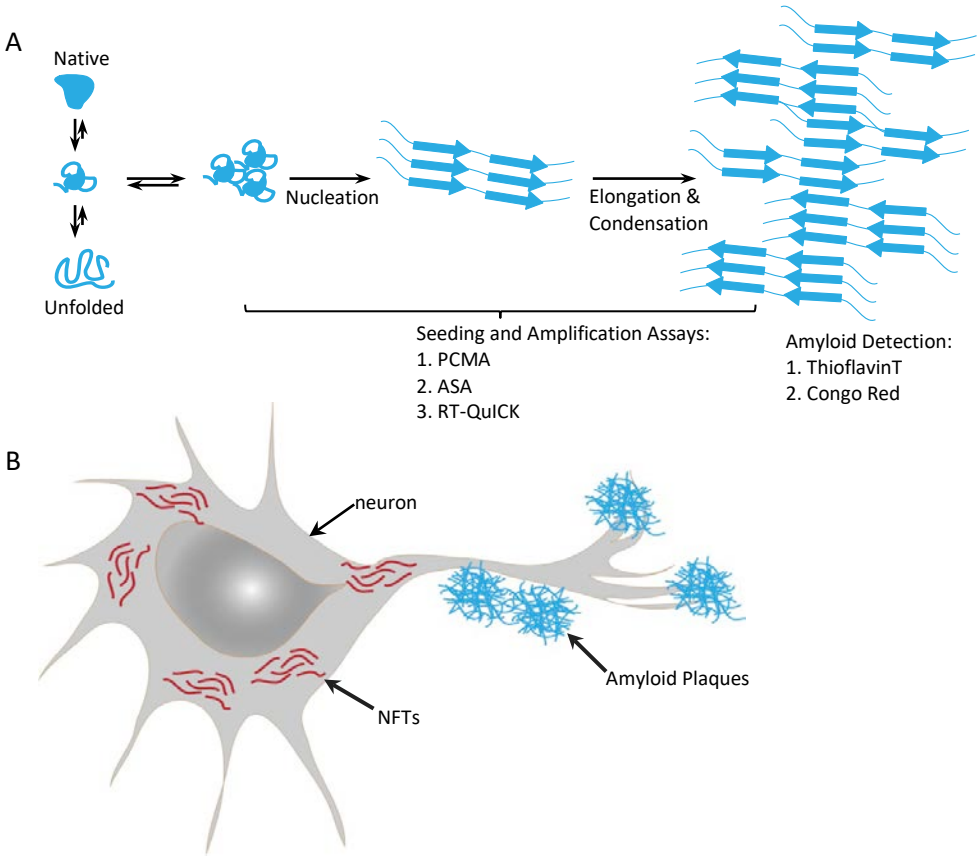
A
Native
Unfolded
Nucleation
Elongation &
Condensation
Seeding and Amplification Assays:
1. PCMA
2. ASA
3. RT-QuICK
Amyloid Detection:
1. ThioflavinT
2. Congo Red
B
neuron
Amyloid Plaques
NFTs

Manuscript II

Publication Status: Formatted as a research article for submission to *Prion*

Title: Site-specific mutations in the Hsp104 N-domain impair [PSI$^+$] prion curing in *Saccharomyces cerevisiae*

Authors: Shannon E. May[1,2], Christopher J. LaBreck[3] and Jodi L. Camberg[1,2,3]

Author Affiliations:

[1] Interdisciplinary Neurosciences Program, University of Rhode Island, Kingston, RI 02881

[2] George and Anne Ryan Institute for Neuroscience, University of Rhode Island, Kingston, RI 02881

[3] Department of Cell and Molecular Biology, College of the Environment and Life Sciences, University of Rhode Island, Kingston, RI 02881

Author Contributions: S.E.M. designed experiments, performed experiments, interpreted data and wrote paper; C.J.L. performed experiments and edited paper, J.L.C. designed experiments, interpreted data, and wrote paper.

Abstract

Molecular chaperone proteins are required for maintaining protein homeostasis by facilitating proper folding of nascent polypeptides, misfolded proteins and unfolded proteins. Hsp104 belongs to the AAA+ (ATPases associated with diverse cellular activities) superfamily of ATPases that share similar domain organization. In *Saccharomyces cerevisiae*, heat shock protein 104 (Hsp104) regulates prion inheritance and coordinates with Hsp70 and Hsp40 to disassemble aggregated proteins, including amyloids. In the yeast prion model system of [PSI^+], overexpression of Hsp104 cures yeast cells of the [PSI^+] prion. Previous research showed that [PSI^+] prion curing mediated by Hsp104 overexpression requires the N-domain of Hsp104 (1). To further investigate the biochemical mechanism of amyloid recognition and prion curing by Hsp104 overexpression, we constructed an *hsp104* gene library containing mutations in the N-terminal domain and screened clonal isolates in *Saccharomyces cerevisiae* using the [PSI^+] colorimetric assay. Using a novel, quantitative fluorescence-based assay we identified several specific sites in the N-domain of Hsp104 that are essential for [PSI^+] curing by Hsp104 overexpression. This study provides novel insight into chaperone-mediated recognition and disassembly of amyloids, which are expressed in yeast as prions and are pervasive in human neurodegenerative disorders, such as Alzheimer's disease, Parkinson's disease, and Huntington's disease.

Introduction

Prions are amyloidogenic protein conformations that propagate from cell to cell in either a functional or pathogenic capacity (2, 3, 4). Prions are non-genetic elements that self-template and are inherited in a non-Mendelian manner; reversion of the prion fold to the native fold, also referred to as prion curing, is reversible (5). Budding yeast have been shown to contain as many as eight propagating prions (4). One of the most extensively studied prions in yeast is Sup35, which confers the phenotype [PSI^+].

Sup35 is a translation termination protein that exists in at least two conformations: the native conformation and the prion conformation (6). The [psi^-] phenotype in *S. cerevisiae* is characterized by the presence of soluble, natively folded Sup35 protein (Sup35p), which recognizes stop codons and subsequently releases polypeptides from the ribosome (7). In yeast, Sup35 can adopt the prion conformation and subsequently aggregate into insoluble amyloid fibrils, thus decreasing the pool of soluble Sup35 protein (8). The [PSI^+] phenotype is characterized by low levels of soluble Sup35p and high levels of insoluble Sup35, which results in translation termination errors from read-through of nonsense codons (9). Therefore, the presence or absence of [PSI^+] in yeast can be determined by monitoring translation efficiency of a nonsense codon present in the adenine biosynthesis gene *ade2.* This mutation, *ade2-1 ochre,* leads to accumulation of aminoimidazole ribotide (AIR), a red-colored intermediate produced during in the formation of purine bases, in cells with functional Sup35 (10, 11). The [PSI^+] red/white colorimetric assay is reliably used to monitor translation fidelity as a marker of prion phenotype in yeast. The accumulation of amyloid aggregates (prions) alleviates the accumulation of the red-pigmented metabolite in strains carrying mutations in the adenine biosynthesis

pathway (11). The prion conformation of Sup35 protein, referred to as the [PSI$^+$] phenotype, thus suppresses nonsense mutations and colonies appear white on solid media (12). This traditional [PSI$^+$] assay is both qualitative and binary; the phenotype [psi$^-$] can be identified by red colonies and the phenotype [PSI$^+$] is associated with white colonies. Strong [PSI$^+$] and weak [PSI$^+$] phenotypes in yeast have been observed in research studies that impaired Hsp70 binding to prion in yeast (13). A strong [PSI$^+$] phenotype refers to strong lack of red pigmentation and mitotic stability (13). Mutations in the middle domain of Hsp104 also affect prion propagation in yeast and yield differential [PSI$^+$] phenotypes that range in color from pink to red yeast colonies (14).

Hsp104 is an ATP-dependent molecular chaperone protein that functions to remodel the Sup35 amyloid and segregate it into daughter cells during division. Hsp104 is a ring-shaped hexameric protein that belongs to the AAA+ (ATPases associated with diverse cellular activities) ATPase protein superfamily (15, 16). Common to all AAA+ proteins are highly conserved nucleotide binding domains that contain Walker motifs (17). Several proteins in the AAA+ superfamily use mechanical force to remodel substrate proteins by hydrolyzing ATP (18). Hsp104 contains two nucleotide-binding domains per subunit that function cooperatively (19, 20). The flexible pore loops of Hsp100 proteins are critical for substrate translocation and protein remodeling. Mutations targeting the pore loops of Hsp100 proteins, such as HslU and ClpX, impair substrate engagement and translocation of polypeptides through the axial channel (21, 22). The mechanism for Hsp104-mediated disaggregation is thought to rely on the threading of polypeptides through an axial channel. Cryoelectron microscopy maps of Hsp104 hexamers bound to different nucleotides suggests that the two nucleotide binding domains of Hsp104 form stacked

rings and a central cavity (23). Research suggests that substrates are disaggregated by Hsp104 by threading and translocation of substrate through the axial channel into the central cavity of Hsp104 due to substrate binding of the NBD1 and NBD2 rings coupled to sequential ATP hydrolysis (23). Conserved tyrosine residues (pore-loop) located in the central channel of Hsp104 bind to and grip polypeptides (24 – 28). The mechanism of disaggregation by substrate threading and translocation is conserved in ClpB, the bacterial homolog of Hsp104 (26, 28, 29, 30). ATP hydrolysis cycles cause changes in the conformation of Hsp104, thus providing the mechanical force required to unfold and translocate polypeptides through the axial pore of Hsp104 (23, 26).

Hsp104 remodels heterogenous aggregates, including amorphous as well as highly ordered amyloid aggregates (31 – 33). Hsp104 reactivates misfolded proteins and is necessary for prion inheritance in *Saccharomyces cerevisiae* (34, 35). It is thought that Hsp104 fragments prions and generates seeds for prion assembly, which catalyzes the propagation of prions in yeast (36). All yeast prions with the exception of [PSI^+] require Hsp104 for prion propagation (37 – 42). Deletion of the *hsp104* gene results in the loss of the prions [PSI^+], [URE3], [PIN^+]/[RNQ^+], [SWI^+], and [MOT3] (35, 41). Hsp104 fragments prion fibrils and generates amyloid seeds, which function as propagation units that accelerate the self-assembly of prions; deletion of *hsp104* is thought to inhibit the fragmentation of prions, resulting in large aggregates that cannot be efficiently transmitted from mother to daughter yeast cells (41). Moreover, overexpression of the Hsp40 yeast protein Ydj1p cures the [URE3] prion, possibly by an Hsp70/Hsp40 mechanism (42). The overexpression of Hsp104 cures yeast of the [PSI^+] and [MCA] prions (41, 43).

The N-terminal domain of Hsp104 (amino acid residues 1 – 147) is dispensable for thermotolerance, protein disaggregation of select substrates, and [PSI$^+$] prion propagation, but is required for [PSI$^+$] loss (prion curing) when Hsp104 is overexpressed in vivo (1). Hsp104 cooperates with the Hsp70/40 chaperone system to disaggregate proteins in vivo (44, 45). Hsp70 acts upstream of Hsp104 and regulates Hsp104 binding to protein aggregates (46). Hsp70 is required for species-specific targeting of client proteins to ClpB and Hsp104, suggesting a conserved mechanism of substrate binding and disaggregation by the Hsp70-Hsp100 chaperone system at the surface of protein aggregates (32). Hsp70 binds to the middle domain of Hsp104, which may facilitate threading of protein substrates through the Hsp104 axial channel (47, 48).

Analysis of the crystallized structure of the N-terminal domain of Hsp104 in *S. cerevisiae* suggests that misfolded proteins may bind to the N-domain (49). The unstructured linker of ClpB is thought to regulate the position of the N-domain and affect substrate binding to aggregates (50). Currently, it is unknown where amyloids (prions) bind to Hsp104. Given that the N-domain is implicated in recognizing amyloid, further investigation into the N-domain of Hsp104 is warranted to better characterize substrate binding to Hsp104. Therefore, we randomly mutagenized the N-domain of Hsp104 and screened clonal isolates in *S. cerevisiae* using the [PSI$^+$] colorimetric assay to monitor changes in prion phenotype and possible impairments of Hsp104 binding to prion substrate. We found several mutations in the Hsp104 N-domain that are impaired for prion curing, thermotolerance, and disaggregation, suggesting an important role of the N-domain in the direct recognition and/or clearance of the Sup35 amyloid.

Results

Curing of [PSI$^+$] by Hsp104 overexpression detected by fluorescence

Although the [PSI$^+$] colorimetric conversion assay has been widely used to qualitatively assess amyloid abundance and prion inheritance, it does not allow for quantitative detection of intermediate phenotypes. Therefore, we developed a novel fluorometric assay to quantitatively characterize different [PSI$^+$] phenotypes in yeast, which are associated with differential translation termination efficiency and [PSI$^+$] prion propagation. Yeast carrying the *ade2-1* nonsense mutation in the adenine biosynthesis pathways accumulate red pigment due to the polymerization of aminoimidazole ribotide (10). The polymerization and oxidation of 4-aminoimidazole ribotide in the yeast vacuole results in the accumulation of an endogenously fluorescent red pigment (51). The red pigment stably persists in the vacuole and fluorescence has been previously observed by excitation at 450 – 490 nm and visualization of emitted light at 520-nm (51). The [PSI$^+$] prion phenotype in yeast can be detected in *ade2-1* mutants by screening yeast cells for white colony color; red colonies of yeast carrying the ade2-1 mutation are [psi$^-$] and contain mostly soluble, functional Sup35 protein (11).

To determine if red pigment accumulation is quantifiable in cell lysates by fluorescence, we cultured [psi$^-$] and [PSI$^+$] yeast on agar plates for five days until red colonies were visible for the [psi$^-$] strain (Figure 1A). We harvested cells from solid media, lysed the cells with glass beads and measured protein concentrations of the soluble lysate. We monitored fluorescence emission spectra of soluble cell extracts, normalized to total protein, following excitation at 488 nm. Fluorescence has also previously been used to separate mixed populations of red and white yeast cells by fluorescence-activated cell sorting (FACS) with an excitation at 488 nm (52). We

observed that [psi$^-$] cell lysates produce a large, broad emission peak at 565 nm; however, a much lower emission peak was detected for [PSI$^+$] cell lysates (Figure 1B).

To determine if the amplitude of the emission peak is dependent on the protein concentration in [psi$^-$] cell lysate, we compared emission spectra over a range of concentrations (0.05 to 0.8 mg ml^{-1}) (Figure 1C). We observed that as protein concentration increased, the amplitude of the emission peak at 565 nm also increased, indicating that the emission detected is concentration-dependent, tracking with soluble protein. This also provided evidence that our novel fluorometric assay was linearized and within the working range of detecting differences in fluorescence signal based on the presence or absence of the [PSI$^+$] prion in adenine biosynthesis yeast mutants.

The adenine biosynthesis pathway metabolite AIR accumulates over time in colonies of [psi$^-$] during incubation at 30 °C. It is detectable as pink colony color at day 3 and continues to develop into a darker red as the colonies age. To confirm that fluorescence associated with AIR-containing [psi$^-$] colonies also accumulates with time, we streaked [psi$^-$] yeast cells onto rich yeast extract/peptone/dextrose (YPD) solid media and incubated the plates for 3, 5 and 7 days at 30°C. At each time point, we harvested the cells, collected soluble cell lysates and measured the peak emission amplitude. We observed that the differences in fluorescence emission intensity of [psi$^-$] and [PSI$^+$] *S. cerevisiae* lysates was highly significant on day 5 (p-value = 0.0007) and day 7 (p-value = 0.006) of growth (Figure 1D). [PSI$^+$] cells do not develop dark red colony color or soluble fluorescence over time. To visualize the fluorescence associated with red pigment accumulation in [psi$^-$] cells, we performed confocal fluorescence microscopy using similar excitation/emission conditions. We compared

the basal fluorescence of [psi$^-$] and [PSI$^+$] yeast cells by confocal microscopy. As expected, we observed a strong fluorescence signal in [psi$^-$] cells at the excitation 488 nm (Figure 1E). However, under the same visualization conditions, we did not observe endogenous fluorescence in [PSI$^+$] cells (Figure 1E).

To determine if red pigment accumulation associated with Hsp104 overexpression in [PSI+] yeast is endogenously fluorescent similar to the wild-type [psi-] phenotype in yeast, we transformed the vector pYS104 (53) into [PSI$^+$] cells containing chromosomal *hsp104*. We observed that curing of [PSI$^+$] prion by Hsp104 overexpression results in a conversion of white colony phenotype to red colony phenotype (Figure 2A). Moreover, the red pigment in [PSI$^+$] yeast overexpressing Hsp104 has a similar endogenous fluorescence signal as [psi$^-$] cells containing the empty pYES2 vector (Figures 2A and 2B). Thus, the fluorometric assay that we developed to quantify [PSI$^+$] phenotype can be used to classify parental [PSI$^+$] and [psi-] yeast strains as well as yeast strains carrying plasmids that modify [PSI$^+$] phenotype.

The Walker B motif in AAA+ proteins is responsible for ATP hydrolysis (54). To determine if a mutation known to impair ATP hydrolysis in Hsp104 also affects [PSI$^+$] phenotype, we constructed the Walker B NBD1 mutation E285Q in *hsp104*. The *S. cerevisiae* containing the Hsp104(E285Q) mutation in the NBD1 domain had a pink colony color on SD-URA solid media, which is associated with a weakly [PSI$^+$] phenotype (Figure 2A). We compared the development of fluorescence signal over time in yeast strains containing the *ade2-1* mutation transformed with pYS104, pYES2, and the Hsp104(E285Q) Walker B mutation. Yeast cells were harvested on days 3, 5, and 7 of growth and analyzed protein lysates using our novel fluorometric assay. Significant differences in emission fluorescence intensities among the different

S. cerevisiae strains occurred on day 5 of growth (p-value = 0.0008) and day 7 of growth (p-value = 0.004). We found that the greatest differences in fluorescence signal among [PSI$^+$] yeast containing empty pYES2 vector, pYS104, and Hsp104(E285Q) occurred at the emission wavelength 565 nm (Figure 2C). The fluorescence intensity of yeast lysates at 565 nm is significantly different between [PSI$^+$] yeast and [psi$^-$] yeast containing empty vector (p-value = 0.0084). Moreover, we found a significant difference in fluorescence intensity at the emission wavelength 565 nm of [PSI$^+$] yeast overexpressing Hsp104 and [PSI$^+$] containing the Walker B mutation Hsp104(E285Q), p-value = 0.0359 (Figure 2C). Confocal microscopy of yeast expressing pYES2, pYS104, and Hsp104(E285Q) showed that the weakly [PSI$^+$] phenotype associated with Hsp104(E285Q) had endogenous fluorescence, which appeared much weaker in intensity than the fluorescence associated with *S. cerevisiae* overexpressing Hsp104 (Figure 2D).

Identification of Hsp104 N-domain residues important for [PSI$^+$] curing in *Saccharomyces cerevisiae*

To identify which amino acids in the Hsp104 N-domain are important for amyloid recognition and curing of the [PSI$^+$] prion phenotype, we performed random mutagenesis and phenotypic screening to monitor *S. cerevisiae* cells for colony color conversion in cells expressing Hsp104 mutant proteins in the plasmid pYS104 (Figure 3A). Using error-prone PCR amplification, we generated random mutations in *hsp104* in the region spanning the N-domain (amino acid residues 1 – 307). Next, the mutagenized fragments were used as primers to amplify a plasmid containing full-length *hsp104,* and DpnI-digested PCR products were subsequently transformed into *E. coli*. Mutagenized pYS104 plasmids were isolated from clonal isolates that grew on

ampicillin selection plates. In total, 127 plasmids extracted from *E. coli* were transformed into [PSI$^+$] *S. cerevisiae* and screened for conferring a color change from white to red. Clonal isolates that had an intermediate or weak [PSI$^+$] phenotype (pink), or loss of Hsp104 function (white) were sequenced and mapped to the Hsp104 N-domain structure (Figure 3B). Mutations identified in the screen included seven frameshift mutations, five single and two double substitution mutations. High-level expression of plasmid-encoded Hsp104 wild type and mutant proteins was confirmed by Western blot using antibodies directed against Hsp104 (Figure 3C).

We found five mutations in the N-domain of Hsp104 that are associated with intermediate [PSI$^+$], or weakly [PSI$^+$], phenotype in yeast: A133D, L54P, H34D/E138V, L36V, and P81L (Figure 4A). Moreover, we observed that cells cured of [PSI$^+$] reverted to a strongly [PSI$^+$] phenotype in cells carrying the mutation V69F in *hsp104* (Figure 4A). The double mutation A99T/V74A in *hsp104* resulted in the phenotypic appearance of dark red colonies, which had more red pigmentation than yeast cells overexpressing *hsp104*, on SD-URA solid media. We further investigated double mutations of interest by generating single substitution mutations in the yeast expression plasmid pYS104 using site-directed mutagenesis. We observed that Hsp104 A99T is responsible for the red pigmentation of yeast colonies on SD-URA. Interestingly, the variant Hsp104 V74A was associated with a weakly [PSI$^+$] phenotype. Furthermore, the yeast variant Hsp104 H34D was weakly [PSI$^+$] and the variant Hsp104 E138V was strongly [PSI$^+$] (Figure 4A).

Functional analyses of Hsp104 N-domain mutants in vivo

The phenotypic [PSI$^+$] colorimetric differences that we observed among the hsp104 N-domain variants could have been caused by variable expression of Hsp104 among yeast strains. To determine if variable Hsp104 expression was responsible for the phenotypic differences among our strains, we performed immunoblots using an antibody against Hsp104. *S. cerevisiae* strains containing H34D, L36V, L54P, V69F, V74A, P81L, A99T, A133D, and E138V all expressed Hsp104 protein. Mapping the N-domain mutations to the crystal structure of the Hsp104 N-domain of *S. cerevisiae* (55) containing mutations shows that the following mutations are near the surface: L54P, V74A, P81L, A133D, and E138V (Figure 4B). Thus, it is possible that these residues may contact amyloid substrate and participate in substrate binding.

Yeast strains carrying mutations in *hsp104* show maximal differences in fluorescence intensity at 565 nm when excited at 488 nm. One-way ANOVA of the fluorescence intensities was used to determine that the means of the fluorescence intensity for each strain at the emission wavelength 565 nm is significantly different ($p < 0.0001$) (Figure 4C). Confocal microscopy was used to visualize the endogenous fluorescence of *S. cerevisiae* carrying the Hsp104(V69F) mutation, which is associated with loss of prion curing (Figure 4D). We observed reduced endogenous fluorescence in this yeast strain (Figure 4D), as expected from the conversion of colony color from red to white on SD-URA solid media.

Characterization of Hsp104 N-domain variants by thermotolerance assays

Hsp104 is required for thermotolerance in yeast. To determine if the mutations that we identified in the N-domain are impaired for thermotolerance, we carried out

thermotolerance assays with different strains of yeast containing mutations in *hsp104*. Yeast strains were grown to mid-logarithmic phase of growth and Hsp104 expression was induced by mild heat shock at 37°C for 30 minutes. Yeast cells were exposed to extreme heat shock at 52°C at 0, 5, and 10 minutes and serially diluted fivefold on SD-URA solid media. Heat shock at 52°C for 15 minutes and 30 minutes resulted in no colony growth on SD-URA plates (data not shown). We assessed the cell viability of the yeast strains carrying mutations in the Hsp104 N-domain after five days of growth at 30°C and found that cells expressing Hsp104(H34D), Hsp104(V69F), Hsp104(A133D), and Hsp104(E138V) had reduced viability and thus impaired thermotolerance (Figure 5B) compared to yeast strains that were not subjected to heat shock at 52°C (Figure 5A). It should also be noted that all cells have endogenous expression of Hsp104 from the chromosome and loss of function phenotypes likely emerge from dominant-negative mutations.

To determine if the Hsp104 variants H34D, L36V, L54P, V69F, V74A, P81L, A99T, A133D, and E138V have impaired disaggregation and/or reactivation of aggregated proteins, we grew yeast strains containing Hsp104 mutations to early mid-logarithmic growth, incubated the liquid cultures in 37°C for 30 minutes, heat shocked the cells at 52°C for 15 minutes, recovered the yeast cells at 30°C for 20 minutes and extracted soluble and insoluble protein fractions using mechanical lysis with glass beads. We monitored protein aggregate load in insoluble yeast protein fractions by SDS-PAGE and Coomassie stain (Figure S1). We observed that yeast containing the mutation Hsp104(L54P) had a 1.8-fold increase in thermal aggregate accumulation compared to yeast cells overexpressing wild-type Hsp104 (Figure 6). The mutation Hsp104(V74A) was associated with a1.8-fold increase in thermal aggregates and yeast containing Hsp104(P81L) had a 1.9-fold increase in thermal aggregate load

compared to wild-type Hsp104 (Figure 6). Therefore, the *hsp104* mutations L54P, V74A, and P81L are associated with impaired reactivation of protein aggregates.

Discussion

The amino acid residues 1 – 163 in the N-domain of ClpB are thought to be important for early recognition of polypeptide substrates targeted for disaggregation (56 – 58). Research does not support that the entire N-domain is essential for thermotolerance or prion propagation (1). However, the inversion of Hsp104 residues 110 – 121 (inversion of nucleotides 330 – 363) in the N-domain results in loss of both thermotolerance and prion propagation (59). Hsp104 overexpression has been shown to convert [PSI^+] yeast to a [psi^-] phenotype, thus "curing" yeast of the Sup35 amyloid (35, 54). By contrast, Hsp104 lacking the N-domain (Hsp104ΔNTD) does not cure [PSI^+] yeast of Sup35 amyloid (1). It has been suggested that the N-domain of Hsp104 may fine-tune substrate recognition to prevent the nonspecific disaggregation of polypeptides and directly bind to amyloid substrates (60). Here, we provide evidence that specific residues in the N-domain of Hsp104 are necessary for substrate recognition of Sup35 amyloid.

Hsp104 and its bacterial homolog ClpB are highly conserved and are found throughout bacteria, fungi, plants, and lower eukaryotes. Hsp104 disaggregates thermal aggregates and remodels stable, ordered aggregates, such as fibrillar Sup35 and Ure2 (61 – 63). Previous studies have provided evidence that the N-domain of ClpB is important for recognition of substrate proteins and remodeling of aggregates; a hydrophobic substrate-binding site in the N-terminal domain of ClpB was identified by Rosenzweig and coworkers. Specifically, the residues W6A, L14A, L91A, L111A

were found to be important for ClpB binding to aggregates (64). A separate study found that the ClpB N-domain residues T7A, D103A, E109A are involved in substrate binding based on luciferase reactivation assays and the observation that the N-domain supports the casein-induced activation of ClpB ATPase activity (58). Mapping these residues to the *E. coli* ClpB structure modeled on the crystal structure of *T. thermophilus* ClpB shows that the following residues are surface-exposed and are likely involved in direct substrate recognition of aggregated proteins: T7, L91, L14, D103, and E109 (Figure 7A).

Pairwise alignments of the Hsp104 N-domain and the ClpB N-domain were conducted using the EMBOSS Needle tool from EMBL-EBI (65, 66). The alignment of the Hsp104 N-domain (amino acid residues 1 – 165) to the ClpB N-domain (amino acid residues 1 – 149) using EMBOSS Needle results in a similarity score of 45.2%. The amino acid residue H34 is a highly conserved residue; the residue is conserved in the *S. cerevisiae* Hsp104 and *E. coli* ClpB N-domain sequences (Figure 7B). The mutation H34D identified during phenotypic screening is associated with an intermediate [PSI^+] phenotype, which suggests that prion curing mediated by overexpression of Hsp104 is impaired. Notably, the biochemical change from histidine, a positively charged residue, to aspartic acid, a negatively charged residue may result in major functional changes of Hsp104. An additional mutation, A133D, occurs at a highly conserved site between the *S. cerevisiae* Hsp104 and *E. coli* ClpB sequences. The substitution of alanine, a nonpolar amino acid, with aspartic acid, a negatively charged amino acid, may change the binding properties and functional interactions of Hsp104. Notably, the mutations at H34D and A133D are associated with impaired thermotolerance and prion curing by Hsp104 overexpression. Furthermore, the *hsp104* mutations L36V and V69F are conserved residues and are

associated with weakly [PSI$^+$] and strongly [PSI$^+$] phenotypes in *S. cerevisiae*, respectively. The *hsp104* mutations L54P, V74A, P81L, A99T, and E138V are semi-conserved residues. Therefore, it is possible that the sites H34 and A133 in ClpB and Hsp104 are evolutionary conserved and are important for direct binding to aggregated proteins.

Thermotolerance assays conducted in this study suggest that *hsp104* mutations H34D, V69F, and A133D are associated with impaired cell viability after exposure to extreme thermal stress. Thus, these amino acid residues in Hsp104 may be important for thermotolerance. Based on our results, we propose a model of Hsp104-mediated disassembly of amyloid protein that involves initial substrate recognition by the Hsp70/40 co-chaperone system, binding of Hsp70 to the middle domain of Hsp104 to deliver substrate to Hsp104, and binding of amyloid substrate to the N-domain of Hsp104 before substrate translocation through the axial channel of Hsp104 into the central cavity for disaggregation (Figure 7C). Our results suggest that surface-exposed Hsp104 residues, including A133D, bind to Sup35 amyloid. The Hsp104 residues P81L, V74A, and L54P are associated with increased thermal aggregate load after extreme heat shock, suggesting a role for these residues in protein disaggregation. Thus, these residues may be involved in the recognition of amyloid fibrils. Our results suggest that conserved residues H34 and A133 in the N-domain may engage amyloid substrate and enable Hsp104 to translocate Sup35, or other aggregated substrates through the axial channel for unfolding and reactivation in collaboration with Hsp70/40.

The mutations in the Hsp104 N-domain identified by [PSI$^+$] colorimetric screening in *S.cerevisiae* V69F and E138V are associated with complete loss of Hsp104-mediated curing of Sup35 prion as evidence by the reversion of colony color

from red, a [psi$^-$] phenotype, to white, a strongly [PSI$^+$] phenotype. Furthermore, the mutations Hsp104(H34D), Hsp104(L36V), Hsp104(L54P), Hsp104(V74A), Hsp104(P81L), and Hsp104(A133D) caused a conversion from the [psi$^-$] phenotype to a weakly [PSI$^+$] phenotype as evidenced by the colorimetric change in yeast colonies from red to pink or pale orange-pink. It is possible that these point mutations in *hsp104* impair the oligomerization of Hsp104, thereby rendering wild-type Hsp104 protein non-functional. Future research should address this hypothesis to determine if oligomerization of Hsp104 is affected by the point mutations H34D, L36V, L54P, V69F, V74A, P81L, and A133D described here. Moreover, in vitro disaggregation assays, ATP activity assays, and binding assays of Hsp104 containing the mutations H34D, L36V, L54P, V69F, V74A, P81L, A99T, and A133D would provide more mechanistic information about the point mutations in Hsp104 that are associated with complete or partial loss of Hsp104-mediated curing of Sup35 prion. Here, we provide evidence that the N-domain of Hsp104 recognizes amyloid fibrils and is essential for substrate recognition of Sup35 prion.

Materials and Methods

The [PSI$^+$] yeast strain used in this study is strain PSI+ [BSC783/4a], ATCC® MYA-536™. The genotype of this strain is: MATa SUQ5 ade2-1 ura3-1 his3-11 his3-15 leu2-3 leu2-112 [PSI+]. The [psi-] yeast strain used in this study is a prion-deficient mutant derived from the BSC783/4a strain and is designated 783/4a psi-, ATCC® MYA-537™. The [psi-] strain has the genotype MATa SUQ5 ade2-1 ura3-1 his3-11 his3-15 leu2-3 leu2-112 [psi-]. Both yeast strains are haploid and have previously been used in prion studies (67). Yeast strains were grown at 30°C in synthetic dextrose media minus uracil solid media (SD-URA; 1.7 g yeast nitrogen base, 5 g

ammonium sulfate, 20 g dextrose per liter, and 17 g agar per liter) and yeast extract/peptone/dextrose media (YPD; containing 1% yeast extract, 2% bactopeptone, 2% glucose, and 40 mg of adenine sulfate per liter).

Mutagenesis

The Megawhop cloning method has been used to construct mutant libraries of specific protein domains (66). First, mutations in the N-domain of Hsp104 were introduced into the gene *hsp104* using an error-prone DNA polymerase (Agilent Genemorph II Random Mutagenesis kit). The DNA fragment generated from the random mutagenesis polymerase chain reaction, or the “megaprimer”, was used to amplify the template pYS104 vector, resulting in nicked plasmid DNA (68). Parental plasmid DNA was removed by DpnI digestion and the digestion reaction products were transformed into *Escherichia coli*. Transformants were grown on LB Lennox media containing ampicillin. Plasmids recovered from *E. coli* were then purified and screened in *Saccharomyces cerevisiae* using a fluorescence-based [PSI^{+}] assay. Site-directed mutagenesis of *hsp104* on the vectorpYS104 (54) was carried out using the QuikChange Mutagenesis kit (Agilent Genomics). Primers were designed to introduce the following substitutions into hsp104: A99T, V74A, H34D, and E138V (Table 3). Yeast transformants were grown on synthetic dextrose plates lacking uracil and were replica plated.

Yeast Whole Cell Extraction and Western Blot

Yeast whole cell lysates were extracted under non-denaturing conditions as previously described. Yeast cells were grown on synthetic dextrose solid media lacking uracil and supplemented with 2 % galactose at 30°C. After five days of growth, yeast cells were scraped off the solid media and pelleted at 3,000 x *g* for 5 minutes at 4°C. Cells were washed twice with ice-cold phosphate buffered saline and resuspended in yeast lysis buffer (50 mM Tris pH 8.0, 5 mM EDTA, 0.5 mM NaCl, 5% glycerol, 1% Triton X-100) containing protease inhibitors. Yeast cells were lysed by vortexing cells resuspended in lysis buffer with 0.5 mm glass beads (Scientific Industries, Inc.) eight times with two-minute cooling periods on ice between each vortex. The protein concentration of lysates was quantified using the bicinchoninic acid assay (Pierce BCA Protein Assay kit) and protein concentrations were subsequently normalized. Hsp104 antibody (Thermo Fisher Scientific) was diluted 1:1,000 in Tris buffer containing 0.1% Tween-20 and 0.05% nonfat milk. All Western blot bands were normalized to beta-actin (Abcam) or GAPDH (Thermo Fisher Scientific).

Fluorescence [PSI^{+}] Assay

Yeast whole cell lysates were normalized to a final protein concentration of 0.5 mg/mL. Using a quartz cuvette, 80 µL of lysate was excited at 488 nm at PMT 750 V. Emission wavelengths were captured between 500 and 800 nm. The excitation slit width was 10 nm and the emission wavelength was 20 nm.

Thermotolerance Assay

Thermotolerance experiments were conducted with yeast strains as previously described (69, 70). Briefly, yeast cells were grown in SD-URA media to mid-logarithmic phase (OD_{600} of 0.400 – 0.600) in SD-URA media. The synchronized liquid cultures of yeast were incubated for 30 minutes at 37°C with vigorous aeration to induce the expression of Hsp104. Subsequently, yeast cultures were moved to a 52°C water bath and 1 mL aliquots of cultures were removed, transferred to ice briefly, and serial diluted five-fold in SD-URA media before spot plating onto SD-URA + 2% galactose solid media 0 minutes and 5 minutes after heat shock at 52°C to determine cell viability.

To measure thermal aggregate accumulation in [PSI^+] yeast containing mutations in *hsp104*, yeast cultures were grown in 30°C to mid-logarithmic phase in 5 mL of SD-URA media and pretreated at 37°C for 30 minutes with vigorous aeration. Cultures were then transferred to a 52°C water bath for 15 minutes. Subsequent to the extreme heat shock, yeast cultures were incubated at 30°C with vigorous aeration to allow cells to recover from the thermal stress. Yeast cells were harvested by centrifugation and protein was extracted by glass bead lysis in lysis buffer. Equal volumes (5 µL) of insoluble yeast protein were boiled in LDS sample buffer; the final sodium dodecyl sulfate (SDS) concentration of the protein samples was 2%. The insoluble protein samples were loaded in a 3 – 8% Tris-acetate gel and electrophoresed at 150V in Tris-acetate running buffer containing SDS. Gels were incubated in Coomassie stain to observe total protein levels across lanes. Intensity of each full lane was analyzed using ImageJ software (National Institute of Health ImageJ).

Statistical analyses

Differences in mean fluorescence intensities were measured using an unpaired, one-tailed t-test with alpha level equal to 0.05. Analysis of variance tests and post-hoc Tukey's multiple comparison tests were conducted to determine differences in fluorescence intensities across more than two yeast strains. Statistical analyses were carried out using Graphpad Prism version 6.0, GraphPad Software, La Jolla, California, USA (www.graphpad.com).

Pairwise protein alignment

Protein sequences were globally aligned using the EMBOSS Needle tool (66) from the European Bioinformatics Institute (EMBL-EBI) (65). The default settings in EMBOSS Needle were used for protein alignment.

Disclosure of Potential Conflicts of Interest

The authors do not have any conflict of interest or financial disclosures.

Acknowledgements

We thank Arnob Dutta for assisting with yeast protocol development. We thank Sue Wickner and Shannon Doyle for helpful discussions. Fluorescence microscopy and sequencing were performed at the Rhode Island Genomics and Sequencing Center, which is supported in part by the National Science Foundation (MRI Grant No. DBI-

0215393 and EPSCoR Grant No. 0554548 & EPS-1004057), the US Department of Agriculture (Grant Nos. 2002-34438-12688, 2003-34438-13111, and 2008-34438-19246) and the University of Rhode Island.

Funding

Research reported in this publication was supported by the National Institute of General Medical Sciences of the National Institutes of Health under Award Number R01GM118927 to J. Camberg. The content is solely the responsibility of the authors and does not necessarily represent the official views of the National Institutes of Health.

References

1. Hung GC and Masison DC. N-terminal domain of yeast Hsp104 chaperone is dispensable for thermotolerance and prion propagation but necessary for curing prions by Hsp104 overexpression. *Genetics Society of America.* 2006; 173, 611 – 622.
2. Pruisner SB. Prions. *Proc Natl Acad Sci USA*; 1998: 95: 13363 – 13383.
3. Crow ET, Li L. Newly identified prions in budding yeast, and their possible functions. *Semin Cell Dev Biol.* 2011; 22: 452 – 9.
4. Cascarina SM, Ross ED. Yeast prions and human prion-like proteins: sequence features and prediction methods. *Cellular and molecular life sciences: CMLS*. 2014; 71:2047 – 63.

5. Wickner RB, Shewmaker FP, Bateman DA, Edskes HK, Gokovskiy A, Dayani Y, and Bezsonov EE. Yeast prions: structure, biology, and prion-handling systems. *Microbiol Mol Biol Rev*. 2015; 79(1): 1 – 17.
6. Wickner RB. [UER3] as an altered URE2 protein: evidence for a prion analog in Saccharomyces cerevisiae. *Science*. 1994; 264: 566 – 569.
7. Stansfield, I, Jones K, Kushnirov VV, Dagkesamaskaya AR, Poznyakovski AI, Paushkin SV et al. The products of the Sup45 (eRF1) and SUP35P genes interact to mediate translation termination in Saccharomyces cerevisiae. *EMBO J*. 1995; 14: 4365 – 4373.
8. Paushkin SV, Kushnirov VV, Smirnov VN, and Ter-Avanesyan MD. Propagation of the yeast prion-like [PSI+] determinant is mediated by oligomerization of the SUP35P-encoded polypeptide chain release factor. *EMBO J*. 1996; 15: 3127 – 3134.
9. Zhou P et al. The yeast non-Mendelian factor [ETA+] is a variant of [PSI+], a prion-like form of release factor eRF3. *EMBO J*. 1999; 18, 1182 – 1191.
10. Smirnov VN, Budowsky EI, Inge-Vechtomov SG, and Serebrjakov NG. Red pigment of adenine-deficient yeast Saccharomyces cerevisiae. *Biochemical and Biophysical Research Communications*. 1967; 27(3), 299 – 306.
11. Silver JM and Eaton NR. Functional blocks of the ad-1 and ad-2 mutants of Saccharomyces cerevisiae. *Biochem Biophys Res Commun*. 1969; 34, 301 – 305.
12. Roman, HL. A system selective for mutations affecting the synthesis of adenine in yeast. *C R Trav Lab Carlsberg Ser Physiol*. 1956; 16:299 – 314.
13. Jones G, Song Y, Chung S, and Masison DC. Propagation of Saccharomyces cerevisiae [PSI+] prion is impaired by factors that regulate Hsp70 substrate binding. *Molecular and Cellular Biology*. 2004; 24(9), 3928 – 3937.

14. Dulle JE, Stein KC, and True HL. Regulation of the Hsp104 middle domain activity is critical for yeast prion propagation. *PLoS One*. 2014; 9(1): e87521.
15. Lee S et al. The structure of ClpB: a molecular chaperone that rescues proteins from the aggregated state. *Cell*. 2003; 115: 229 – 240.
16. Lupas AN and Martin J. AAA proteins. Curr Opin Struct Biol. 2002; 12: 746 – 753.
17. Hanson PI and Whiteheart SW. AAA+ proteins: have engine, will work. *Nature Reviews Molecular Cell Biology*. 2005; 6, 519 – 529.
18. Gai D, Zhao R, Li D, Finkielstein CV, and Chen XS. Mechanisms of conformational change for a replicative hexameric helicase of SV40 large tumor antigen. *Cell*. 2004; 119: 47 – 60.
19. Hattendorf DA and Lindquist SL. Cooperative kinetics of both Hsp104 ATPase domains and interdomain communication revealed by AAA sensor-1 mutants. *EMBO J*. 2002; 21: 12 – 21.
20. Schaupp A, Marcinowski M, Grimminger V, Bösl B, and Walter S. Processing of proteins by the molecular chaperone Hsp104. *J Mol Biol*. 2007; 370(4): 674 – 686.
21. Park E, Rho YM, Koh OJ, Ahn SW, Seong IS, Song JJ, Bang O, Seol JH, Wang J, Eom SH, and Chung CH. Role of the GYVG pore motif of HslU ATPase in protein unfolding and translocation for degradation by HslV peptidase. *J Biol Chem*. 2005; 280(24): 22892 – 8.
22. Siddiqui SM, Sauer RT, and Baker TA. Role of the processing pore of the ClpX AAA+ ATPase in the recognition and engagement of specific protein substrates. *Genes Dev*. 2004; 18(4): 369 – 374.
23. Lum R, Niggemann M, and Glover JR. Peptide and protein binding in the axial channel of Hsp104. Insights into the mechanism of protein unfolding. *J Biol Chem*. 2008; 283: 30139 – 30150.

24. Wendler P, Shorter J, Snead D, Plisson C, Clare DK, Lindquist S, et al. Motor mechanism for protein threading through Hsp40. *Mol Cell*. 2009; 34: 81 – 92.
25. Weber-ban EU, Reid BG, Miranker AD, and Horwich AL. Global unfolding of a substrate protein by the Hsp100 chaperone ClpA. *Nature*. 1999; 401(6748): 90 – 3.
26. Lee S, Choi JM, and Tsai FT. Visualizing the ATPase cycle in a protein disaggregating machine: structural basis for substrate binding by ClpB. *Mol Cell*. 2007; 25: 261 – 271.
27. Weibezahn J, Tessarz P, Schlieker C, Zahn R, Maglica Z, Lee S, et al. Thermotolerance requires refolding of aggregated proteins by substrate translocation through the central pore of ClpB. *Cell*. 2004; 653 – 665.
28. Haslberger T, Bukau B, and Mogk A. Towards a unifying mechanism for ClpB/Hsp104-mediated protein disaggregation and prion propagation. *Biochem Cell Biol*. 2010; 88(1): 63 – 75.
29. Tessarz P, Mogk A, and Bukau B. Substrate threading through the central pore of the Hsp104 chaperone as a common mechanism for protein disaggregation and prion propagation. *Mol Microbiol*. 2008; 68(1): 87 – 97.
30. Doyle SM, Hoskins JR, and Wickner S. Collaboration between the ClpB AAA+ remodeling protein and the DnaK chaperone system. *Proc Natl Acad Sci USA*. 2007; 104: 11138 – 11144.
31. Watanbe YH, Nakazaki Y, Suno R, and Yoshido M. Stability of the two wings of the coiled-coil domain of ClpB chaperone is critical for its disaggregation activity. *Biochem J*. 2009; 421: 71 – 77.
32. Tipton KA, Verges KJ, and Weissman JS. In vivo monitoring of the prion replication cycle reveals a critical role for Sis1 in delivering substrates to Hsp104. *Mol Cell*. 2008; 32: 584 – 591.

33. Winkler J, Tyedmers J, Bukau B, and Mogk A. Hsp70 targets Hsp100 chaperones to substrates for protein disaggregation and prion fragmentation. *J Cell Biol*. 2012; 198: 387 – 404.
34. Sweeny EA, Jackrel ME, Go MS, Sochor MA, Razzo BM, DeSantis ME, Gupta K, and Shorter J. The Hsp104 N-terminal domain enables disaggregase plasticity and potentiation. *Mol Cell.* 2015; 57: 836 – 849.
35. Sanchez Y and Lindquist SL. Hsp104 required for induced thermotolerance. *Science*. 1990; 248(4959): 1112 – 1115.
36. Chernoff YO, Lindquist SL, Ono B, Inge-Vechtomov SG, and Liebman SW. Role of the chaperone protein Hsp104 in propagation of the yeast prion-like factor [psi+]. *Science*. 1995; 268(5212):880 – 884.
37. Shorter J and Lindquist S. Hsp104 catalyzes formation and elimination of self-replicating Sup35 prion conformers. *Science*. 2004; 304(5678): 1793 – 1797.
38. Helsen CW and Glover JR. A new perspective on Hsp104-mediated propagation and curing of the yeast prion [PSI(+)]. *Prion*. 2012; 6(3): 234 – 9.
39. Shorter J and Lindquist S. Hsp104, Hsp70 and Hsp40 interplay regulates formation, growth and elimination of Sup35 prions. *EMBO J*. 2008; 27(20): 2712 – 2724.
40. Doyle SM, Shorter J, Zolkiewski M, Hoskins JR, Lindquist S, and Wickner S. Asymmetric deceleration of ClpB or Hsp104 ATPase activity unleashes protein-remodeling activity. *Nat Struct Mol Biol*. 2007; 14: 114 – 122.
41. Crow ET and Li L. Newly identified prions in budding yeast, and their possible functions. *Semin Cell Dev Biol*. 2011; 22(5): 452 – 459.
42. Sharma D, Stanley RF and Masison DC. Curing of [URE3] prion by the Hsp40 co-chaperone Ydj1p is mediated by Hsp70. *Genetics*. 2009; 181(1): 129 – 137.

43. Volkov KV, Aksenova AY, Soom MJ, Osipov KV, Svitin AV, Kurischko C, Shkundina IS, Ter-Avanesyan MD, Inge-Vechtomov SG, and Mironova LN. Novel non-Mendelian determinant involved in the control of translation accuracy in *Saccharomyces cerevisiae*. *Genetics*. 2000; 160(1):25 – 36.
44. Schlee S, Beinker P, Akhrymuk A, and Reinstein J. A chaperone network for the resolubilization of protein aggregates: direct interaction of ClpB and DnaK. *J Mol Biol*. 2004; 336(1): 275 – 285.
45. Glover JR and Lindquist S. Hsp104, Hsp70 and Hsp40: a novel chaperone system that rescues previously aggregated proteins. *Cell.* 1998; 94: 73 – 82.
46. Acebron SP, Martin I, del Castillo U, Moro F, and Muga A. DnaK-mediated association of ClpB to protein aggregates: A bichaperone network at the aggregate surface. *FEBS Lett*. 2009; 583(18): 2991 – 22996.
47. Sielaff B and Tsai FTF. The M-domain controls Hsp104 protein-remodeling activity in an Hsp70/40-dependent manner. *J Mol Biol*. 2010; 402(1): 30 – 37.
48. Haslberger T, Bukau B, and Mogk A. Towards a unifying mechanism for ClpB/Hsp104-mediated protein disaggregation and prion propagation. *Biochem Cell Biol*. 2010; 88(1): 63 – 75.
49. Wang P, Li J, Weaver C, Lucius A, and Sha B. Crystal structures of Hsp104 N-terminal domains from Saccharomyces cerevisiae and Candida albicans suggest the mechanism for the function of Hsp104 in dissolving prions. *Acta Cryst*. 2017; 73(Pt 4): 365 – 372.
50. Zhang T, Ploetz EA, Nagy M, Doyle SM, Wickner S, Smith PE, and Zolkiewski M. Flexible connection of the N-terminal domain in ClpB modulates substrate binding and the aggregate reactivation efficiency. *Proteins*. 2012; 80(12): 2758 – 2768.

51. Weisman LS, Bacallao R, and Wickner W. Multiple methods of visualizing the yeast vacuole permit evaluation of its morphology and inheritance during the cell cycle. *J Cell Biol*. 1987; 105(4): 1539 – 1547.
52. Bruschi CV and Chuba PJ. Nonselective enrichment for yeast adenine mutants by flow cytometry. *Cytometry*. 1988; 9, 60 – 67.
53. Patino MM, Liu JJ, Glover JR, Lindquist S. Support for the prion hypothesis for inheritance of a phenotypic trait in yeast. *Science*. 1996; 273(5275): 622 – 626.
54. Walker JE, Saraste M, Runswick MJ, and Gay NJ. Distantly related sequences in the alpha- and beta-subunits of ATP synthase, myosin, kinases and other ATP-requiring enzymes and a common nucleotide binding fold. *EMBO J*. 1982; 1(8): 945 – 951.
55. Lee J, Sung N, Mercado JM, Hryc CF, Chang C, Lee S, and Tsai FTF. Overlapping and specific functions of the Hsp104 N domain define its role in protein disaggregation. *Sci Rep*. 2017; 7(1): 11184.
56. Barnett ME, Nagy M, Kedzierska S, and Zolkiewski M. The amino-terminal domain of ClpB supports binding to strongly aggregated proteins. *Journal of Biological Chemistry*. 2005; 280(41): 3940 – 3945.
57. Lee S, Sowa ME, Choi J-M, and Tsai FTF. The ClpB/Hsp104 molecular chaperone—a protein disaggregating machine. *Journal of Structural Biology*. 2004; 146: 99 – 105.
58. Liu Z, et al. Conserved amino acid residues within the Amino-terminal domain of ClpB are essential for the chaperone activity. *Journal of Molecular Biology*. 2002; 31: 111 – 120.
59. Kurahashi H and Nakamura Y. Channel mutations in Hsp104 hexamer distinctively affect thermotolerance and prion-specific propagation. *Molecular Microbiology*. 2007; 63(6): 1669 – 1683.

60. Grimminger-Marquardt V and Lashuel HA. Structure and function of the molecular chaperone Hsp104 from yeast. *Biopolymers*. 2009; 93(3): 252 – 276.
61. Parsell DA et al. Hsp104 is a highly conserved protein with two essential nucleotide-binding sites. *Nature*. 1991; 353: 270 – 273.
62. Shorter J and Lindquist S. Destruction or potentiation of different prions catalyzed by similar hsp104 remodeling activities. *Mol Cell*. 2006; 23: 425 – 438.
63. Thomas JG and Baneyx F. Roles of the *Escherichia coli* small heat shock proteins IbpA and IbpB in thermal stress management: comparison with ClpA, ClpB, and HtpG In vivo. *J Bacteriol*. 1998; 180: 5165 – 5172.
64. Rosenzweig R, et al. ClpB N-terminal domain plays a regulatory role in protein disaggregation. *Proc Natl Acad Sci USA*. 2015; E6872 – E6881.
65. McWilliam H, Li W, Uludag M, Squizzato S, Park YM, Buso N, Crowley AP, and Lopez R. Analysis Tool Web Services from the EMBL-EBI. Nucelic Acids Research. 2013; W1: W597 – W600.
66. Needleman SB and Wunsch CD. A general method applicable to the search for similarities in the amino acid sequence of 2 proteins. *J Mol Biol*. 1970; 48(3): 443 – 453.
67. Eaglestone SS, et al. Translation termination efficiency can be regulated in *Saccharomyces cerevisiae* by environmental stress through a prion-mediated mechanism. *EMBO J*. 1999; 18: 1974 – 1981.
68. Naylor K, Ingerman E, Okreglak V, Marino M, Hinshaw JE, and Nunnari J. Mdv1 interacts with assembled dnm1 to promote mitochondrial division. *J Biol Chem*. 2006; 281: 2177 – 2183.
69. Miyazaki K. Megawhop cloning: a method of creating random mutagenesis libraries via megaprimer PCR of whole plasmids. *Methods in Enzymology*. 2011; 498: 399 – 406.

70. Jung G, Jones G, and Masison DC. Amino acid residue 184 of yeast Hsp104 chaperone is critical for prion-curing by guanidine, prion propagation, and thermotolerance. *Proc Natl Acad Sci USA*. 2002; 99: 9936 – 9941.
71. Lindquist S and Kim G. Heat-shock protein 104 expression is sufficient for thermotolerance in yeast. *Proc Natl Acad Sci USA*. 1996; 93: 5301 – 5306.

Table 1. Yeast strains used in the study.

Strain	Genotype	Ploidy	Source
783/4a PSI+ [BSC783/4a]	MATa SUQ5 ade2-1 ura3-1 his3-11 his3-15 leu2-3 leu2-112 [PSI+]	Haploid	ATCC MYA-536
783/4a psi-	MATa SUQ5 ade2-1 ura3-1 his3-11 his3-15 leu2-3 leu2-112 [psi-]	Haploid	ATCC MYA-537

Table 2. Mutations of interest in Hsp104 N-domain identified by [PSI$^+$] assay.

Random Mutation in Hsp104	**Colony Phenotype**	**Function**	**Phenotype**
V69F	White	-	Strongly [PSI$^+$]
L54P	Orange-pink	+/-	Weakly [PSI$^+$]
A133D	Dark orange-pink	+/-	Weakly [PSI$^+$]
H34D and E138V	Light orange-pink	+/-	Weakly [PSI$^+$]
H34D	Orange-pink	+/-	Weakly [PSI$^+$]
E138V	Light pink	+/-	Weakly [PSI$^+$]
V74A and A99T	Dark red	+	[psi$^-$]
V74A	Light pink	+/-	Weakly [PSI$^+$]
A99T	Dark red	+	[psi$^-$]
P81L	Light pink	-	Strongly [PSI$^+$]
Q113A	Light orange-pink	+/-	Weakly [PSI$^+$]
L36V	Orange-pink	+/-	Weakly [PSI$^+$]

Table 3. Primers used for site-directed mutagenesis.

Primer	DNA Sequence (5' to 3')
Hsp104 H34D Forward	CAATGAAGGCAGCTAGAATATCTATAGGTTGTAATTGTGGATG
Hsp104 H34D Reverse	CATCCACAATTACAACCTATAGATATTCTAGCTGCCTTCATTG
Hsp104 A99T Forward	TTGTTTTTGAATCTTAGCAGTGTCTTGAAGGACTTTCCC
Hsp104 A99T Reverse	GGGGAAAGTCCTTCAAGACACTGCTAAGATTCAAAAACAA
Hsp104 V74A Forward	CAGGTTGCTGTTGAGGAATTCTTGCTAGATTTCTATTAACCACTTTC
Hsp104 V74A Reverse	GAAAGTGGTTAATAGAAATCTAGCAAGAATTCCTCAACAGCAACCTG
Hsp104 E138V Forward	GTTGCTTGATGGCCACAATATCTACTTGAGCTTCC
Hsp104 E138V Reverse	GGAAGCTCAAGTAGATATTGTGGCCATCAAGCAAC
Hsp104 E285Q Forward	CTTACCATTACCCATTAACATGTGAATCTGATCAATGAATAACACAATTAGAGTCTT
Hsp104 E285Q Reverse	AAGACTCTAATTGTGTTATTCATTGATCAGATTCACATGTTAATGGGTAATGGTAAG

Figure 1. Red pigment in *S. cerevisiae ade2-1* mutants is intrinsically fluorescent.

A.) Red pigment accumulates in the [psi$^-$] yeast strain that contains the *ade2-1* mutation. Yeast with soluble Sup35 accumulates red pigmentation.

B.) The [psi$^-$] and [PSI$^+$] yeast strains have intrinsic fluorescence at 488 nm.

C.) The fluorescence signal associated with red pigment accumulation is dependent on the protein concentration of [psi$^-$] lysates; fluorescence signal increases with increasing protein concentration.

D.) The fluorescence signal is time-dependent; the maximal colorimetric differences between [PSI$^+$] and [psi$^-$] strains occurs on day 5 of growth at 30°C. The greatest difference between fluorescence signal of [PSI$^+$] and [psi$^-$] yeast occurs on day 5 (p-value = 0.0006) and day 7 (p-value = 0.006).

E.) *S. cerevisiae* carrying the *ade2-1* mutation and the [psi$^-$] phenotype accumulate red pigment, which has intrinsic fluorescence. Yeast cells with the [PSI$^+$] phenotype grow into white colonies on solid SD-URA plates + 2 % galactose and do not have endogenous fluorescence. Wavelength excitation 488 nm; Wavelength emission 520 nm. Scale bar indicates 5 μm.

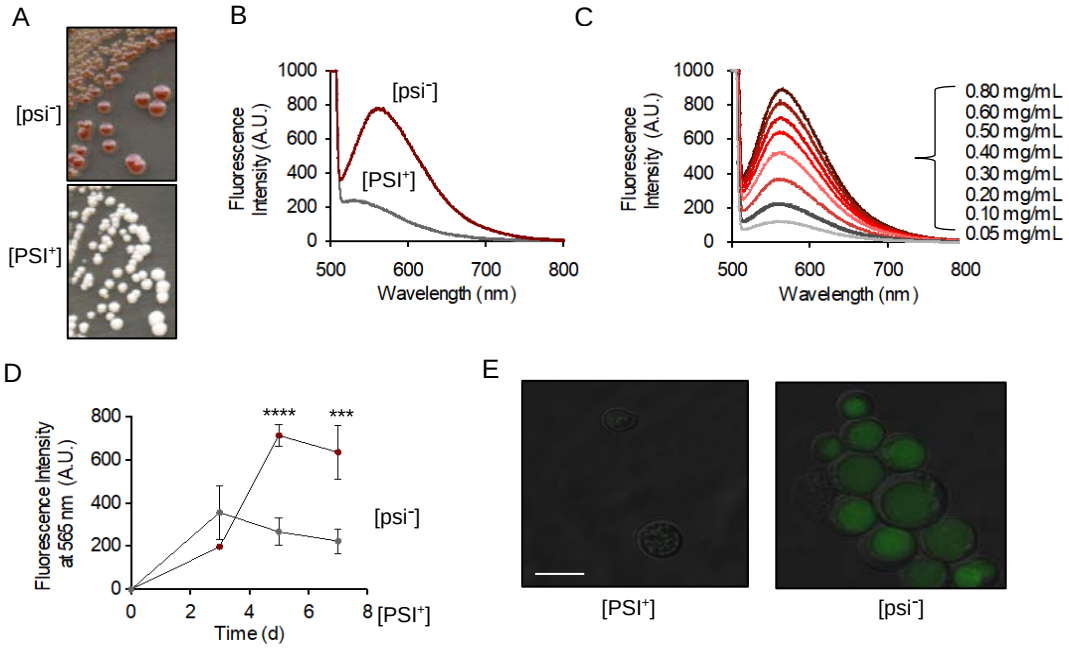
A
[psi-]
[PSI+]
B
Fluorescence Intensity (A.U.)
1000
800
600
400
200
0
500
600
700
800
Wavelength (nm)
[psi-]
[PSI+]
C
Fluorescence Intensity (A.U.)
Wavelength (nm)
0.80 mg/mL
0.60 mg/mL
0.50 mg/mL
0.40 mg/mL
0.30 mg/mL
0.20 mg/mL
0.10 mg/mL
0.05 mg/mL
D
Fluorescence Intensity at 565 nm (A.U.)
****
***
[psi-]
[PSI+]
Time (d)
E
[PSI+]
[psi-]

Figure 2. Red pigment accumulation and endogenous fluorescence in yeast [PSI$^+$] and [psi$^-$] strains.

A.) Streaks of [PSI$^+$] yeast strains containing Hsp104, empty vector (pYES2), and Hsp104 E285Q. The Walker B mutation in the NBD1 domain of Hsp104 (E285Q) is weakly [PSI$^+$], as evidenced by the pink colony phenotype on SD-URA solid media. B.) Overexpression of Hsp104 in [PSI$^+$] yeast results in red pigment accumulation, which has intrinsic fluorescence at 488 nm comparable to [psi$^-$] yeast. Red pigmentation develops over time in yeast strains containing overexpressed Hsp104 in the vector pYS104. The maximal differences in fluorescence between [PSI$^+$] yeast containing empty vector and [PSI$^+$] yeast cured by Hsp104 occurs on day 5 of growth (p-value = 0.0008) and day 7 of growth (p-value = 0.0035). Unpaired, one-tailed t-tests.

C.) The differences in fluorescence signal between [PSI$^+$] yeast containing empty vector pYES2 and pYS104 vector overexpressing Hsp104 is significant (p = 0.0255) Fluorescence intensity at 565 nm is highly significantly different between [PSI$^+$] yeast and [psi-] yeast containing empty vector (p-value = 0.0084). Yeast containing the Hsp104 Walker B mutant E285Q shows significantly less fluorescence than [PSI$^+$] yeast overexpressing Hsp104 (p-value = 0.0359). Unpaired, one-tailed t-tests.

D.) The intermediate [PSI$^+$] phenotype has a similar emission profile as [PSI$^+$]. Wavelength excitation 488 nm, wavelength emission 520 nm. Scale bar shown indicates 5 μm.

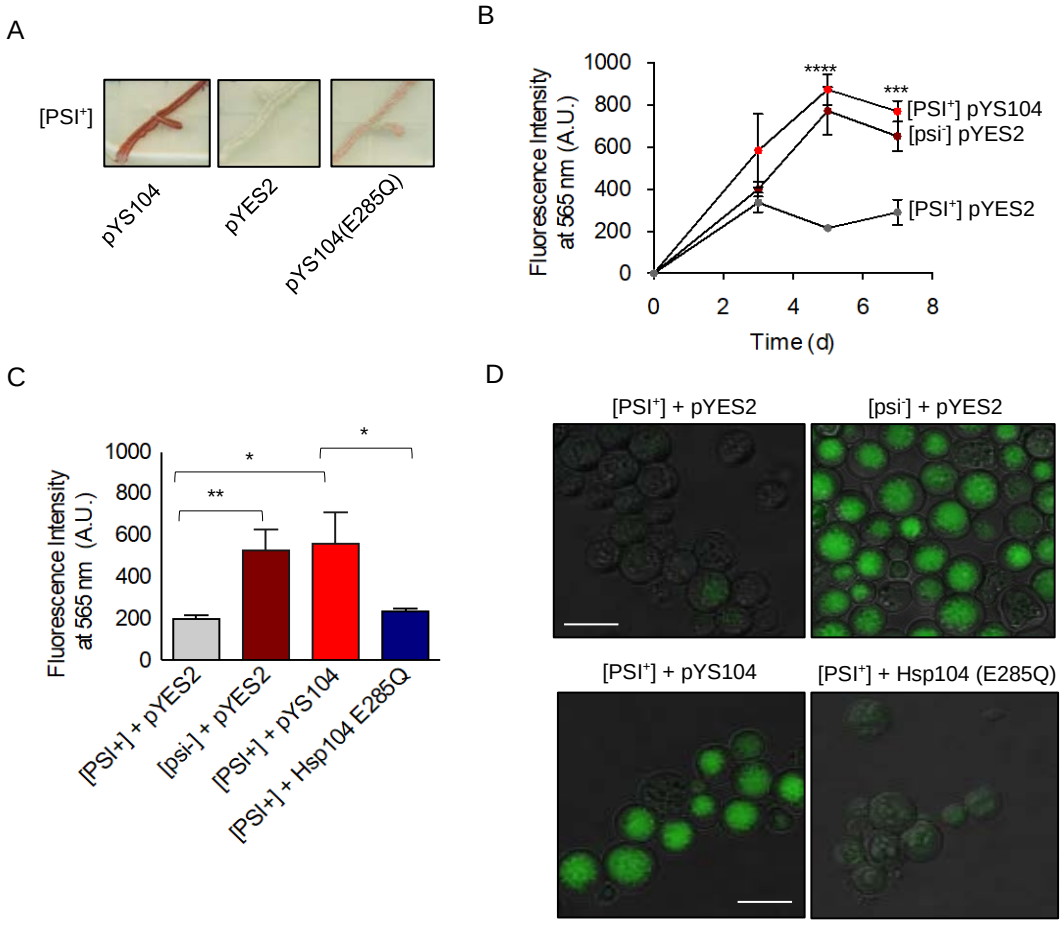
A
[PSI+]
pYS104
pYES2
pYS104(E285Q)
B
Fluorescence Intensity at 565 nm (A.U.)
Time (d)
****
***
[PSI+] pYS104
[psi-] pYES2
[PSI+] pYES2
C
Fluorescence Intensity at 565 nm (A.U.)
**
*
*
[PSI+] + pYES2
[psi-] + pYES2
[PSI+] + pYS104
[PSI+] + Hsp104 E285Q
D
[PSI+] + pYES2
[psi-] + pYES2
[PSI+] + pYS104
[PSI+] + Hsp104 (E285Q)

Figure 3. Selection of mutations in the N-terminal domain of Hsp104.

A.) Random mutagenesis of the N-terminal domain of Hsp104 was carried out using an error-prone DNA polymerase and primers that targeted the N-domain of Hsp104. The products of the random mutagenesis PCR were used as primers in a subsequent PCR to amplify the plasmid pYS104. The PCR products were transformed into chemically competent *E. coli*. Plasmids were isolated from *E. coli* and transformed into electrically competent *S. cerevisiae* for [PSI^{+}] colorimetric screening.

B.) The colorimetric [PSI^{+}] assay screens for [psi^{-}] and [PSI^{+}] phenotypes. Yeast strains that carried mutations in Hsp104 associated with loss of prion curing appear white on SD-URA solid media and were sequenced and further analyzed. Here, a red box marks yeast strains that have loss-of-function Hsp104.

C.) Protein expression levels of Hsp104 in yeast strains. Mutants of interest were further screened for analysis by determining protein expression levels of induced lysates. Western blot Hsp104 protein is made in all [PSI^{+}] *S. cerevisiae* strains containing mutations in Hsp104.

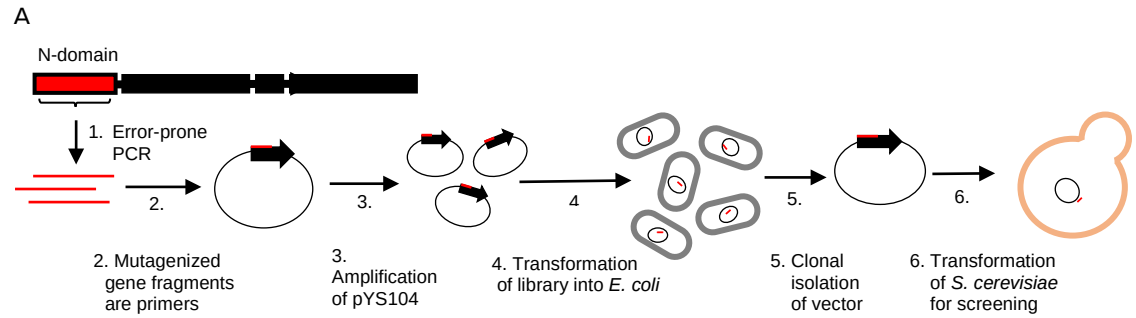
A
N-domain
1. Error-prone PCR
2.
3.
4
5.
6.
2. Mutagenized gene fragments are primers
3. Amplification of pYS104
4. Transformation of library into E. coli
5. Clonal isolation of vector
6. Transformation of S. cerevisiae for screening


B

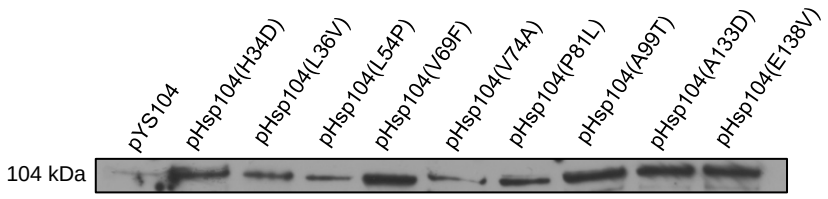
C
pYS104
pHsp104(H34D)
pHsp104(L36V)
pHsp104(L54P)
pHsp104(V69F)
pHsp104(V74A)
pHsp104(P81L)
pHsp104(A99T)
pHsp104(A133D)
pHsp104(E138V)
104 kDa

Figure 4. Functional analyses of *hsp104* mutations of interest.

A.) Yeast strains carrying point mutations in *hsp104* on day 3 of growth at 30 °C.

B.) Model of Hsp104 N-terminal domain in *S. cerevisiae* (PDB 6AMN; Lee, J. et al., 2017) containing mutations H34D (cyan), L36V (yellow), L54P (light blue), V69F (green), V74A (orange), P81L (violet), A99T (magenta), A133D (light pink), and E138V (wheat).

C.) Yeast strains carrying mutations in *hsp104* show maximal differences in fluorescence intensity at 565 nm when excited at 488 nm. One-way ANOVA of the fluorescence intensities was used to determine that the means of the fluorescence intensity of each strain at 565 nm is significantly different ($p < 0.0001$).

D.) Confocal fluorescence microscopy of yeast cells grown on day 5 of growth. [PSI^+] yeast carrying empty vector pYES2 (white colonies on SD-URA solid media) has decreased endogenous fluorescence compared to [PSI^+] yeast overexpressing Hsp104 and [psi^-] yeast containing pYES2. The loss-of-function V69F mutation in Hsp104 is associated with reduced endogenous fluorescence (pale pink colonies on SD-URA solid media). Wavelength excitation 488 nm; wavelength emission 520 nm.

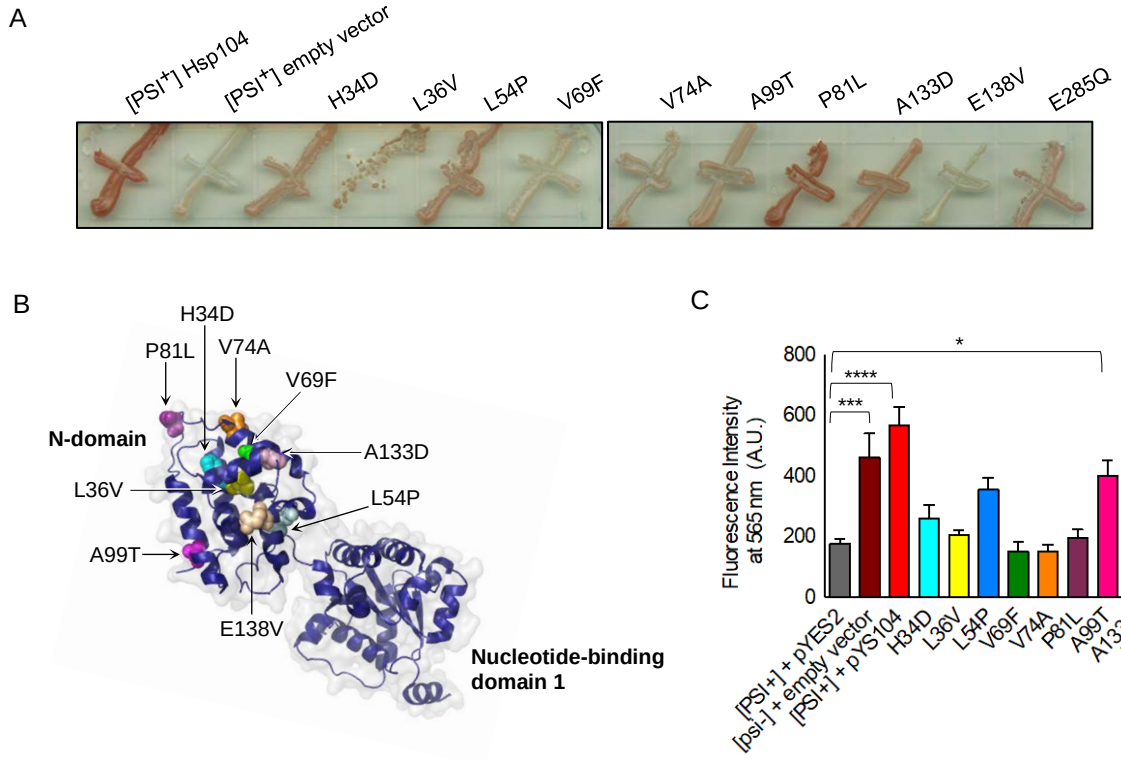
A
[PSI+] Hsp104
[PSI+] empty vector
H34D
L36V
L54P
V69F
V74A
A99T
P81L
A133D
E138V
E285Q
B
H34D
P81L
V74A
V69F
N-domain
A133D
L36V
L54P
A99T
E138V
Nucleotide-binding domain 1
C
Fluorescence Intensity at 565 nm (A.U.)
800
600
400
200
0
*
****
***
[PSI+] + pYES2
[psi-] + empty vector
[PSI+] + pYS104
H34D
L36V
L54P
V69F
V74A
P81L
A99T
A133D
E138V
E285Q
D
[PSI+] + pYES2
[psi-] + pYES2
[PSI+] + pYS104
[PSI+] + Hsp104 V69F

Figure 5. Impaired thermotolerance of [PSI$^+$] yeast containing mutations in the N-domain of Hsp104. Hsp104 NTD mutants were incubated at 37°C for 30 minutes and subsequently transferred to 52°C for A.) 0 minutes of heat shock and B.) 5 minutes and yeast cultures were fivefold serially diluted onto SD-URA + 2% galactose solid media. Plates were grown at 30°C for 5 days.

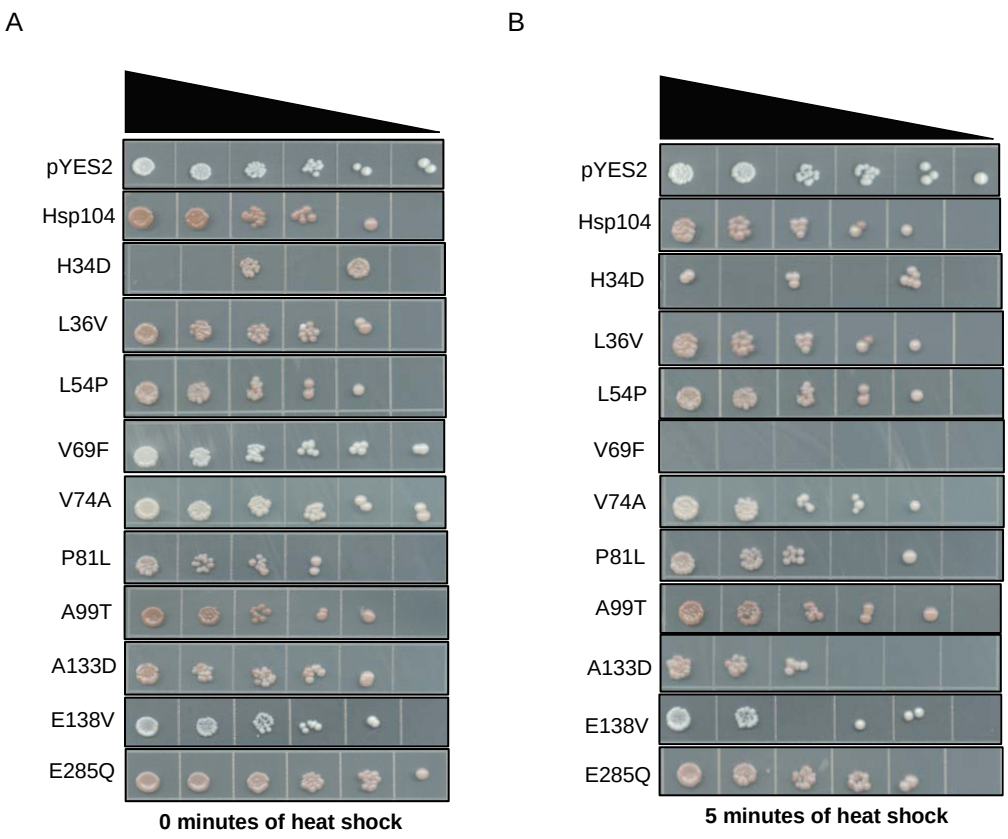
A
B
pYES2
Hsp104
H34D
L36V
L54P
V69F
V74A
P81L
A99T
A133D
E138V
E285Q
0 minutes of heat shock
5 minutes of heat shock

Figure 6. Thermal aggregates accumulate in *S. cerevisiae* containing mutations in the Hsp104 N-domain. Yeast cells carrying mutations in *hsp104* were grown in SD-URA + 2% galactose liquid media until early logarithmic growth. Cultures were incubated at 37°C for 30 minutes before heat shock at 52°C for 15 minutes. Cells recovered at 30°C for 20 minutes after heat shock. Insoluble protein fractions were electrophoresed on a 3-8% Tris-acetate gel and Coomassie stained. Cells with the mutation Hsp104(L54P) had a 1.8-fold increase in thermal aggregate accumulation compared to cells overexpressing wild-type Hsp104. Furthermore, mutations Hsp104(V74A) and Hsp104(P81L) were associated with a 1.8-fold and 1.9-fold increase in thermal aggregate load compared to wild-type Hsp104.

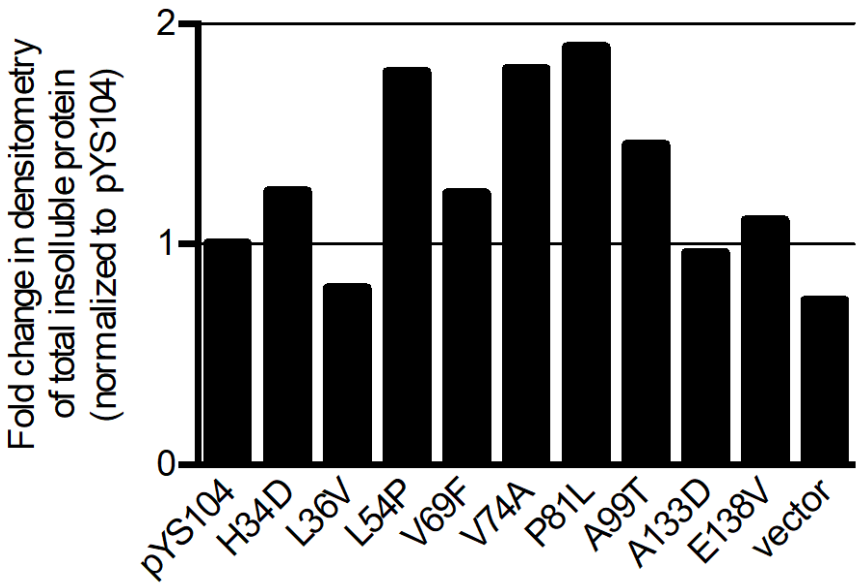
Fold change in densitometry
of total insolluble protein
(normalized to pYS104)
2
1
0
pYS104
H34D
L36V
L54P
V69F
V74A
P81L
A99T
A133D
E138V
vector

Figure 7. The role of the N-domain of Hsp104 in substrate binding of amyloid fibrils.

A.) *E. coli* ClpB N-domain modeled on *T. thermophilus* ClpB crystal structure; PDB 1QVR (Lee S, et al., 2003). The ClpB mutations T7 (yellow), L91 (orange), L14 (pink), D103 (red), and E109 (green) are surface-exposed.

B.) Protein alignment of *S.cerevisiae* Hsp104 N-domain (a.a. 1 – 165) and *E.coli* ClpB N-domain (a.a. 1 – 149). Residues highlighted in yellow are Hsp104 N-domain mutations. Residues highlighted in gray are identical. Red arrows denote highly conservative mutations. EMBOSS Needle (EMBL-EBI) pairwise protein alignment.

C.) Model of Amyloid Binding to Hsp104. (I) Hsp70, bound to nucleotide exchange factor (NEF) and Hsp40, binds to amyloid protein substrate. Hsp104 is a hexameric protein with an axial channel and tyrosine pore loops. (II) Hsp70 binds to the middle domain of Hsp104 and a segment of the amyloid binds to the N-domain of Hsp104. Hsp104 pore loops translocate polypeptides through the axial channel. (III) Amyloid protein is threaded through the axial channel of Hsp104, driven by the movement of the pore loops coupled to rounds of ATP hydrolysis. (III) Amyloid protein is reactivated by Hsp104 into natively folded proteins.

A

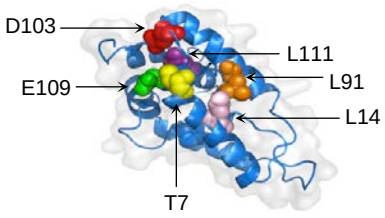

B

```
Hsp104   1 MNDQTQFTERALTILTLAQKLASDHQHPQLQPIHILAAFIETPEDGSV-P     49
ClpB     1 -MRLDRLTNKFQLALADAQSLALGHDNQFIEPLHLMSALL-NQEGGSVSP     48
Hsp104  50 YLQNL-IEKGRYDYDLFKKVNRNLVRIPQQQPAPAEITPSYALGKVLQD     98
ClpB    49 LLTSAGINAGQLRTD-----INQALNRLPQVEGTGGDVQPSQDLVRVLNL     93
Hsp104  99 AAKIQKQQKDSFIAQD-HILFALFNDSSIQQIFKEAQVDIEAIKQQALEL    147
ClpB    94 CDKLAQKRGDNFISSELFVLAALESRGTLADILKAAGATTANITQAIEQM    143
Hsp104 148 RGNTRIDSRGADTNTPLE    165
ClpB   144 RGGESV------------    149
```

C

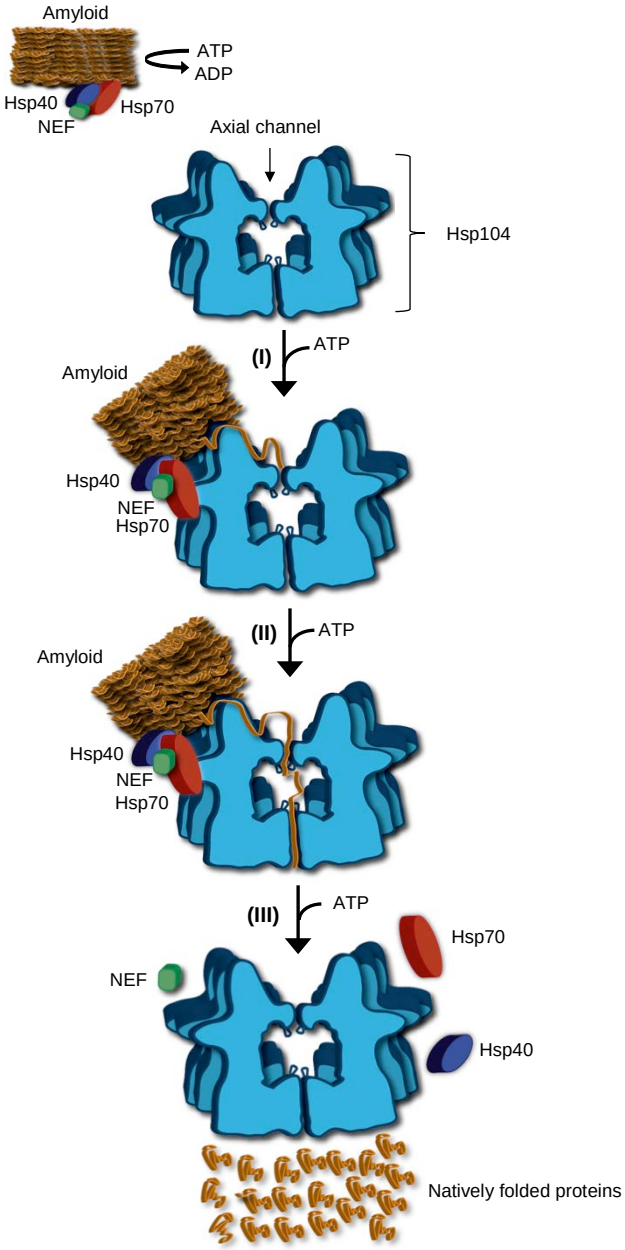

Figure S1. Thermal aggregates in *S. cerevisiae* strains containing mutations in the N-domain of Hsp104. Yeast lysates were loaded on a 3 – 8% Tris-acetate gel and electrophoresed at 150V. The gel was subsequently Coomassie stained. Yeast containing L54P, V74A, and P81L mutations in Hsp104 show increased thermal aggregates in response to heat shock at 52°C.

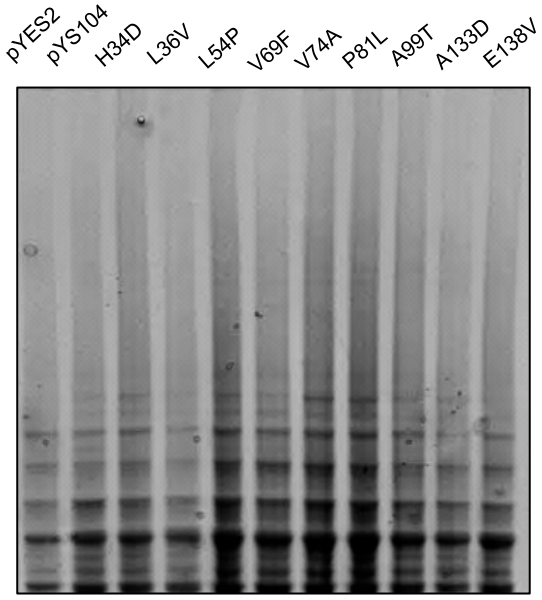
pYES2
pYS104
H34D
L36V
L54P
V69F
V74A
P81L
A99T
A133D
E138V

Manuscript III

Publication Status: Published in *Frontiers in Molecular Biosciences*, 2017

Title: The protein chaperone ClpX targets native and non-native aggregated substrates for remodeling, disassembly and degradation with ClpP

Authors: Shannon May*, Christopher J. LaBreck*, Marissa G. Viola*, Joseph Conti, Jodi L. Camberg#

Author Affiliations:

Department of Cell and Molecular Biology, The University of Rhode Island, Kingston, Rhode Island, United States of America

*These authors contributed equally.

#**Corresponding author**: Jodi L. Camberg, 120 Flagg Road, Kingston, RI, 02881;

Tel: (401) 874-4961; Email: cambergj@uri.edu

Abstract

ClpX is a member of the Clp/Hsp100 family of ATP-dependent chaperones and partners with ClpP, a compartmentalized protease, to degrade protein substrates bearing specific recognition signals. ClpX targets specific proteins for degradation directly or with substrate-specific adaptor proteins. Native substrates of ClpXP include proteins that form large oligomeric assemblies, such as MuA, FtsZ and Dps in *Escherichia coli*. To remodel large oligomeric substrates, ClpX utilizes multivalent targeting strategies and discriminates between assembled and unassembled substrate conformations. Although ClpX and ClpP are known to associate with protein aggregates in *E. coli*, a potential role for ClpXP in disaggregation remains poorly characterized. Here, we discuss strategies utilized by ClpX to recognize native and non-native protein aggregates and the mechanisms by which ClpX alone, and with ClpP, remodels the conformations of various aggregates. We show that ClpX promotes the disassembly and reactivation of aggregated Gfp-ssrA through specific substrate remodeling. In the presence of ClpP, ClpX promotes disassembly and degradation of aggregated substrates bearing specific ClpX recognition signals, including heat-aggregated Gfp-ssrA, as well as polymeric and heat-aggregated FtsZ, which is a native ClpXP substrate in *E. coli*. Finally, we show that ClpX is present in insoluble aggregates and prevents the accumulation of thermal FtsZ aggregates in vivo, suggesting that ClpXP participates in the management of aggregates bearing ClpX recognition signals.

Introduction

Maintaining cellular proteostasis relies on chaperone pathways that promote native protein folding. Typical strategies include targeting misfolded, unfolded, and aggregated polypeptides for reactivation or degradation (Bukau and Horwich, 1998;Wickner et al., 1999;Stoecklin and Bukau, 2013). Misfolded proteins are generated during polypeptide elongation and as a complication of environmental stress (Powers and Balch, 2013). The challenges imposed on chaperone systems by proteotoxic stress are especially relevant in pathogenic organisms like *E. coli*, which experience extreme fluctuations in environmental conditions leading to accumulation of protein aggregates and subsequent proteotoxicity (Mogk et al., 2011). Protein quality control systems reactivate, degrade and remove damaged and aggregated proteins. Under thermal stress in *E. coli*, the heat shock response provides a cellular defense mechanism and upregulates heat shock protein and chaperone levels to restore proteostasis (Mogk et al., 2011).

In addition to preventing protein aggregation, chaperone proteins mediate aggregate clearance through proteolysis of non-native proteins and aggregation reversal (Hartl et al., 2011;Mogk et al., 2011). Clearance of misfolded proteins in *E. coli* is carried out by AAA+ (ATPases Associated with diverse cellular Activities) proteins, which initiate substrate recognition, unfolding, and translocation into a proteolytic chamber (ClpP, HslV) (Snider and Houry, 2008;Sauer and Baker, 2011). Several AAA+ proteins, such as Lon and FtsH, contain both AAA+ chaperone and proteolytic domains within a single protomer (Sauer and Baker, 2011). The chaperone-protease Lon recognizes exposed aromatic and hydrophobic residues, which may contribute to less stringent substrate selectivity and favor degradation of unfolded or misfolded proteins (Gur and Sauer, 2008).

The Clp ATPases of the AAA+ superfamily can be separated into two functional categories: degradation or disaggregation machines. Degradation machines, including ClpX, ClpA, and HslU form complexes with peptidases ClpP or HslV to remove misfolded proteins or specific substrates (Zolkiewski, 2006). Disaggregation machines, including Hsp104 and its bacterial homolog ClpB, disaggregate and reactivate aggregated proteins by an ATP-dependent mechanism and can function in cooperation with the Hsp70/DnaK system independent of protein degradation (Zolkiewski, 1999;Dougan et al., 2002;Doyle et al., 2007;Sweeny and Shorter, 2016). Through a collaborative mechanism, Hsp70, with Hsp40, binds first to a polypeptide segment of an aggregated protein and then the substrate is remodeled by Hsp104/ClpB (Zietkiewicz et al., 2004;Zietkiewicz et al., 2006;Acebron et al., 2009).

E. coli substrates that are degraded by ClpXP include a variety of cellular proteins, metabolic enzymes and several proteins capable of forming large conformational assemblies, including FtsZ, Dps and MinD (Flynn et al., 2003;Stephani et al., 2003;Neher et al., 2006;Camberg et al., 2009;Camberg et al., 2014;Conti et al., 2015). ClpXP can associate with cellular aggregates in *E. coli* and can promote removal of cellular inclusions, but direct protein disaggregation in vitro is not well characterized for ClpX (Vera et al., 2005;Winkler et al., 2010). An early study suggested that ClpX, in the absence of ClpP, could protect the lambda O phage protein from aggregation and resolubilize lambda O aggregates (Wawrzynow et al., 1995). In *Bacillus subtilis*, ClpX also localizes to protein aggregates, suggesting that it may be involved in protein disaggregation 76 ler et al., 2000;Kain et al., 2008;Kirstein et al., 2008)Simmons et al., 2008). ClpX and ClpX substrates are present in polar protein aggregates in *E. coli* under stress in vivo, suggesting that

ClpX associates with aggregated proteins and participates in their removal (Kain et al., 2008;Maisonneuve et al., 2008;Simmons et al., 2008).

ClpXP comprises an asymmetric, hexameric ring of ClpX docked to two stacked heptameric rings of the ClpP serine protease (Wang et al., 1997;Glynn et al., 2009). Although ClpX has been shown to independently remodel substrates, such as MuA, in the presence of ClpP, hydrophobic 'IGF' loops on the bottom surface of the ClpX hexamer contact hydrophobic pockets on the ClpP tetradecamer, allowing unfolded substrates to access the ClpP proteolytic chamber (Kim et al., 2001;Abdelhakim et al., 2010;Baker and Sauer, 2012). Nucleotide binding by ClpX protomers, in the cleft between the large and small AAA+ subdomains, regulate the position of the subdomains relative to each other; these conformational changes enable ClpX to couple substrate translocation to ATP hydrolysis (Glynn et al., 2009;Baker and Sauer, 2012). Substrates are then translocated into the ClpP chamber for degradation (Baker and Sauer, 2012).

Substrates bind to the ClpX N-domain and to residues in the ClpX central channel (pore-loops) (Bolon et al., 2004;Park et al., 2007;Martin et al., 2008;Baker and Sauer, 2012). The N-domain of ClpX is separated from the AAA+ domain by a flexible linker and can dimerize independently. The N-domain is important for direct recognition of some substrates, including FtsZ and MuA, as well as adaptor proteins, but is not required for direct recognition of the ssrA-tag (Abdelhakim et al., 2008;Martin et al., 2008;Camberg et al., 2009;Baker and Sauer, 2012). Adaptor proteins, such as RssB or SspB, promote the interaction and engagement of specific substrates, such as RpoS or ssrA-tagged substrates, respectively (Sauer and Baker, 2011). The ssrA tag is an 11-residue degron appended to a nascent polypeptide

when the ribosome stalls during protein synthesis, targeting the misfolded protein for subsequent degradation (Gottesman et al., 1998;Levchenko et al., 2000).

ClpXP is implicated in the degradation of diverse cellular substrates and more than 100 substrates have been reported (Flynn et al., 2003;Neher et al., 2006). Native substrates of ClpX contain recognition motifs at the N- or C-termini (Flynn et al., 2003). Notably, the essential cell division protein FtsZ in *E. coli* has two distinct ClpX motifs: one in the flexible linker region and one near the C-terminus (Camberg et al., 2014). FtsZ is a tubulin homolog that assembles into linear polymers in vitro and forms the septal ring critical for division in vivo, called the Z-ring (Erickson et al., 2010). ClpXP degrades approximately 15% of FtsZ proteins during the cell cycle in *E. coli* and is capable of degrading both monomers and polymers in vitro (Camberg et al., 2009). ClpXP degrades polymers more efficiently, which is consistent with a common strategy of multivalent recognition of substrates by AAA+ ATPases (Davis et al., 2009;Camberg et al., 2014;Ling et al., 2015). In addition to FtsZ, several other ClpXP substrates form large oligomeric structures, including the tetrameric phage protein MuA, the dodecameric bacterial protein Dps, and the bacterial cell division ATPase MinD (Stephani et al., 2003;Neher et al., 2006;Abdelhakim et al., 2010;Conti et al., 2015). Like FtsZ, alternate monomeric and oligomeric conformations of MuA are also differentially recognized by ClpX (Abdelhakim et al., 2008;Abdelhakim et al., 2010;Ling et al., 2015).

78

In this study, we use engineered and native substrates to investigate the role of ClpX and ClpXP in the disassembly and degradation of protein aggregates that bear specific ClpX recognition signals. We observed that ClpX, with and without ClpP, destabilizes Gfp-ssrA aggregates in vitro. The native ClpXP substrate FtsZ forms several discrete conformations, including linear ordered polymers and also heat-

induced aggregates. Our results show that ClpXP disassembles both heat-induced and linear polymers containing FtsZ. Finally, we also demonstrate that thermal stress promotes aggregation of FtsZ, which is exacerbated in cells deleted for *clpX* or *clpP*. Together, these results show bona fide chaperone activity for ClpX in vitro and suggest that ClpX, with or without ClpP, may play a broader role in rescue and disassembly of protein aggregates.

Materials and Methods

Bacterial strains and plasmids

E. coli strains and plasmids used in this study are described in Table 1. An expression plasmid encoding FtsZ(ΔC67) was constructed by introducing a TAA stop codon (at residue 317 of FtsZ) into pET-FtsZ by site-directed mutagenesis (Camberg et al., 2009).

Expression and purification of proteins

Gfp-ssrA was purified as previously described (Yakhnin et al., 1998). ClpX, ClpP, FtsZ, and FtsZ(ΔC67) were each overexpressed in *E. coli* BL21 (λDE3) and purified as described (Maurizi et al., 1994;Grimaud et al., 1998;Camberg et al., 2009;Camberg et al., 2014). ClpX(E185Q) was purified as described for wild type ClpX, except the expression strain, *E. coli* MG1655 Δ*clpX* carrying plasmid pClpX(E185Q), was induced with 1% arabinose (Table 1) (Camberg et al., 2011). Gfp(uv) containing an N-terminal histidine tag was overexpressed in *E. coli* BL21 (λDE3) and grown to an OD_{600} of 1.0 and induced for 3 hours at 30 ºC. Cells were

lysed by French press in purification lysis buffer (20 mM HEPES, pH 7.5, 5 mM $MgCl_2$, 50 mM KCl, and 10% glycerol). Soluble extracts were bound to TALON metal affinity resin (GE Healthcare), eluted with an imidazole gradient, and imidazole was removed by buffer exchange. Protein concentrations are reported as FtsZ monomers, ClpX hexamers, ClpP tetradecamers, and Gfp or Gfp-tagged monomers. For polymerization assays, FtsZ was labeled with Alexa Fluor 488 and active protein (FL-FtsZ) was collected after cycles of polymerization and depolymerization as described (Gonzalez et al., 2003;Camberg et al., 2014).

Dynamic light scattering

Dynamic light scattering (DLS) measurements were made using a Zetasizer Nano ZS (Malvern Instruments). To determine size distribution, FtsZ (5 μM), aggFtsZ (5 μM), Gfp-ssrA (1.5 μM) and aggGfp-ssrA (1.5 μM) in reaction buffer (50 mM HEPES, pH 7.5, 100 mM KCl and 10 mM $MgCl_2$) were added to polystyrene cuvettes and scanned at 23 °C with a detector angle of 173° and a 4 mW, 633 nm He–Ne laser. The reported intensity-weighted hydrodynamic diameters are based on 15 scans.

Heat denaturation, aggregation, disassembly and reactivation of aggregated substrates

To heat-inactivate Gfp substrates, Gfp-ssrA (1.5 μM) or Gfp(uv) (1.5 μM) was added, where indicated, to buffer containing HEPES (50 mM, pH 7.5), KCl (100 mM), $MgCl_2$ (10 mM), glycerol (10%) and dithiothreitol (DTT) (2 mM) in a volume of 800 μl and incubated at 85 °C for 15 minutes. Immediately following heat-treatment, the denatured substrate was placed on ice for 2 minutes and added to a reaction (50 μl) containing ClpX, (0.3 μM), ClpX (E185Q) (0.3 μM), ClpP (0.3 μM), ATP (4 mM),

ATPγS (1 mM), or ADP (2 mM), where indicated. Samples containing ATP were supplemented with an ATP-regenerating system containing phosphocreatine (5 mg ml^{-1}) and creatine kinase (CK) (60 µg ml^{-1}). Fluorescence recovery was monitored by measuring fluorescence in a Cary Eclipse fluorometer with excitation and emission wavelengths set at 395 nm and 510 nm, respectively. Readings were corrected for background signal by subtracting the fluorescence of buffer. Rates were calculated by fitting to a one-phase association model in GraphPad Prism (version 6.0b). Disaggregation was monitored by 90º-angle light scatter with excitation and emission wavelengths set to 550 nm. Readings were corrected for background signal by subtracting the scatter of the buffer and then plotted as percent of the initial turbidity. Heat-induced aggregation of Gfp-ssrA with time was monitored by 90º-angle light scatter with the temperature of the cuvette holder set to 80 ºC using a circulating water bath.

To inactivate native FtsZ substrates, FtsZ and FtsZ(ΔC67) (5 µM) were heated for 15 minutes in reaction buffer (20 mM HEPES, pH 7.5, 100 mM KCl, 10 mM $MgCl_2$) in a volume of 120 µl at 65 ºC, then cooled on ice for 40 seconds, and held at 23 °C until addition to reactions (60 µl volume) containing ClpX (0.5 µM or 1 µM), ClpX(E185Q) (0.5 µM), ClpP (1 µM), ATP (4 mM) and an ATP-regenerating system (phosphocreatine at 5 mg ml^{-1} and creatine kinase at 60 µg ml^{-1}), where indicated. Disaggregation was monitored by 90º-angle light scatter with excitation and emission wavelengths set to 450 nm. Readings were corrected for background signal by subtracting the scatter of the buffer and then plotted as percent of the initial turbidity. Heat-induced aggregation of FtsZ with time was monitored by 90º-angle light scatter with the temperature of the cuvette holder set to 65 ºC using a circulating water bath.

Polymerization and GTP hydrolysis assays

FL-FtsZ was incubated with the GTP analog GMPCPP (0.5 mM) in the presence of increasing concentrations of ClpX and ClpP (0, 0.25, 0.5 or 1 μM) as indicated and in the presence of phosphocreatine at 5 mg ml^{-1} and creatine kinase at 60 μg ml^{-1}. Samples were incubated for 3 minutes in buffer containing MES (50 mM, pH 6.5), KCl (100 mM) and $MgCl_2$ (10 mM) at 23 ºC, then centrifuged at 129,000 x *g* in a Beckman TLA 120.1 rotor for 30 minutes. Pellets were resuspended in 0.2 M NaCl with 0.01% Triton X-100 (100 μl) and the fluorescence associated with FL-FtsZ for supernatants and pellets was measured using a Cary Eclipse spectrophotometer. GTP hydrolysis rates for FtsZ and FtsZ(ΔC67) were measured before and after aggregation using the Biomol Green (Enzo Life Sciences) detection reagent as described (Camberg et al., 2014).

Heat shock of wild type and deletion strains

E. coli wild type and deletion strains were grown overnight, diluted 1:100 in fresh Lennox broth the next day and grown at 30 °C to an OD of 0.4. All strains were incubated in a water bath at 50 °C for 1 hour, followed by recovery at 30 °C for 35 minutes. Cells were harvested by centrifugation and lysed with Bacterial Protein Extraction Reagent (B-PER) (ThermoFisher Scientific) (2 ml) and lysozyme (25 μg ml^{-1}). Insoluble fractions were collected by centrifugation at 15,000 x *g* for 5 minutes at 4 °C, resuspended in lithium dodecyl sulfate sample buffer and analyzed by reducing SDS-PAGE. Total proteins were transferred to a nitrocellulose membrane and visualized by Ponceau (Fisher Scientific) staining and membranes were immunoblotted using antibodies to ClpX and FtsZ (Camberg et al., 2009;2011). Band

intensities were analyzed by densitometry (NIH ImageJ), normalized to the intensity of the average of the 'no heat' sample, and evaluated for significance by the Mann-Whitney test. Where indicated, to test a mild heat shock condition, cells were incubated in a water bath at 42 °C for 30 minutes, followed by recovery at 30 °C for 35 minutes, and analyzed as described.

Results

ClpXP degrades aggregates in vitro

To determine if ClpX can remodel protein substrates from the aggregated state, we used the fusion protein, Gfp-ssrA, which forms aggregates upon heat treatment (Zietkiewicz et al., 2004;Zietkiewicz et al., 2006). Gfp-ssrA is rapidly degraded by ClpXP and has been extensively studied to understand substrate targeting by ClpXP. The Gfp moiety is widely used in protein disaggregation assays because it forms non-fluorescent aggregates when heated, but is disaggregated and reactivated by several chaperone systems (Zietkiewicz et al., 2004;Zietkiewicz et al., 2006). Therefore, we heated Gfp-ssrA at 85 °C for 15 minutes to induce aggregation (aggGfp-ssrA), resulting in an 86% loss of fluorescence emitted (Figure 1A). Next, to measure the distribution of aggregates by size after heating, we performed dynamic light scattering (DLS) of untreated and heat-denatured Gfp-ssrA. We observed that without heating, the particle sizes are uniform with an average hydrodynamic diameter of 8-10 nm (Figure 1B). After heating, aggregates are approximately 500-600 nm, and there is a narrow distribution of particle sizes and no small particles (i.e., less than 100 nm) (Figure 1C). Upon heat-treatment, aggregation of Gfp-ssrA (1.5 μM) occurs rapidly and plateaus by 10 minutes by 90°-angle light scattering (Figure

1D). The heat inactivation is irreversible since incubation of aggregated Gfp-ssrA (aggGfp-ssrA) alone does not lead to appreciable fluorescence reactivation, which is consistent with previous reports using Gfp (Figure S1) (Zietkiewicz et al., 2004). To determine if ClpXP can bind to aggregates and degrade them, we incubated aggGfp-ssrA with ClpXP and monitored turbidity by 90°-angle light scattering. Incubation of aggGfp-ssrA with ClpXP led to a 35% loss of turbidity in 2 hours (Figure 1E). However, when ClpXP was omitted from the reaction, there was very little change in turbidity over time (5% loss in 2 hours) (Figure 1E). This suggests that ClpXP targets aggregated substrates for degradation. To determine if degradation is required to reduce turbidity, we omitted ClpP and observed that ClpX is capable of reducing sample turbidity by 15% in 2 hours (Figure 1E). Finally, when ATP was omitted from the reaction containing ClpXP, we observed a less than 10% reduction in the turbidity of the reaction (Figure 1E). To confirm that ClpXP degrades aggGfp-ssrA, we incubated aggGfp-ssrA with combinations of ClpX, ClpP and ATP, and sampled degradation reactions after 2 hours. We observed that in the presence of ClpXP, aggGfp-ssrA is degraded, but not when ClpP or ATP was omitted (Figure 1F). Together, these results demonstrate that ClpXP targets aggregates for ATP-dependent degradation and that ClpX is also capable of promoting disassembly in the absence of ClpP.

FtsZ is a well-characterized ClpXP substrate that is essential for cell division and forms linear polymers in vitro in the presence of GTP (Erickson et al., 2010). We previously showed that ClpXP binds to GTP-stimulated FtsZ polymers and promotes FtsZ degradation (Camberg et al., 2009). ClpXP also recognizes and degrades non-polymerized FtsZ, but less efficiently than polymerized FtsZ (Camberg et al., 2009). In vitro, FtsZ rapidly aggregates when heated at 65 °C and this aggregation is

associated with an increase in overall light scatter and a 97% loss of GTPase activity (Figure 2A and 2B). FtsZ, which purifies as a mixture of monomers (40.4 kDa) and dimers (80.8 kDa), has an average hydrodynamic diameter of 10-15 nm by DLS (Figure 2C). Heat treatment of FtsZ (5 μM) at 65 °C produces several particle sizes, including small (30-40 nm) and large aggregates (>300 nm) (Figure 2D). To determine if ClpXP reduces the turbidity associated with aggregated FtsZ (aggFtsZ), we incubated aggFtsZ with ClpXP and ATP and observed a 40% loss of turbidity after incubation with ClpXP for 2 hours (Figure 2E). However, in the absence of ClpXP, the light scatter signal remained stable for aggFtsZ (Figure 2E). Incubation of ClpX with aggFtsZ also resulted in a 25% loss in light scatter, suggesting that ClpX also promotes disassembly of aggregates similar to what we observed for aggGfp-ssrA (Figure 2E and 1E).

Next, to confirm that aggFtsZ is degraded by ClpXP, we assembled reactions containing combinations of aggFtsZ, ClpX, ClpP and ATP and sampled these reactions at 0 and 120 minutes for analysis by SDS-PAGE. We observed that in the presence of ClpXP and ATP, 50% of the total aggFtsZ in the reaction is lost to degradation after 120 minutes (Figure 2F). Omission of either ClpP or ATP from the reaction prevents loss of aggFtsZ (Figure 2F). These results indicate that ClpXP degrades aggFtsZ. Furthermore, the amount of aggFtsZ after incubation with ClpX is unchanged despite the decrease in light scatter detected, suggesting that ClpX can disaggregate aggFtsZ (Figure 2E and 2F).

In addition to forming aggregates upon heating, FtsZ also assembles into a linear head-to-tail polymer, which is a native, ordered aggregate, and distinct from the disordered aggregates which are induced by heating (aggFtsZ). We compared the loss of aggFtsZ by ClpXP to a similar reaction monitoring loss of native polymerized

FtsZ, which is a known substrate of ClpXP. Like aggFtsZ, we also observed a ~50% loss of polymeric FtsZ, stabilized by the GTP analog GMPCPP, after 120 minutes in reactions containing ClpXP and ATP (Figure 2F). GMPCPP promotes the assembly of stable polymers that are far less dynamic than polymers assembled with GTP (Lu et al., 2000). To test if ClpXP disassembles GMPCPP-stabilized FtsZ polymers, we incubated pre-assembled polymers with ClpXP and ATP. Then, we collected polymers by high-speed centrifugation. In these assays, we used active fluorescent FtsZ, labeled with Alexa fluor 488 (FL-FtsZ), to quantify the amount of polymerized FtsZ in the pellet fraction and soluble FtsZ in the supernatant. We observed that after incubation of GMPCPP-stabilized FtsZ polymers with increasing concentrations of ClpXP (0 μM to 1 μM), few FtsZ polymers were recovered in the pellet fractions containing ClpXP (26% of the total FtsZ was recovered in the reaction containing 1 μM ClpXP), indicating that ClpXP is highly effective at promoting the disassembly of GMPCPP-stabilized FtsZ polymers (Figure 2G).

ClpX reactivates heat-aggregated Gfp-ssrA

Incubation of ClpX with aggGfp-ssrA resulted in loss of turbidity, suggesting that ClpX may function independently of ClpP to reactivate substrates (Figure 1E). Reactivation of misfolded proteins may occur through binding and stabilization of intermediates enabling proteins to adopt the native folded conformation, or through ATP-dependent chaperone-assisted unfolding. To determine if ClpX, which recognizes the ssrA amino acid sequence, is able to reactivate aggGfp-ssrA, we monitored fluorescence of aggGfp-ssrA in the presence and absence of ClpX and ATP. AggGfp-ssrA regains very little fluorescence alone, approximately 20 units, which is 8% of the initial fluorescence lost upon heating; however, in the presence of

ClpX, fluorescence recovers rapidly in the first 10 minutes of the reaction and then plateaus, regaining approximately 85 units, which is 27% of the initial fluorescence lost upon heating (Figure 3A).

ClpX catalyzes ATP-dependent unfolding of substrates (Kim et al., 2000;Singh et al., 2000). To determine if ATP is essential for reactivation, we incubated aggGfp-ssrA with ClpX under various nucleotide conditions including with ATP, the ATP analog ATPγS, ADP and omission of nucleotide. We observed an 82% slower rate of fluorescence reactivation when ClpX and aggGfp-ssrA were incubated with ATPγS than with ATP (0.02 AU min^{-1} and 0.11 AU min^{-1}, respectively), and no recovery over background with ADP or without nucleotide (Figure 3B). Reactivation by ClpX and ATP is prevented in the presence of ClpP, and the residual fluorescence after heat treatment is lost upon degradation (Figure S2). Together, these results indicate that ClpX requires ATP to reactivate Gfp-ssrA and, surprisingly, that ATPγS is also capable of promoting reactivation, although at a much slower rate than ATP (Figure 3B).

Reactivation and disaggregation by ClpX requires a specific recognition sequence

Next, we determined if a ClpX recognition motif is important for efficient recognition of aggregated substrates by ClpX. We compared reactivation of aggGfp-ssrA with heat-aggregated Gfp (aggGfp) without an ssrA tag. We observed that after incubation with ClpX and ATP for 60 minutes, approximately 30 units of fluorescence were recovered, which is 8% of the initial pre-heat fluorescence, indicating that aggGfp is a poor substrate for reactivation by ClpX (Figure 4A). In contrast, aggGfp-

ssrA recovered 33% (>100 units) of the initial pre-heat fluorescence after incubation with ClpX (Figure 4A).

Two regions of FtsZ are important for promoting degradation of *E. coli* FtsZ by ClpXP, one in the unstructured linker region (amino acids 352-358) and one near the C-terminus (residues 379 through 383) (Camberg et al., 2014). Using a truncated FtsZ mutant protein, FtsZ(ΔC67), which is deleted for 67 C-terminal amino acid residues, including both regions involved in ClpX recognition, we tested if ClpXP reduces the light scatter in reactions containing heat-aggregated FtsZ(ΔC67) [aggFtsZ(ΔC67)]. We heated FtsZ(ΔC67) at 65 °C for 15 minutes, the condition that promotes aggregation of full length FtsZ, and confirmed that heat treatment resulted in an 84% loss of GTP hydrolysis activity and an increase in light scatter, which is stable over time (Figure 4B and 4C). In the presence of ClpXP, we observed no decrease in light scatter for aggFtsZ(ΔC67) after incubation for 120 minutes (Figure 4C), which is expected since FtsZ(ΔC67) is a poor substrate for ClpXP degradation (Figure S3). Together, these results demonstrate that for ClpX to recognize aggregates and promote disaggregation, disassembly and/or reactivation, a ClpX recognition motif is required.

Impaired reactivation by ClpX(E185Q)

ATP is required for reactivation of aggGfp-ssrA, however, it is unknown if this event requires ATP-hydrolysis and substrate unfolding. Therefore, we used the ClpX mutant protein ClpX(E185Q), which has a mutation in the Walker B motif and is defective for ATP-hydrolysis, but interacts with substrates (Hersch et al., 2005;Camberg et al., 2014). We observed that ClpX(E185Q) is defective for

disaggregation of aggGfp-ssrA by monitoring turbidity by 90°-angle light scatter of reactions containing aggGfp-ssrA, ClpX(E185Q) and ATP (Figure 5A). We also tested if aggFtsZ is disassembled by ClpX(E185Q), and observed no reduction in light scatter in reactions containing aggFtsZ, ClpX(E185Q) and ATP after 120 minutes compared to ClpX (Figure 5B). Finally, we tested if reactivation of aggGfp-ssrA requires ATP hydrolysis using ClpX(E185Q) instead of ClpX. We observed that ClpX(E185Q) promotes a small amount of reactivation of aggGfp-ssrA and restores fluorescence, but to a much lesser extent than the level observed for wild type ClpX (Figure 5C). These results suggest that ATP hydrolysis by ClpX is required to promote efficient reactivation of aggGfp-ssrA and disassembly of large complexes containing aggFtsZ or aggGfp-ssrA (Figure 5A, 5B and 5C).

ClpXP prevents accumulation of FtsZ aggregates in vivo under extreme thermal stress

ClpX and ClpP were previously reported to localize to protein aggregates in *E. coli*, suggesting that ClpXP may target aggregates in vivo for direct degradation (Winkler et al., 2010). We used the native ClpXP substrate FtsZ, which aggregates upon heat treatment, to determine if ClpX and/or ClpXP modulates FtsZ aggregate accumulation after thermal stress by comparing the levels of FtsZ present in insoluble cell fractions (Figure 2A and 6A). Wild type cells and cells deleted for *clpX*, *clpP*, *clpB*, *clpA*, *dnaK, lon*, *hslU* and *hslV* were exposed to heat shock and insoluble protein fractions were collected and analyzed by immunoblot. We observed that FtsZ was present in the insoluble fraction of wild type cells (BW25113), and this amount was 42% higher in cells exposed to heat shock at 50 °C (Figure 6A and S4A). However, FtsZ levels were even higher in the insoluble fractions of Δ*clpX* and Δ*clpP* strains

compared to the parental strain (2.4-fold and 2.3-fold, respectively), although the amount of total protein was similar to the wild type strain exposed to heat shock (Figure S4B). We detected less protein overall in the Δ*dnaK* strain after recovery, but this strain also had poor viability after heat shock and recovery (Figure S4C). In addition, we also detected ClpX in the insoluble fraction in all strains except the *clpX* deletion strain (Figure S4A). Next, we conducted a mild heat shock, 42 °C for 30 minutes, followed by recovery, and observed that deletion of *clpB* had a larger effect on the accumulation of insoluble FtsZ than deletion of *clpX* (Figure S4D). To determine the relative contributions of either *clpB* or *clpX* during a 40 minute recovery period after incubation at 50 °C, we analyzed insoluble FtsZ levels at 20 minute time intervals during recovery (Fig. 6B). Notably, we observed that in cells deleted for *clpX*, insoluble FtsZ was present immediately after heat treatment and continued to accumulate throughout the recovery period to a greater extent than in wild type or *clpB* deletion cells. These results suggest that ClpXP prevents accumulation of FtsZ aggregates in cells exposed to extreme thermal stress. Since we observed that insoluble FtsZ levels were elevated in Δ*clpB* strains exposed to mild heat shock (Figure S4D), we repeated the recovery time course in *clpX* and *clpB* deletion strains after mild heat shock, 42 °C for 30 minutes, to monitor insoluble FtsZ levels (Figure S4E). We observed that insoluble FtsZ accumulates during the recovery period in *clpB* deletion strains after mild heat shock (Figure S4E).

Finally, if ClpXP is active in cells after severe heat shock, then it should not be a thermolabile protein. To determine if ClpXP remains active after exposure to 50 °C in vitro, we incubated ClpXP in buffer at 50 °C for one hour, and then measured activity after addition of Gfp-ssrA by monitoring the loss of Gfp-ssrA fluorescence. We observed that ClpXP remained active for unfolding and degradation of Gfp-ssrA after

incubation at 50 °C for one hour (Figure S4F). As a control, ClpXP was also incubated in buffer at 30 °C for one hour and then assayed for activity. We observed that ClpXP incubated at 30 °C was more active than ClpXP incubated at 50 °C, suggesting that a partial loss of activity had occurred at high temperature (Figure S4F). However, this assay was performed in the complete absence of other cellular chaperones or substrates and suggests that some ClpXP likely continues to retain activity after exposure to heat stress, while some may become inactivated.

Discussion

Here, using both a native and an engineered aggregated substrate, we demonstrate that ClpXP has the operational capacity to disassemble and degrade large aggregates that have ClpX degrons. In this study, FtsZ, a native substrate of ClpXP in *E. coli*, was aggregated in vitro by thermal stress, and we further show that FtsZ also aggregates in vivo when cells are exposed to high temperature (Figure 2A and 6A). The observation that FtsZ is aggregation prone is in agreement with a prior study reporting the presence of FtsZ in intracellular aggregates of Δ*rpoH* cells incubated at 42 °C by mass spectrometry (Tomoyasu et al., 2001). FtsZ aggregates are cleared in vitro and in vivo by ClpXP, and ClpXP does not require the assistance of additional chaperones (Figure 2E, 2F and 6A). Moreover, in the absence of ClpP, ClpX also promotes disassembly of FtsZ and Gfp-ssrA aggregates indicating that disassembly can also occur by a proteolysis-independent mechanism, although disaggregation is more efficient in the presence of ClpP. ClpXP-mediated disassembly of Gfp-ssrA aggregates requires ATP in experiments monitoring turbidity

(Figure 1E). In addition, the Walker B mutation in ClpX, E185Q, which impairs ATP hydrolysis, also impairs disaggregation of aggGfp-ssrA and, to a lesser extent, aggFtsZ. Aggregate disassembly and resolubilization by ClpX was previously described using the substrate lambda O protein, and here we show disassembly of aggregates and kinetic monitoring using two additional substrates, as well as reactivation of Gfp-ssrA fluorescence (Wawrzynow et al., 1995). Reactivation of Gfp-ssrA is largely dependent on ATP hydrolysis (Figure 3B), since ClpX(E185Q) only weakly promotes reactivation of aggregated Gfp-ssrA (Figure 5C), yet ClpX(E185Q) is capable of stable interactions with substrates in the presence of ATP, although they are not unfolded (Hersch et al., 2005;Camberg et al., 2014). It is unlikely that there are soluble, unfolded Gfp-ssrA monomers in solution after heating, since we did not detect them by DLS and it has been demonstrated that soluble, unfolded Gfp rapidly refolds, in 20 to 30 seconds, by a spontaneous reaction that does not require chaperones (Figure 1C) (Makino et al., 1997;Tsien, 1998;Zietkiewicz et al., 2004). Therefore, it is likely that large aggregates contain loosely associated unfolded proteins, which can be removed and reactivated by ClpX and, in the case of Gfp-ssrA, allowed to spontaneously refold. As expected, recognition by ClpX is highly specific, as Gfp without an ssrA-tag is not reactivated (Figure 4A).

We also detected partial disaggregation of aggFtsZ by ClpX, but not by ClpX(E185Q) (Figure 5B). Aggregation of FtsZ is induced at 65 °C, but the aggregates formed by FtsZ are smaller than those formed by Gfp-ssrA (30 nm and 600 nm, respectively) (Figure 1C and 2D). FtsZ aggregates likely contain 8-10 monomers, based on the average size of a folded FtsZ monomer, which is approximately 40 Å in diameter (Figure 2D) (Oliva et al., 2004). In contrast, Gfp aggregates in this study likely contain more than 120 subunits, based on an average

size of a folded Gfp monomer, which is approximately 50 Å across the long axis (van Thor et al., 2005). The small size of the FtsZ aggregate may allow it to be more susceptible to disassembly by ClpX than a larger aggregate.

In the model for disassembly of aggregates by ClpXP, ClpX binds to exposed recognition tags on the surface of the aggregate and promotes removal, unfolding and degradation of protomers from within the aggregate (Figure 7A). Removal of protomers eventually leads to destabilization and fragmentation of the aggregate as well as degradation (Figure 1F and 2F). Although this process does not require ClpP, it occurs more robustly when ClpP is present than when ClpP is omitted (Figure 1E and 2E). For aggregated substrate reactivation, ClpX likely engages unfolded protomers from the aggregate, which may be internal or loosely bound to the exterior of the aggregate, unfolds and release them. For small aggregates, this activity may be sufficient to lead to fragmentation and capable of promoting reactivation of substrates such as Gfp-ssrA (Figure 7B).

Finally, we observed large increases in insoluble FtsZ when cells were exposed to two different temperatures, 50 °C, which represents extreme heat shock, and 42 °C, which represents a mild heat sho[93]igure 6A, 6B and S4D). At 42 °C, deletion of *clpB* was associated with a large accumulation of insoluble FtsZ, suggesting that under mild heat stress, ClpB is the major factor that ensures FtsZ solubility (Figure S4D and S4E). However, we observed a remarkably different result after heat shock at 50 °C and throughout the recovery period. Specifically, in a *clpX* deletion strain, large amounts of insoluble FtsZ accumulate during the recovery period to a greater extent than in a *clpB* deletion strain (Figure 6A and 6B). It is unknown if ClpXP and ClpB are processing FtsZ aggregates directly in vivo, because we did not observe a reduction of aggregated FtsZ during the recovery period for any strain. FtsZ

is typically present at very high levels (5,000 to 20,000 copies per cell) and is essential for cell division in *E. coli* (Bramhill, 1997). Interestingly, FtsZ also forms linear polymers as part of its normal biological function to promote cell division, and polymers are efficiently recognized, disassembled and degraded by ClpXP (Figure 2F and 2G) (Camberg et al., 2009;Camberg et al., 2014;Viola et al., 2017). Given the diverse conformational plasticity of FtsZ, its use as a model disaggregation and remodeling substrate will be informative for studies of targeting and processing of multisubunit substrates by AAA+ proteins. As with FtsZ, many other ClpXP substrates are detectable in protein aggregates in cells (Flynn et al., 2003;Maisonneuve et al., 2008). Moreover, a previous study showed that ClpXP is important for cell viability under thermal stress conditions in cells depleted of DnaK (Tomoyasu et al., 2001). Given that it is estimated that 2-3% of *E. coli* proteins are ClpXP substrates, ClpXP likely serves as an additional mechanism to manage accumulation of aggregation-prone proteins in vivo, particularly under extreme stress conditions (Flynn et al., 2003;Maisonneuve et al., 2008).

Funding

This work was funded by an Institutional Development Award (IDeA) from the National Institute of General Medical Sciences of the National Institutes of Health (#P20GM103430 to J. Camberg). The funders had no role in study design, data collection and interpretation, or the decision to submit the work for publication.

Acknowledgements

We thank Sue Wickner, Joel Hoskins, Shannon Doyle, Eric DiBiasio, David Vierra and Katherine Kellenberger for helpful discussions, Paul Johnson and Janet Atoyan for sequencing assistance. Sequencing was performed at the Rhode Island Genomics and Sequencing Center, which is supported in part by the National Science Foundation under EPSCoR Grants Nos. 0554548 & EPS-1004057.

References

Abdelhakim, A.H., Oakes, E.C., Sauer, R.T., and Baker, T.A. (2008). Unique contacts direct high-priority recognition of the tetrameric Mu transposase-DNA complex by the AAA+ unfoldase ClpX. *Mol. Cell.* 30**,** 39-50.

Abdelhakim, A.H., Sauer, R.T., and Baker, T.A. (2010). The AAA+ ClpX machine unfolds a keystone subunit to remodel the Mu transpososome. *Proc. Natl. Acad. Sci. USA* 107**,** 2437-2442.

Acebron, S.P., Martin, I., Del Castillo, U., Moro, F., and Muga, A. (2009). DnaK-mediated association of ClpB to protein aggregates. A bichaperone network at the aggregate surface. *FEBS Lett.* 583**,** 2991-2996.

Baba, T., Ara, T., Hasegawa, M., Takai, Y., Okumura, Y., Baba, M., Datsenko, K.A., Tomita, M., Wanner, B.L., and Mori, H. (2006). Construction of *Escherichia coli* K-12 in-frame, single-gene knockout mutants: the Keio collection. *Mol. Syst. Biol.* 2**,** 2006 0008.

Baker, T.A., and Sauer, R.T. (2012). ClpXP, an ATP-powered unfolding and protein-degradation machine. *Biochim. Biophys. Acta.* 1823**,** 15-28.

Bolon, D.N., Wah, D.A., Hersch, G.L., Baker, T.A., and Sauer, R.T. (2004). Bivalent tethering of SspB to ClpXP is required for efficient substrate delivery: a protein-design study. *Mol. Cell.* 13**,** 443-449.

Bramhill, D. (1997). Bacterial cell division. *Annu. Rev. Cell Dev. Biol.* 13**,** 395-424.

Bukau, B., and Horwich, A.L. (1998). The Hsp70 and Hsp60 chaperone machines. *Cell.* 92**,** 351-366.

Camberg, J.L., Hoskins, J.R., and Wickner, S. (2009). ClpXP protease degrades the cytoskeletal protein, FtsZ, and modulates FtsZ polymer dynamics. *Proc. Natl. Acad. Sci. USA.* 106**,** 10614-10619.

Camberg, J.L., Hoskins, J.R., and Wickner, S. (2011). The interplay of ClpXP with the cell division machinery in *Escherichia coli*. *J. Bacteriol.* 193**,** 1911-1918.

Camberg, J.L., Viola, M.G., Rea, L., Hoskins, J.R., and Wickner, S. (2014). Location of dual sites in *E. coli* FtsZ important for degradation by ClpXP; one at the C-terminus and one in the disordered linker. *PLoS One.* 9**,** e94964.

Conti, J., Viola, M.G., and Camberg, J.L. (2015). The bacterial cell division regulators MinD and MinC form polymers in the presence of nucleotide. *FEBS Lett.* 589**,** 201-206.

Datsenko, K.A., and Wanner, B.L. (2000). One-step inactivation of chromosomal genes in *Escherichia coli* K-12 using PCR products. *Proc. Natl. Acad. Sci. USA.* 97**,** 6640-6645.

Davis, J.H., Baker, T.A., and Sauer, R.T. (2009). Engineering synthetic adaptors and substrates for controlled ClpXP degradation. *J. Biol. Chem.* 284**,** 21848-21855.

Dougan, D.A., Mogk, A., and Bukau, B. (2002). Protein folding and degradation in bacteria: to degrade or not to degrade? That is the question. *Cell. Mol. Life Sci.* 59**,** 1607-1616.

Doyle, S.M., Hoskins, J.R., and Wickner, S. (2007). Inaugural Article: Collaboration between the ClpB AAA+ remodeling protein and the DnaK chaperone system. *Proc. Natl. Acad. Sci. USA.* 104**,** 11138-11144.

Erickson, H.P., Anderson, D.E., and Osawa, M. (2010). FtsZ in bacterial cytokinesis: cytoskeleton and force generator all in one. *Microbiol. Mol. Biol. Rev.* 74**,** 504-528.

Flynn, J.M., Neher, S.B., Kim, Y.I., Sauer, R.T., and Baker, T.A. (2003). Proteomic discovery of cellular substrates of the ClpXP protease reveals five classes of ClpX-recognition signals. *Mol. Cell.* 11**,** 671-683.

Glynn, S.E., Martin, A., Nager, A.R., Baker, T.A., and Sauer, R.T. (2009). Structures of asymmetric ClpX hexamers reveal nucleotide-dependent motions in a AAA+ protein-unfolding machine. *Cell.* 139**,** 744-756.

Gonzalez, J.M., Jimenez, M., Velez, M., Mingorance, J., Andreu, J.M., Vicente, M., and Rivas, G. (2003). Essential cell division protein FtsZ assembles into one monomer-thick ribbons under conditions resembling the crowded intracellular environment. *J. Biol. Chem.* 278**,** 37664-37671.

Gottesman, S., Roche, E., Zhou, Y., and Sauer, R.T. (1998). The ClpXP and ClpAP proteases degrade proteins with carboxy-terminal peptide tails added by the SsrA-tagging system. *Genes Dev.* 12**,** 1338-1347.

Grimaud, R., Kessel, M., Beuron, F., Steven, A.C., and Maurizi, M.R. (1998). Enzymatic and structural similarities between the *Escherichia coli* ATP-dependent proteases, ClpXP and ClpAP. *J. Biol. Chem.* 273**,** 12476-12481.

Gur, E., and Sauer, R.T. (2008). Recognition of misfolded proteins by Lon, a AAA(+) protease. *Genes Dev.* 22**,** 2267-2277.

Hartl, F.U., Bracher, A., and Hayer-Hartl, M. (2011). Molecular chaperones in protein folding and proteostasis. *Nature.* 475**,** 324-332.

Hersch, G.L., Burton, R.E., Bolon, D.N., Baker, T.A., and Sauer, R.T. (2005). Asymmetric interactions of ATP with the AAA+ ClpX6 unfoldase: allosteric control of a protein machine. *Cell.* 121**,** 1017-1027.

Kain, J., He, G.G., and Losick, R. (2008). Polar localization and compartmentalization of ClpP proteases during growth and sporulation in *Bacillus subtilis*. *J. Bacteriol.* 190**,** 6749-6757.

Kim, Y.I., Burton, R.E., Burton, B.M., Sauer, R.T., and Baker, T.A. (2000). Dynamics of substrate denaturation and translocation by the ClpXP degradation machine. *Mol. Cell.* 5**,** 639-648.

Kim, Y.I., Levchenko, I., Fraczkowska, K., Woodruff, R.V., Sauer, R.T., and Baker, T.A. (2001). Molecular determinants of complex formation between Clp/Hsp100 ATPases and the ClpP peptidase. *Nat. Struct. Biol.* 8**,** 230-233.

Kirstein, J., Strahl, H., Moliere, N., Hamoen, L.W., and Turgay, K. (2008). Localization of general and regulatory proteolysis in *Bacillus subtilis* cells. *Mol. Microbiol.* 70**,** 682-694.

Kruger, E., Witt, E., Ohlmeier, S., Hanschke, R., and Hecker, M. (2000). The clp proteases of *Bacillus subtilis* are directly involved in degradation of misfolded proteins. *J. Bacteriol.* 182**,** 3259-3265.

Levchenko, I., Seidel, M., Sauer, R.T., and Baker, T.A. (2000). A specificity-enhancing factor for the ClpXP degradation machine. *Science.* 289**,** 2354-2356.

Ling, L., Montano, S.P., Sauer, R.T., Rice, P.A., and Baker, T.A. (2015). Deciphering the Roles of Multicomponent Recognition Signals by the AAA+ Unfoldase ClpX. *J. Mol. Biol.* 427**,** 2966-2982.

Lu, C., Reedy, M., and Erickson, H.P. (2000). Straight and curved conformations of FtsZ are regulated by GTP hydrolysis. *J. Bacteriol.* 182**,** 164-170.

Maisonneuve, E., Fraysse, L., Moinier, D., and Dukan, S. (2008). Existence of abnormal protein aggregates in healthy *Escherichia coli* cells. *J. Bacteriol.* 190**,** 887-893.

Makino, Y., Amada, K., Taguchi, H., and Yoshida, M. (1997). Chaperonin-mediated folding of green fluorescent protein. *J. Biol. Chem.* 272**,** 12468-12474.

Martin, A., Baker, T.A., and Sauer, R.T. (2008). Diverse pore loops of the AAA+ ClpX machine mediate unassisted and adaptor-dependent recognition of ssrA-tagged substrates. *Mol. Cell.* 29**,** 441-450.

Maurizi, M.R., Thompson, M.W., Singh, S.K., and Kim, S.H. (1994). Endopeptidase Clp: ATP-dependent Clp protease from *Escherichia coli*. *Methods Enzymol.* 244**,** 314-331.

Mogk, A., Huber, D., and Bukau, B. (2011). Integrating protein homeostasis strategies in prokaryotes. *Cold Spring Harb. Perspect. Biol.* 3.

Neher, S.B., Villen, J., Oakes, E.C., Bakalarski, C.E., Sauer, R.T., Gygi, S.P., and Baker, T.A. (2006). Proteomic profiling of ClpXP substrates after DNA damage reveals extensive instability within SOS regulon. *Mol. Cell.* 22**,** 193-204.

Oliva, M.A., Cordell, S.C., and Lowe, J. (2004). Structural insights into FtsZ protofilament formation. *Nat. Struct. Mol. Biol.* 11**,** 1243-1250.

Park, E.Y., Lee, B.G., Hong, S.B., Kim, H.W., Jeon, H., and Song, H.K. (2007). Structural basis of SspB-tail recognition by the zinc binding domain of ClpX. *J. Mol. Biol.* 367**,** 514-526.

Powers, E.T., and Balch, W.E. (2013). Diversity in the origins of proteostasis networks--a driver for protein function in evolution. *Nat. Rev. Mol. Cell Biol.* 14**,** 237-248.

Sauer, R.T., and Baker, T.A. (2011). AAA+ proteases: ATP-fueled machines of protein destruction. *Annu. Rev. Biochem.* 80**,** 587-612.

Simmons, L.A., Grossman, A.D., and Walker, G.C. (2008). Clp and Lon proteases occupy distinct subcellular positions in *Bacillus subtilis*. *J. Bacteriol.* 190**,** 6758-6768.

Singh, S.K., Grimaud, R., Hoskins, J.R., Wickner, S., and Maurizi, M.R. (2000). Unfolding and internalization of proteins by the ATP-dependent proteases ClpXP and ClpAP. *Proc. Natl. Acad. Sci. USA.* 97**,** 8898-8903.

Snider, J., and Houry, W.A. (2008). AAA+ proteins: diversity in function, similarity in structure. *Biochem. Soc. Trans.* 36**,** 72-77.

Stephani, K., Weichart, D., and Hengge, R. (2003). Dynamic control of Dps protein levels by ClpXP and ClpAP proteases in Escherichia coli. *Mol. Microbiol.* 49**,** 1605-1614.

Stoecklin, G., and Bukau, B. (2013). Telling right from wrong in life - cellular quality control. *Nat. Rev. Mol. Cell Biol.* 14**,** 613-615.

Sweeny, E.A., and Shorter, J. (2016). Mechanistic and Structural Insights into the Prion-Disaggregase Activity of Hsp104. *J. Mol. Biol.* 428**,** 1870-1885.

Tomoyasu, T., Mogk, A., Langen, H., Goloubinoff, P., and Bukau, B. (2001). Genetic dissection of the roles of chaperones and proteases in protein folding and degradation in the Escherichia coli cytosol. *Mol. Microbiol.* 40**,** 397-413.

Tsien, R.Y. (1998). The green fluorescent protein. *Annu. Rev. Biochem.* 67**,** 509-544.

Van Thor, J.J., Georgiev, G.Y., Towrie, M., and Sage, J.T. (2005). Ultrafast and low barrier motions in the photoreactions of the green fluorescent protein. *J. Biol. Chem.* 280**,** 33652-33659.

Vera, A., Aris, A., Carrio, M., Gonzalez-Montalban, N., and Villaverde, A. (2005). Lon and ClpP proteases participate in the physiological disintegration of bacterial inclusion bodies. *J. Biotechnol.* 119**,** 163-171.

Viola, M.G., Labreck, C.J., Conti, J., and Camberg, J.L. (2017). Proteolysis-Dependent Remodeling of the Tubulin Homolog FtsZ at the Division Septum in *Escherichia coli*. *PLoS One.* 12**,** e0170505.

Wang, J., Hartling, J.A., and Flanagan, J.M. (1997). The structure of ClpP at 2.3 A resolution suggests a model for ATP- dependent proteolysis. *Cell.* 91**,** 447-456.

Wawrzynow, A., Wojtkowiak, D., Marszalek, J., Banecki, B., Jonsen, M., Graves, B., Georgopoulos, C., and Zylicz, M. (1995). The ClpX heat-shock protein of *Escherichia coli*, the ATP-dependent substrate specificity component of the

ClpP-ClpX protease, is a novel molecular chaperone. *EMBO J.*. 14**,** 1867-1877.

Wickner, S., Maurizi, M.R., and Gottesman, S. (1999). Posttranslational quality control: folding, refolding, and degrading proteins. *Science.* 286**,** 1888-1893.

Winkler, J., Seybert, A., Konig, L., Pruggnaller, S., Haselmann, U., Sourjik, V., Weiss, M., Frangakis, A.S., Mogk, A., and Bukau, B. (2010). Quantitative and spatio-temporal features of protein aggregation in *Escherichia coli* and consequences on protein quality control and cellular ageing. *EMBO J* 29**,** 910-923.

Yakhnin, A.V., Vinokurov, L.M., Surin, A.K., and Alakhov, Y.B. (1998). Green fluorescent protein purification by organic extraction. *Protein Expr. Purif.* 14**,** 382-386.

Zietkiewicz, S., Krzewska, J., and Liberek, K. (2004). Successive and synergistic action of the Hsp70 and Hsp100 chaperones in protein disaggregation. *J. Biol. Chem.* 279**,** 44376-44383.

Zietkiewicz, S., Lewandowska, A., Stocki, P., and Liberek, K. (2006). Hsp70 chaperone machine remodels protein aggregates at the initial step of Hsp70-Hsp100-dependent disaggregation. *J. Biol. Chem.* 281**,** 7022-7029.

Zolkiewski, M. (1999). ClpB cooperates with DnaK, DnaJ, and GrpE in suppressing protein aggregation. A novel multi-chaperone system from *Escherichia coli*. *J. Biol. Chem.* 274**,** 28083-28086.

Zolkiewski, M. (2006). A camel passes through the eye of a needle: protein unfolding activity of Clp ATPases. *Mol. Microbiol.* 61**,** 1094-1100.

TABLE 1. *E. coli* strains and plasmids used in this study

Strain or Plasmid	Genotype	Source, reference, or construction
Strains		
BW25113	F$^-$, DE(*araD-araB*)567, lacZ4787(del)(::rrnB-3), *LAM*-, *rph-1*, DE(*rhaD-rhaB*)*568*, *hsdR514*	Datsenko and Wanner, 2000
JW0429	F-, *Δ(araD-araB)567*, *ΔlacZ4787*(::rrnB-3), *Δlon-725::kan*, *λ*$^-$, *rph-1*, *Δ(rhaD-rhaB)568*, *hsdR514*	Baba et al., 2006
JW0428	F-, *Δ(araD-araB)56, ΔlacZ4787*(::rrnB-3), *ΔclpX724::kan*, *λ*$^-$, *rph-1*, *Δ(rhaD-rhaB)568*, *hsdR514*	Baba et al., 2006
JW0427	F-, *Δ(araD-araB)567*, *ΔlacZ4787*(::rrnB-3), *ΔclpP723::kan*, *λ*$^-$, *rph-1*, *Δ(rhaD-rhaB)568*, *hsdR514*	Baba et al., 2006
JW2573	F-, *Δ(araD-araB)567*, *ΔlacZ4787*(::rrnB-3), *ΔclpB757::kan*, *λ*$^-$, *rph-1*, *Δ(rhaD-rhaB)568*, *hsdR514*	Baba et al., 2006
JW0866	F-, *Δ(araD-araB)567*, *ΔlacZ4787*(::rrnB-3), *ΔclpA783::kan*, *λ*$^-$, *rph-1*, *Δ(rhaD-rhaB)568*, *hsdR514*	Baba et al., 2006
JW3902	F-, *Δ(araD-araB)567*, *ΔlacZ4787*(::rrnB-3), *ΔhslU790::kan*, *λ*$^-$, *rph-1*, *Δ(rhaD-rhaB)568*, *hsdR514*	Baba et al., 2006
JW3903	F-, *Δ(araD-araB)567*, *ΔlacZ4787*(::rrnB-3), *ΔhslV720::kan*, *λ*$^-$, *rph-1*, *Δ(rhaD-rhaB)568*, *hsdR514*	Baba et al., 2006
JW0013	F-, *Δ(araD-araB)567*, *ΔlacZ4787*(::rrnB-3), *ΔdnaK734::kan*, *λ*$^-$, *rph-1*, *Δ(rhaD-rhaB)568*, *hsdR514*	Baba et al., 2006
JW0462	F-, *Δ(araD-araB)567*, *ΔlacZ4787*(::rrnB-3),*ΔhtpG757::kan*, *λ*$^-$, *rph-1*, *Δ(rhaD-rhaB)568*, *hsdR514*	Baba et al., 2006
JC0259	MG1655 *ΔclpX::kan*	Camberg et al., 2011

Plasmids		
pET-ClpX	*kan*	Camberg et al. 2009
pET-ClpP	*kan*	Maurizi et al. 1994
pET-FtsZ	*kan*	Camberg et al. 2009
pET-FtsZ(ΔC67)	*kan*	This study
pET-H_6-Gfp(uv)	*kan*	This study
pBad-Gfp-ssrA	*amp*	Singh et al., 2000
pClpX(E185Q)	*amp*	Camberg et al., 2011

Figure 1. Disaggregation and degradation of aggregated Gfp-ssrA by ClpXP.

(A) The fluorescence emission spectra (450-600 nm) of Gfp-ssrA (1.0 μM) (green) and heat-treated Gfp-ssrA (1.0 μM) (black) (85 °C for 15 minutes) were measured using an excitation wavelength of 395 nm. Plotted curves are representative of three

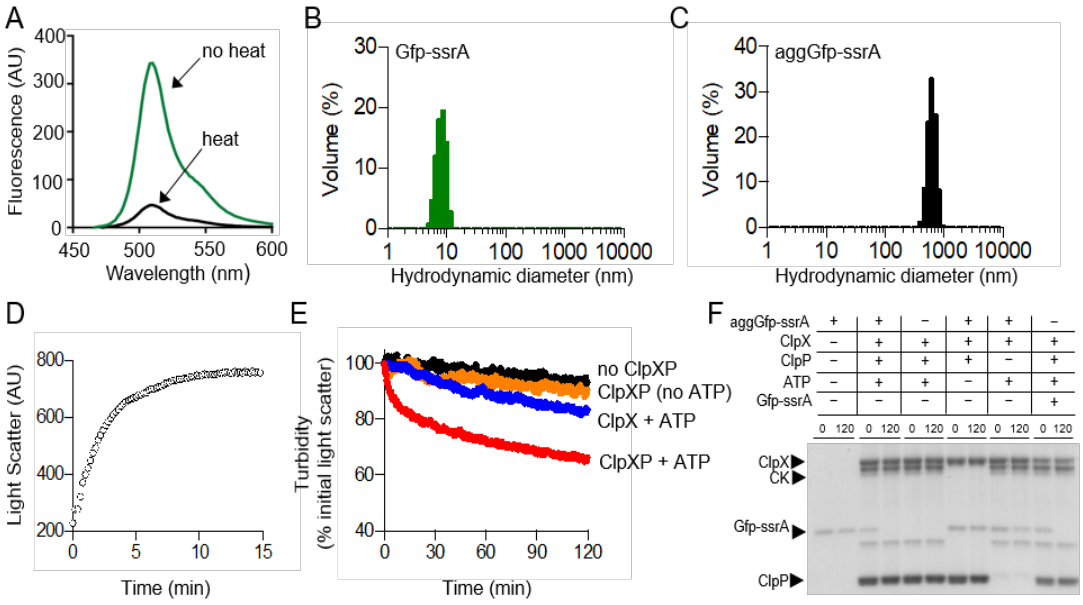
A
Fluorescence (AU)
400
300
200
100
0
450
500
550
600
Wavelength (nm)
no heat
heat
B
Gfp-ssrA
Volume (%)
30
20
10
0
1
10
100
1000
10000
Hydrodynamic diameter (nm)
C
aggGfp-ssrA
Volume (%)
40
30
20
10
0
1
10
100
1000
10000
Hydrodynamic diameter (nm)
D
Light Scatter (AU)
800
600
400
200
0
5
10
15
Time (min)
E
Turbidity
(% initial light scatter)
100
80
60
40
0
30
60
90
120
Time (min)
no ClpXP
ClpXP (no ATP)
ClpX + ATP
ClpXP + ATP
F
aggGfp-ssrA
ClpX
ClpP
ATP
Gfp-ssrA
0 120
ClpX
CK
Gfp-ssrA
ClpP

Figure 2. Aggregation and disaggregation of native ClpXP substrate FtsZ.

(A) Aggregation by 90°–angle light scatter was measured for FtsZ (5 μM) (black circles) in a cuvette attached to a circulating water bath at 65 °C for 30 minutes as described in *Materials and Methods*. The curve shown is representative of at least three replicates. **(B)** Rates of GTP hydrolysis were measured for FtsZ (5 μM) (gray) and aggFtsZ (5 μM) (black) with GTP (1 mM) for 15 minutes at 30 °C, as described in *Materials and Methods*. The average rate was determined from at least four replicates. **(C)** DLS was performed for FtsZ (5 μM) (gray) as described to determine particle size (nm) distribution. **(D)** DLS was performed for aggFtsZ (5 μM) (black) as described to determine particle size (nm) distribution. **(E)** Disaggregation of aggFtsZ (5 μM) was monitored by 90°-angle light scatter as described in *Materials and Methods.* Disaggregation reactions contained aggFtsZ (5 μM) (black circles) or aggFtsZ (5 μM) and ClpX (1 μM) (blue circles), or aggFtsZ (5 μM), ClpX (1 μM), and ClpP (1 μM) (red circles), with ATP (4 mM) and a regenerating system. Light scattering was monitored for 120 minutes. The curves shown are representative of at least three replicates. **(F)** Degradation was monitored for FtsZ and aggFtsZ as described in *Materials and Methods* in reactions containing FtsZ (6 μM), aggFtsZ (6 μM), ClpX (0.5 μM), ClpP (0.5 μM), ATP (4 mM) and a regenerating system, where indicated. For degradation of FtsZ, GMPCPP (0.5 mM) was included to promote the assembly of stable polymers. Degradation reactions were incubated at 23 °C for 120 minutes. To detect protein loss due to degradation, samples from 0 and 120 minutes were analyzed by SDS-PAGE to solubilize any remaining aggregates.

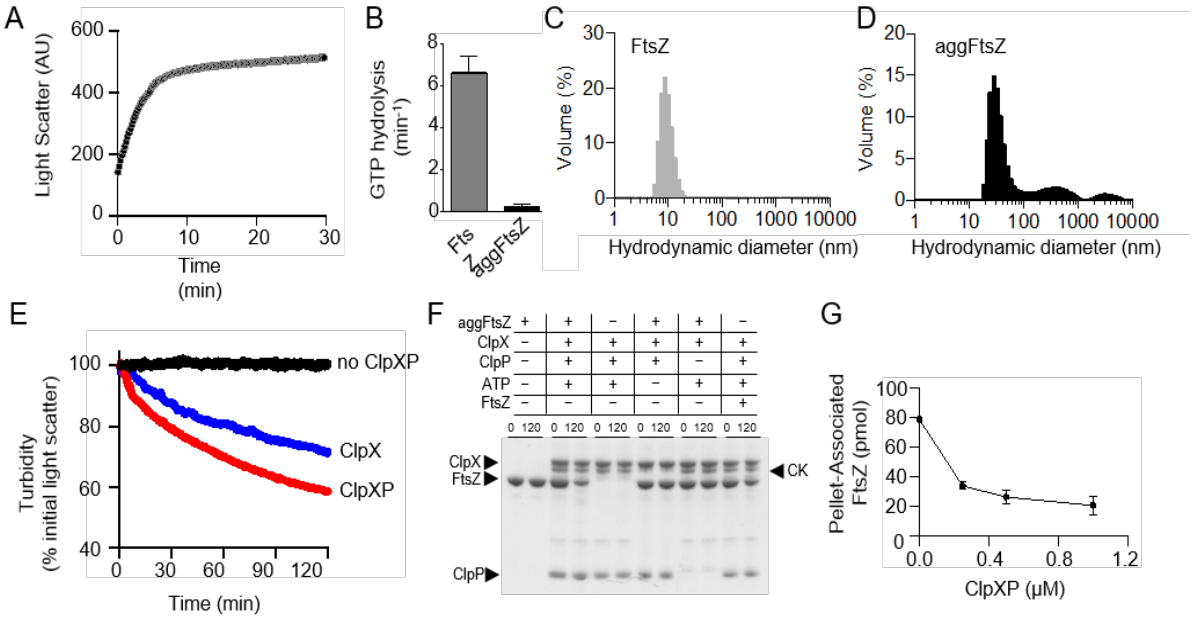
A
Light Scatter (AU)
600
400
200
0
0
10
20
30
Time
(min)
B
GTP hydrolysis
(min-1)
8
6
4
2
0
FtsZ
aggFtsZ
C
FtsZ
Volume (%)
30
20
10
0
1
10
100
1000
10000
Hydrodynamic diameter (nm)
D
aggFtsZ
Volume (%)
20
15
10
5
0
1
10
100
1000
10000
Hydrodynamic diameter (nm)
E
Turbidity
(% initial light scatter)
100
80
60
40
0
30
60
90
120
Time (min)
no ClpXP
ClpX
ClpXP
F
aggFtsZ
ClpX
ClpP
ATP
FtsZ
0 120 0 120 0 120 0 120 0 120
ClpX
FtsZ
CK
ClpP
G
Pellet-Associated
FtsZ (pmol)
100
80
60
40
20
0
0.0
0.4
0.8
1.2
ClpXP (μM)

Figure 3. Reactivation of aggregated Gfp-ssrA in the presence of ClpX.

(A) Reactivation of aggGfp-ssrA (1.0 μM) was monitored as described in *Materials and Methods* in the absence (black circles) and presence (blue circles) of ClpX (0.3 μM), ATP (4 mM), and a regenerating system. Fluorescence emission (AU) was monitored for 30 minutes. The curves shown are representative of at least three replicates.

(B) Reactivation of aggGfp-ssrA (1.0 μM) was monitored in the absence (black circles) or presence of ClpX (0.3 μM), ATP (4 mM) and a regenerating system (blue circles), ATPγS (2 mM) (orange circles), ADP (2 mM) (green circles), or no nucleotide (gray circles), where indicated. Fluorescence emission (AU) was monitored for 60 minutes. The curves shown are representative of at least three replicates.

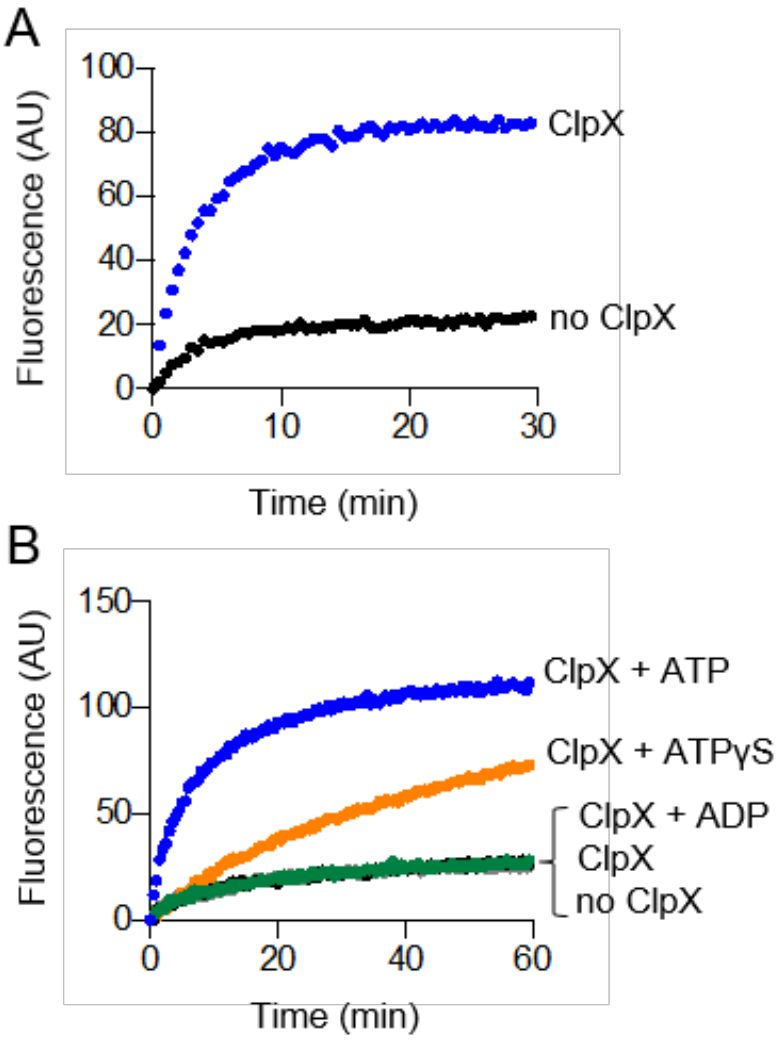

Figure 4. Aggregation and disaggregation of ClpXP substrates with and without recognition motifs.

(A) Reactivation of aggGfp-ssrA (1.0 μM) alone (dark gray circles) or in the

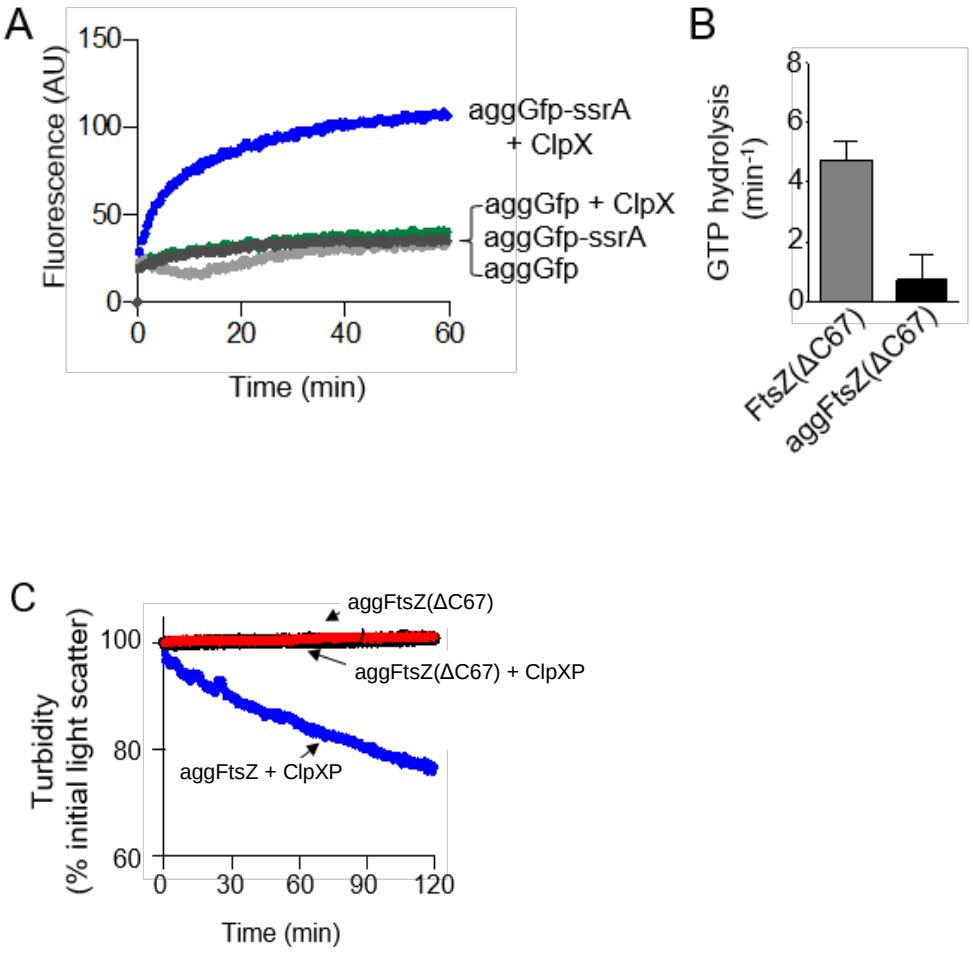
A
Fluorescence (AU)
150
100
50
0
0
20
40
60
Time (min)
aggGfp-ssrA
+ ClpX
aggGfp + ClpX
aggGfp-ssrA
aggGfp
B
GTP hydrolysis
(min-1)
8
6
4
2
0
FtsZ(ΔC67)
aggFtsZ(ΔC67)
C
Turbidity
(% initial light scatter)
100
80
60
0
30
60
90
120
Time (min)
aggFtsZ(ΔC67)
aggFtsZ(ΔC67) + ClpXP
aggFtsZ + ClpXP

Figure 5. **Disaggregation and reactivation of ClpX substrates in the presence of ClpX(E185Q).**

(A) Disaggregation was monitored by 90°-angle light scatter, as described in *Materials and Methods* for aggGfp-ssrA (1.0 μM) alone (black circles) or in the presence of ClpX (0.5 μM) (blue circles) or ClpX (E185Q) (0.5 μM) (open circles), where indicated, with ATP (4 mM), and a regenerating system. Light scattering was monitored for 120 minutes. The curves shown are representative of at least three replicates.

(B) Disaggregation was monitored by 90°-angle light scatter for aggFtsZ (5 μM), ClpX (0.5 μM) or ClpX(E185Q) (0.5 μM) where indicated, ATP (4 mM), and a regenerating system for 120 minutes as described in *Materials and Methods*. The curves shown are representative of at least three replicates.

(C) Reactivation was monitored as described in *Materials and Methods* for aggGfp-ssrA (1.0 μM) alone (black circles) or in the presence of ClpX (0.3 μM) (blue circles) or ClpX (E185Q) (0.3 μM) (open circles), with ATP (4 mM) and a regenerating system, where indicated. Fluorescence emission (AU) was monitored for 90 minutes. The curves shown are representative of at least three replicates.

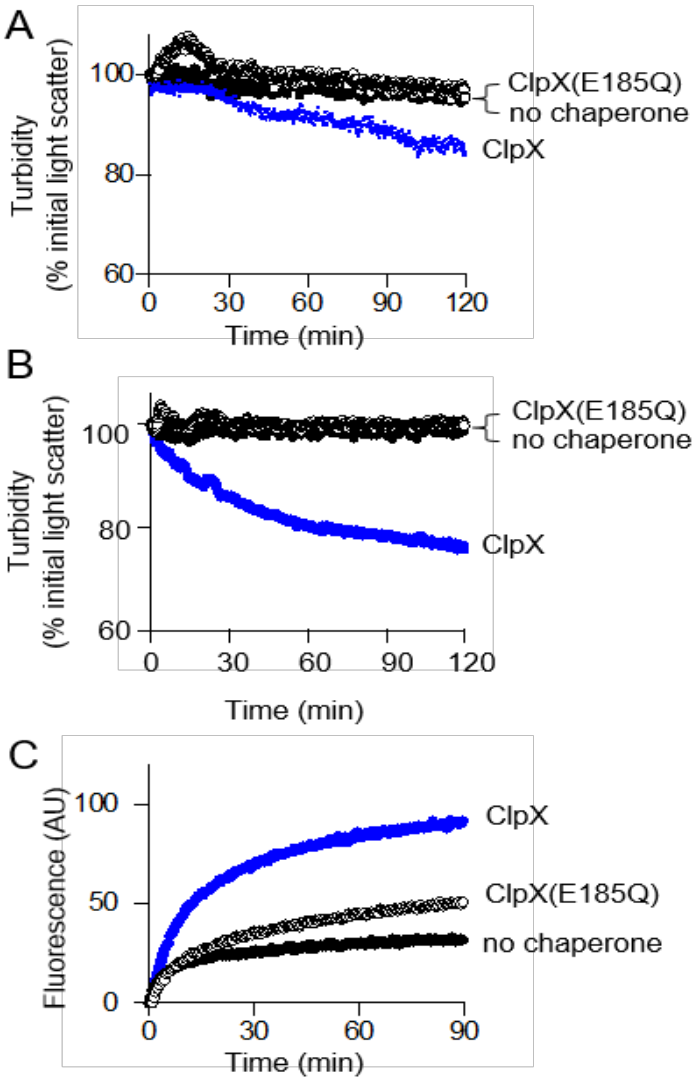
A
Turbidity
(% initial light scatter)
100
80
60
0
30
60
90
120
Time (min)
ClpX(E185Q)
no chaperone
ClpX
B
Turbidity
(% initial light scatter)
100
80
60
0
30
60
90
120
Time (min)
ClpX(E185Q)
no chaperone
ClpX
C
Fluorescence (AU)
100
50
0
0
30
60
90
Time (min)
ClpX
ClpX(E185Q)
no chaperone

Figure 6. FtsZ aggregation in deletion strains after heat shock.

(A) FtsZ levels were compared in insoluble cell extracts prepared from single gene deletion strains (Table 1) after heat shock at 50°C for 1 hour and recovery (30°C) as described in *Materials and Methods*. Cells were collected and insoluble protein extracts were analyzed by immunoblotting using anti-FtsZ antibodies. Relative FtsZ levels were quantified by densitometry from four independent experiments. Where indicated, '*' represents a *p*-value of 0.03.

(B) Insoluble FtsZ levels were monitored during the 30°C recovery period (0, 20 and 40 minutes) after heat shock at 50°C for 60 minutes in wild type, Δ*clpB* and Δ*clpX* deletion strains.

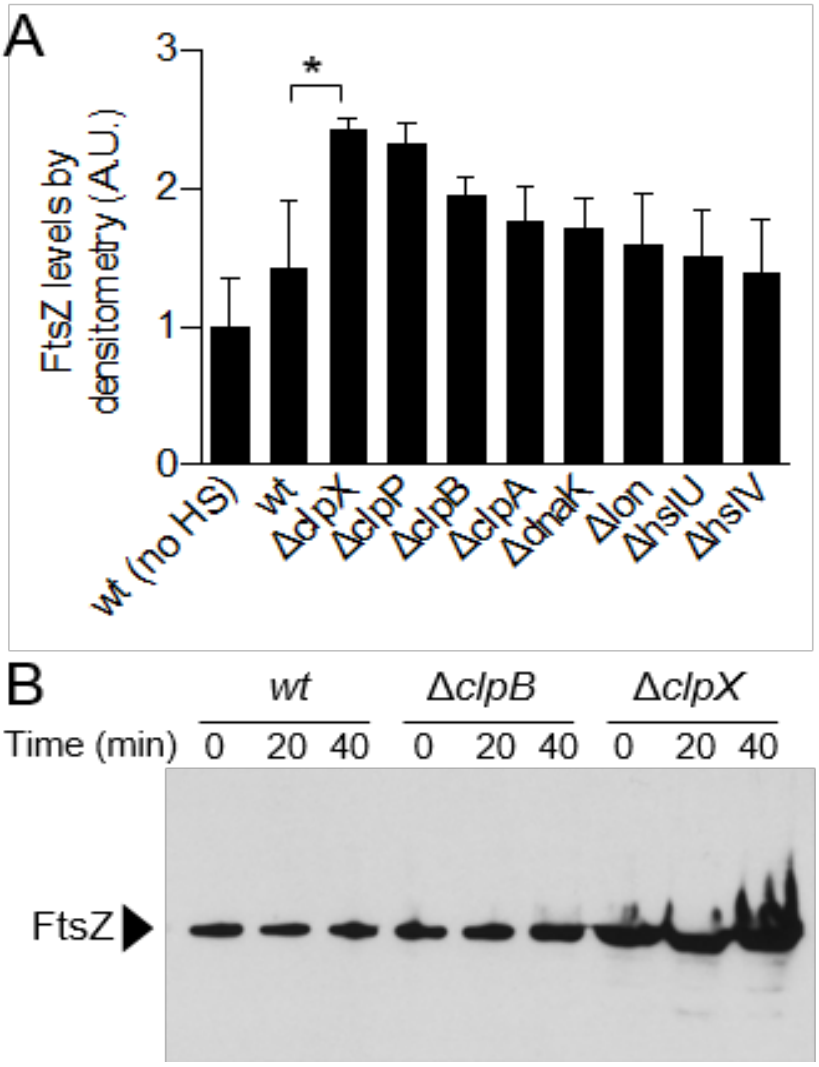
A
FtsZ levels by densitometry (A.U.)
3
2
1
0
*
wt (no HS)
wt
ΔclpX
ΔclpP
ΔclpB
ΔclpA
ΔdnaK
Δlon
ΔhslU
ΔhslV
B
wt
ΔclpB
ΔclpX
Time (min)
0 20 40 0 20 40 0 20 40
FtsZ

Figure 7. Model of aggregate disassembly.

(A) ClpXP binds to aggregated substrates bearing a ClpX-recognition motif. ClpXP unfolds and degrades protomers from within the aggregate, leading to fragmentation and disassembly in an ATP-dependent manner.

(B) ClpX binds to aggregates that contain unfolded proteins bearing a ClpX-recognition motif. Unfolded proteins loosely associated with the aggregate surface are reactivated by ClpX through a direct protein interaction that requires ATP-dependent unfolding.

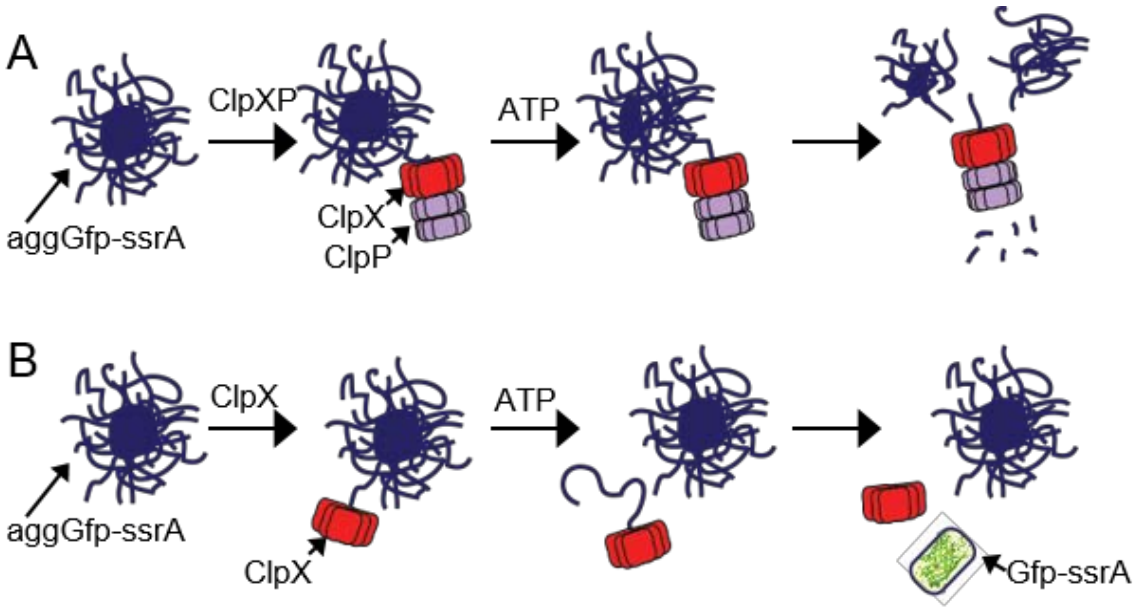
A
ClpXP
ATP
aggGfp-ssrA
ClpX
ClpP
B
ClpX
ATP
aggGfp-ssrA
ClpX
Gfp-ssrA

Supplemental Figure S1. Heat-aggregation of Gfp-ssrA.

The fluorescence emission of aggGfp-ssrA (1.0 μM) (black circles) was monitored as described in Materials and Methods for 90 minutes.

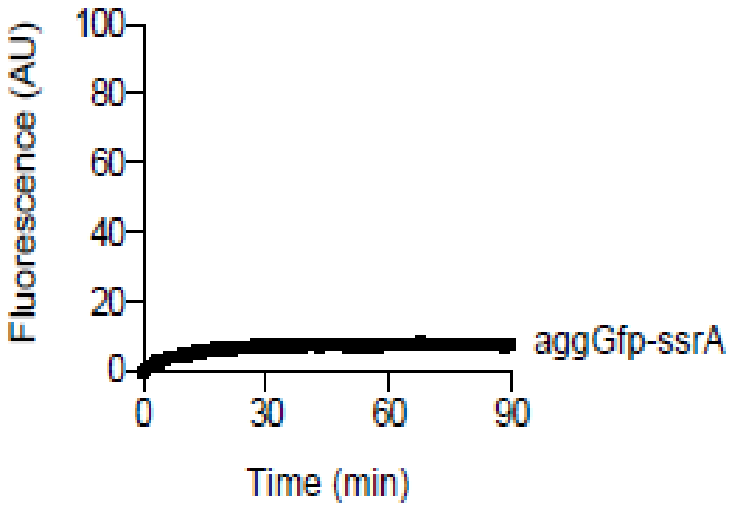
Fluorescence (AU)
100
80
60
40
20
0
0
30
60
90
Time (min)
aggGfp-ssrA

Supplemental Figure S2. Unfolding and degradation of aggregated Gfp-ssrA by ClpXP. Unfolding and degradation were monitored for aggGfp-ssrA **(**1.0 μM) alone (black circles) or in the presence of ClpP (0.3 μM) (gold circles), ClpX (0.3 μM) and ClpP (0. μM) (red circles) with ATP (4 mM), where indicated. Fluorescence emission (AU) was monitored as described in *Materials and Methods.*

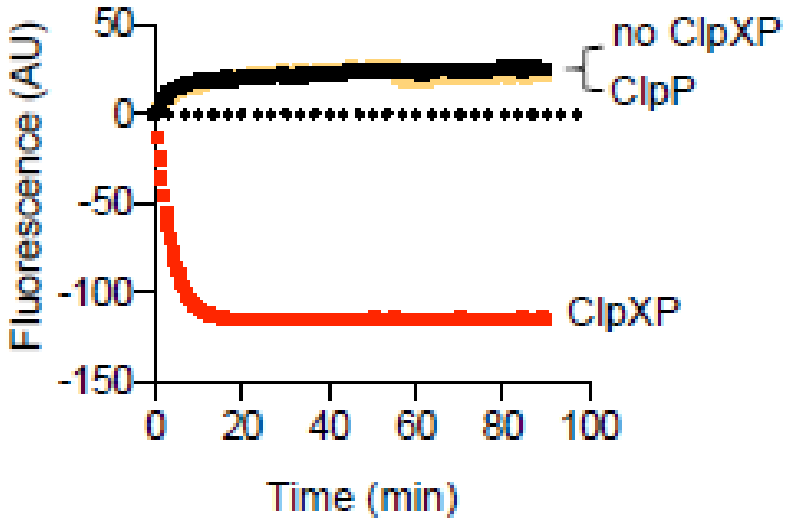
50
0
-50
-100
-150
Fluorescence (AU)
0
20
40
60
80
100
Time (min)
no ClpXP
ClpP
ClpXP

Supplemental Figure S3. Degradation of FtsZ and FtsZ(ΔC67) by ClpXP. Degradation was monitored for FtsZ (6 μM) and FtsZ(ΔC67), ClpXP (0.5 μM), ATP (4 mM), GMPCPP (0.5 mM), and a regenerating system where indicated at 23°C for 120 minutes as described in *Materials and Methods*, and samples were analyzed by SDS-PAGE and Coomassie stain.

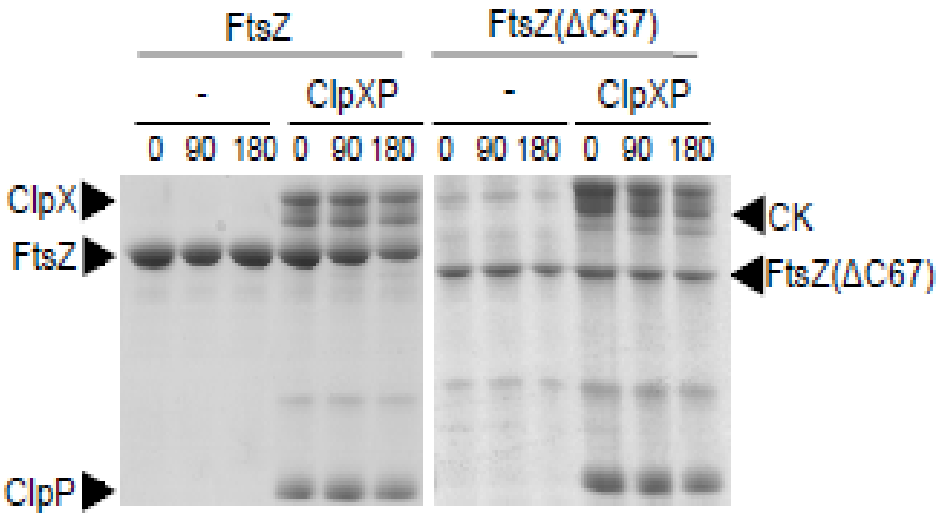
FtsZ
FtsZ(ΔC67)
-
ClpXP
-
ClpXP
0 90 180 0 90 180 0 90 180 0 90 180
ClpX
FtsZ
ClpP
CK
FtsZ(ΔC67)

Supplemental Figure S4. Insoluble FtsZ in deletion strains after heat-treatment.

(A) Single gene deletion strains (Table 1) were incubated at 50 °C for 1 hour and recovered as described in *Materials and Methods*. Cells from deletion strains were collected and insoluble protein extracts were collected as described and analyzed by reducing SDS-PAGE. Immunoblots were performed with antibodies to FtsZ or ClpX as described.

(B) Total protein present in insoluble cell extracts shown in (A) after heat shock at 50 °C and recovery was detected by transferring proteins to a nitrocellulose membrane and staining with Ponceau.

(C) Cell viability for all strains in (A) was determined by measuring colony forming units (CFU ml^{-1}) of cultures before heating ('pre-HS'), after heat treatment at 50 °C for 1 hour ('post-HS'), and after 35 minutes of recovery at 30 °C ('post-rec').

(D) FtsZ levels were compared in single gene deletion strains after heat shock at 42 °C for 30 minutes and recovery (30 °C) as described in *Materials and Methods*. Cells were collected and insoluble protein extracts were analyzed by immunoblotting with antibodies to FtsZ as described.

(E) Insoluble FtsZ levels were monitored in wild type, Δ*clpX* and Δ*clpB* deletion strains before heat shock (50 °C for one hour or 42 °C for 30 minutes, where indicated) and during the 30 °C recovery period (0, 20 and 40 minutes). At the indicated times, cells were collected from cultures and insoluble protein extracts were analyzed by immunoblotting with antibodies to FtsZ as described.

Supplemental Figure S4. Insoluble FtsZ in deletion strains after heat-treatment.

(F) Thermal stability of ClpXP was assayed by incubation of ClpX (0.5 μM) and ClpP (0.7 μM) in phosphate buffered saline supplemented with ATP (4 mM) MgCl2 (10 mM), glycerol (15%), Triton X-100 (0.005%), and TCEP (1 mM). Reactions containing ClpXP were added to a preheated quartz cuvette attached to a circulating water bath set to 50 °C or 30 °C, where indicated, and incubated for one hour. The circulating water bath was rapidly cooled to 30 °C, the reactions were supplemented with ATP and regenerating system, Gfp-ssrA (0.2 μM) was added, and fluorescence was monitored with time in the absence (black) or presence of ClpXP, treated at 50 °C (red) or 30 °C (aqua).

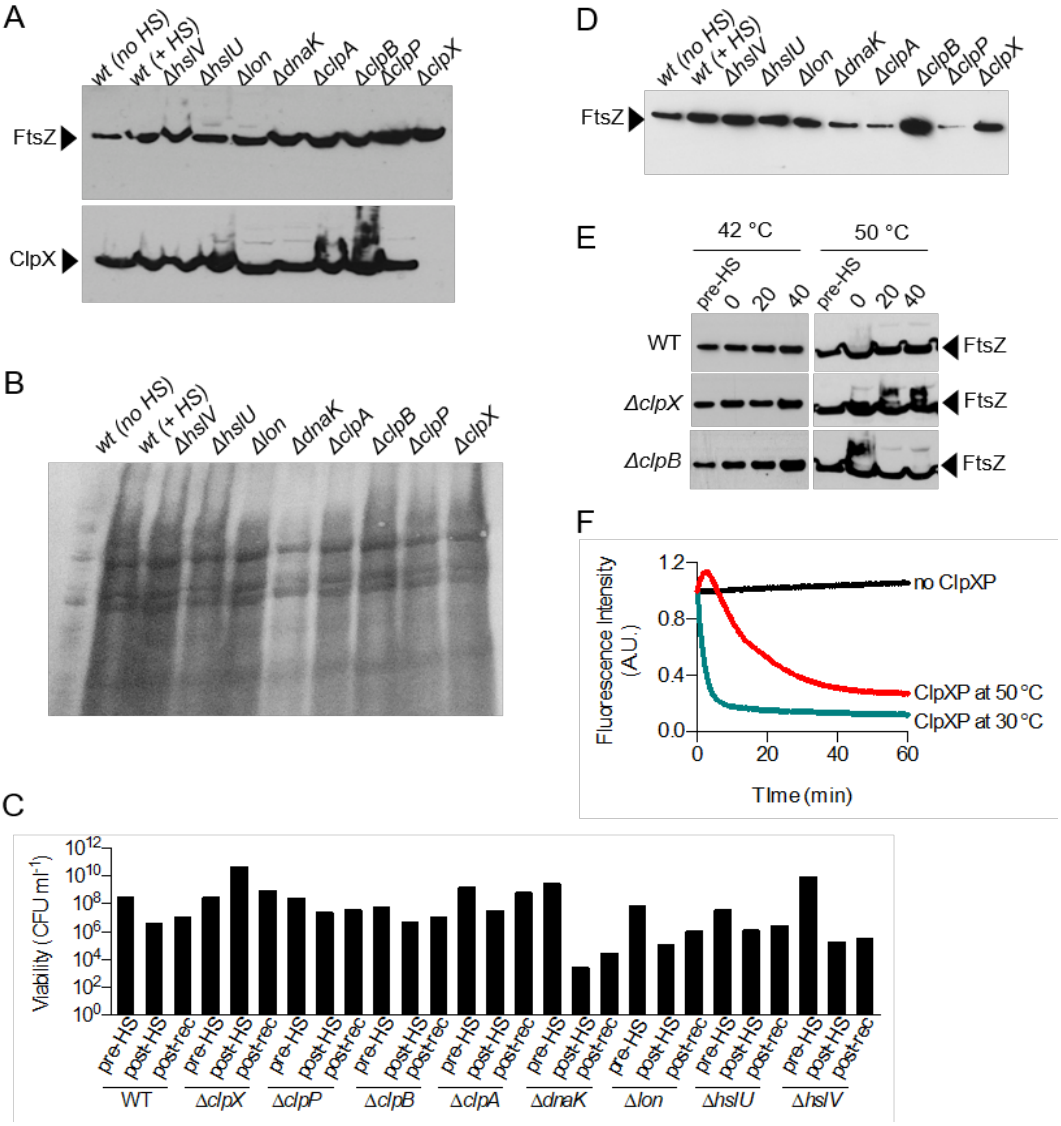
A
wt (no HS)
wt (+ HS)
ΔhslV
ΔhslU
Δlon
ΔdnaK
ΔclpA
ΔclpB
ΔclpP
ΔclpX
FtsZ
ClpX
B
C
Viability (CFU ml-1)
pre-HS
post-HS
post-rec
WT
ΔclpX
ΔclpP
ΔclpB
ΔclpA
ΔdnaK
Δlon
ΔhslU
ΔhslV
D
E
42 °C
50 °C
0
20
40
WT
ΔclpX
ΔclpB
F
Fluorescence Intensity (A.U.)
no ClpXP
ClpXP at 50 °C
ClpXP at 30 °C
TIme (min)

Manuscript IV

Publication Status: Formatted as a research article for submission to *Neurotoxicology*

Title: ATP-dependent chaperone protein expression in an Alzheimer's disease model of tau hyperphosphorylation

Authors: Shannon E. May[1,2], Nasser Zawia[1,2,3] and Jodi L. Camberg[1,2,4]

Author Affiliations:

[1] Interdisciplinary Neurosciences Program, University of Rhode Island, Kingston, RI 02881

[2] George and Anne Ryan Institute for Neuroscience, University of Rhode Island, Kingston, RI 02881

[3]Department of Biopharmaceutical Sciences, College of Pharmacy, University of Rhode Island, Kingston, RI 02881

[4] Department of Cell and Molecular Biology, College of the Environment and Life Sciences, University of Rhode Island, Kingston, RI 02881

Author Contributions: S.E.M. designed experiments, performed experiments, interpreted data and wrote paper; J.L.C. designed experiments, interpreted data, and wrote paper.

Address correspondence to: Jodi L. Camberg, 120 Flagg Road, CBLS, Room 470, University of Rhode Island, Kingston, RI 02881

Abstract

Alzheimer's disease is characterized by the hyperphosphorylation, mislocalization, and aggregation of tau into neurofibrillary tangles (Noble et al., 2013). Tau is an intrinsically disordered protein that lacks secondary structure, which provides the protein with flexibility (Mandelkow et al., 2012). In Alzheimer's disease, tau changes conformation and becomes filamentous, forming ordered aggregates and is abnormally hyperphosphorylated. The extent of neurofibrillary tangle accumulation within the brain tissue of patients with Alzheimer's disease highly correlates to disease severity and progression (Braak and Braak, 1991). It is thought that tau hyperphosphorylation causes deficits in neuronal functioning by whereby pathologically phosphorylated tau protein triggers the conformational change of tau into fibrils and highly ordered, fibrillar aggregates (Alonso et al., 2001). Here, we model tau hyperphosphorylation in vitro by treating human neuroblastoma SH-SY5Y cells with the protein phosphatase 2 (PP2A) inhibitor okadaic acid (Zhang and Simpkins, 2010). We find that chaperone protein levels change in response to different exposures of okadaic acid, indicating that chaperone proteins may be involved in Alzheimer's disease pathogenesis.

Introduction

Alzheimer's disease is characterized by the accumulation of filamentous amyloid-beta and tau protein into extracellular amyloid-beta plaques and intracellular neurofibrillary tangles (Crews and Masliah, 2010). The pathology of Alzheimer's disease is thought to arise from alternative processing of the amyloid precursor protein by beta-secretase and gamma-secretase, which results in the formation and accumulation of amyloid-beta (Aβ) peptides that are 40 residues (Aβ40) and 42 residues (Aβ42). The accumulation of Aβ42 peptide triggers amyloid fibril formation and deposition of amyloid plaques, which are thought to be cytotoxic and responsible for the neurodegeneration observed in Alzheimer's disease (Kametani and Hasegawa, 2018). However, studies have reported that amyloid plaques in transgenic mouse brain tissue are not closely correlated with neurodegeneration or changes in cognitive functioning (Kim et al., 2007; Kim et al., 2013). Moreover, brain imaging studies have shown that amyloid plaques are distributed in brains of cognitively normal aged patients and are not specific to patients with Alzheimer's disease (Edison et al., 2007; Li et al., 2008; Davis et al., 1999; Fagan et al., 2009; Price et al., 2009; Chetelat et al., 2013). Thus, it is possible that amyloid plaques are not a defining pathological hallmark of Alzheimer's disease, but instead accumulate as a result of aging.

Deficits in amyloid precursor protein metabolic activity are thought to contribute to the formation of a pathological environment that triggers tau pathology (Tanzi and Bertram, 2005). Research from a double transgenic mouse model of Alzheimer's disease that expressed both mutant amyloid precursors protein and wild-type human tau showed that amyloid-beta oligomers accelerate the formation of neurofibrillary tangles and neurodegeneration (Hurtado et al., 2010). Neurofibrillary

tangles are intracellular deposits of paired helical filaments that accumulate in regions of the brain associated with cognitive functioning (Binder et al., 2005) and are associated with cognitive impairments (Santacruz et al., 2005; Di et al., 2016). Both neurofibrillary tangles and amyloid-beta plaques are filamentous aggregates that have a cross-beta structure, similar to the human prion protein structure (Iqbal et al., 2005). The main constituent of the paired helical filaments is abnormally phosphorylated tau protein, referred to as hyperphosphorylated tau (Grundke-Iqbal et al., 1986; Kosik et al., 1986; Ihara et al., 1986).

Microtubule-associated tau protein is transcribed from the *MAPT* gene on chromosome 17 and alternative splicing of exon2, exon3, and exon10 results in six different tau isoforms in the adult human brain (Goedert et al., 2010). The six isoforms of tau range from 37 to 46 kDa and differ based on the number of N-terminal inserts and C-terminal microtubule-binding regions (Guo et al., 2017). In the *MAPT* gene, exons 2 and 3 encode for 29 amino acid residue regions that are located in the N-terminal domain of tau protein. Exons 9 – 12 encode for the microtubule-binding repeats in the C-terminal domain of tau (Guo et al., 2017). The longest tau isoform contains 2 N-terminal domain inserts and 4 microtubule-binding repeats (Mandelkow et al., 2012). The domain architecture of tau is divided into an acidic N-terminal projection domain (residues 1 – 150), a proline-rich domain (residues 151 – 243), a microtubule-binding domain, and the C-terminal domain (Mandelkow et al., 2012).

Microtubule-associated tau protein functions to stabilize microtubules and support long-distance, microtubule-mediated axonal transport Drubin and Kirschner, 1986; Johnson and Stoothoff, 2004). In a *Drosophila melanogaster* model of Alzheimer's disease, overexpression of amyloid precursor protein caused axonal transport defects and deficits in short-term synaptic plasticity (Rusu et al., 2007).

Impaired axonal transport may therefore cause cognitive dysfunction in Alzheimer's disease. Furthermore, the phosphorylated tau has greater binding affinity for the light chain of kinesin-1, a motor protein involved in axonal transport, whereas dephosphorylated tau shows decreased binding to kinesin-1 in rat cortical neurons (Cuchillo-Ibanez et al., 2008). Although soluble tau protein is primarily localized to the axons of healthy neurons, early in Alzheimer's disease pathology hyperphosphorylated tau dissociates from microtubules and mislocalizes to the somatodendritic compartment (Morris et al., 2011; Braak et al., 2011). Without biologically functional, soluble tau protein, neuronal processes become disrupted. Microtubules become destabilized, axonal transport decreases, and synapses retract (Dubey et al., 2015).

In Alzheimer's disease, tau hyperphosphorylation is thought to result in a toxic gain of function and loss of normal tau function. Tau protein contains more than 45 possible sites for phosphorylation (Hanger et al., 2007). Normally, tau contains 2 – 3 mol phosphate/mol of protein; phosphorylation levels greater than this impair the ability of tau to bind microtubules and regulate microtubule assembly (Köpke et al., 1993; Lindwall et al., 1984; Alonso et al., 1994). Furthermore, hyperphosphorylation of tau is thought to promote misfolding and aggregation of tau protein into paired helical filaments (Alonso et al., 1996). During Alzheimer's disease pathogenesis, tau hyperphosphorylation at various sites occurs before the aggregation of tau fibrils into intracellular neurofibrillary tangles (Figure 1A). Thus, aberrant phosphorylation of tau may cause the aggregation (Köpke et al., 1993). Previous research has shown that treating transgenic mice with kinase inhibitors changes the phosphorylation state of tau, decreases the number of tau-positive aggregates, reduces neurodegeneration, and improves motor function (Noble et al., 2005; LeCorre et al., 2006; Sundaram et

al., 2013). Evidence that hyperphosphorylation of tau at Thr212 induces the self-assembly of tau into fibrils and aggregates in vitro further support the hypothesis that tau hyperphosphorylation induces self-assembly of tau (Alonso et al., 2010). Phosphorylation of the tau phosphorylation sites Thr212, Thr231, and Ser262 results in caspase-3 activation in 85% of transfected PC12 and CHO cells, suggesting that these residues may be important in Alzheimer's disease neurodegeneration (Alonso et al., 2010). However, there is not a consensus in the field that tau hyperphosphorylation causes tau self-assembly into aggregates. Previous research showed that in vitro phosphorylation of tau at the KXGS motifs in the microtubule binding repeat domain does not facilitate tau aggregation into paired helical filaments (Schneider et al., 1999). Analysis of the expression of tau phospho-epitopes in post-mortem brains of patients with different severities of Alzheimer's disease pathology showed differential expression of specific phospho-tau epitopes during neurofibrillary tangle formation and deposition (Augustinack et al., 2002). Therefore, it is possible that specific sites of tau phosphorylation drive the aggregation of tau into paired helical filaments whereas other sites of tau phosphorylation, though important in dissociating tau from microtubules, do not contribute to tau assembly into aggregates.

Protein quality control and Alzheimer's Disease

Neurofibrillary tangles sequester tau protein, preventing tau protein from associating with and stabilizing microtubules (Gendron and Pretrucelli, 2009). Furthermore, protein degradation pathways are dysfunctional in Alzheimer's disease. Paired helical filaments from the brains of patients with Alzheimer's disease and synthetic paired helical filaments both impair the proteasome, which prevents the clearance of pathological protein aggregates (Keck et al., 2003). Protein aggregates are a threat to cell viability because they disrupt membranes and promote misfolding

in the rest of the proteome (Taylor and Dillin, 2011; Gidalevitz et al., 2006). Within the cell, the protein quality control network safeguards against protein aggregation (Balch et al., 2008). When there is cellular stress, such as heat stress, proteins can become structurally damaged and misfold (Powers and Balch, 2013). Heat shock proteins, or molecular chaperone proteins, are upregulated in response to cell stress to manage protein misfolding (Morimoto, 2008). The transcription factor HSF-1 induces heat shock proteins in response to stress. Overexpression of HSF-1 prolongs lifespan in the model organisms *D. melanogaster* and *C. elegans* (Taylor and Dillin, 2011). During aging, the ability to mount a heat shock response to environmental stresses decreases (Ben-Zvi et al., 2009). Irreversibly misfolded proteins are normally removed from cell via two main degradation pathways: the ubiquitin-proteasome system and autophagy (Taylor and Dillin, 2011). With age, autophagy function decreases (Terman et al., 1995). Postmortem brains of patients with AD show extensive autophagosome accumulation within neurites, which may be due to impairment in the clearance of proteins by macroautophagy (Nixon et al., 2005). Thus, the cell's ability to remove pathological protein aggregates declines with age, which makes aged neurons more susceptible to proteotoxic stressors. Additionally, the expression of ATP-dependent chaperone proteins, specifically Hsp90 and Hsp70, declines with age and even more so in Alzheimer's disease (Brehme M et al., 2014).

The role of ATP-dependent chaperones such as Hsp70 and Hsp90 in Alzheimer's disease pathology is not well understood (Figure 1B). Inhibition of Hsp90 decreases the aggregation of tau into neurofibrillary tangles (Salminen et al., 2011) and promotes the elimination of aggregated, hyperphosphorylated tau (Luo et al., 2007). Thus, Hsp90 may be involved in a pathological pathway that promotes the aggregation of tau into paired helical filaments. By contrast, overexpression of Hsp70

increases the association of tau with microtubules, which is necessary for normal axonal transport and cytoskeletal integrity (Duo et al., 2003). Both Hsp70 and Hsp90 bind to tau, suggesting a role for these chaperone proteins in modulating the folding of tau (Miyata et al., 2011; Thompson et al., 2012).

In eukaryotes, Hsp90 is a critical regulator of protein folding, protein trafficking, and cell signaling; Hsp90 has 400 putative substrate proteins that it regulates (Pearl et al., 2006; Barrott and Haystead, 2013). Due to the diverse set of client proteins that Hsp90 interacts with, the conformation and nucleotide occupancy of Hsp90 is tightly regulated by a network of co-chaperone proteins and post-translational modifications, including phosphorylation, methylation, and acetylation (Pearl et al., 2006). It is known that Hsp90 binds more tightly, and thus has greater affinity for Tau P30L, a mutant of tau that is associated with tau aggregation, compared to wild-type tau protein (Luo et al., 2007). Furthermore, inhibiting Hsp90 in cell culture and in human tau transgenic mice mitigates tau aggregation and pathology (Luo et al., 2007). It is thought that Hsp90 stabilizes phosphorylated, pathological tau and prevents its degradation (Tortosa et al., 2009; Jinwal et al., 2010; Dickey et al., 2007). Moreover, the Hsp90 co-chaperone protein ATPase homolog 1 (Aha1) has been shown to increase tau fibrillization into aggregates in vitro and in a mouse model (Shelton et al., 2017). The co-chaperone proteins FKBP51 and FKBP52 also form a complex with Hsp90 and have been shown to accelerate tau aggregation (Blair et al., 2013). In contrast, the co-chaperone protein carboxy terminus of Hsp70-interacting protein (CHIP), an E3 ubiquitin ligase, forms a complex with Hsp90 and targets client proteins to the proteasome for clearance. Previous work has shown that CHIP in complex with Hsp90 targets hyperphosphorylated tau protein for proteasomal degradation (Dickey et al., 2007).

There is strong evidence in the literature for neuroprotective effects of Hsp70 in Alzheimer's disease pathology caused by tau and amyloid-beta aggregation. Research shows that Hsp70 promotes the degradation of hyperphosphorylated tau protein and has been shown to inhibit the aggregation of all six human tau isoforms with greater affinity for tau isoforms containing three microtubule-binding repeats (Voss et al., 2012). In vitro, the addition of Hsp70 to preformed aggregates of oligomeric and prefibrillar tau decreases tau aggregation and rescues fast axonal transport from tau-mediated pathology (Patterson et al., 2011). Furthermore, the overexpression of Hsp70 in transgenic mice resulted in decreased synaptic loss, amyloid-beta plaque load, and cognitive deficits (Hoshino et al., 2011). In vitro, the Overexpression of Hsp70 protected against toxicity associated with amyloid-beta 42 (Magrané et al., 2004).

The proline-directed kinases glycogen synthase kinase-3 and cyclin dependent kinases regulate tau phosphorylation at epitopes associated with Alzheimer's disease pathology (Drewes et al., 1992; Ledesma et al., 1992; Hanger et al., 1992; Arioka et al., 1993). Dysregulation of phosphorylation is thought to be a contributing factor in Alzheimer's disease pathology. Alzheimer's disease is characterized by a decrease in the activity and expression of protein phosphatases (Braithwaite et al., 2012). Specifically, the downregulation of protein phosphatase 2A (PP2A) has been implicated in contributing to the hyperphosphorylation of tau in AD (Braithwaite et al., 2012; Gong et al., 2005). Furthermore, protein phosphatase 2A inhibitor 2 is mislocalized from the nucleus to the cytoplasm in the brains of patients with Alzheimer's disease, which may trigger the hyperphosphorylation of tau (Arif et al., 2014).

In vitro tau phosphorylation by okadaic acid

Okadaic acid is a lipophilic polyether toxin produced by marine dinoflagellates of the *Prorocentrum* and *Dinophysis* genera that accumulates in filter-feeding shellfish; consumption of mollusks containing okadaic acid causes diarrheic shellfish poisoning in humans, which causes damage to the gastrointestinal tract and can be fatal (Dickey et al., 1990; Cembella et al., 1990; Ito et al., 1994; Edebo et al., 1988). Moreover, in vitro analysis of okadaic acid demonstrated that the toxin is absorbed by human digestive cells and can be readily transported into the bloodstream (Ehlers et al., 2011). In addition to enterotoxic effects, okadaic acid has carcinogenic properties. Research has shown that okadaic acid potently promote tumor formation, affecting the liver, skin, and stomach (Suganama et al., 1988; Sontag and Sontag, 2006; Fujiki and Suganama, 2009). Okadaic acid inhibits protein phosphatases, most notably protein phosphatase 2A (PP2A). The IC_{50} value of okadaic acid required to inhibit 50% of PP2A activity is 0.1 – 0.3 nM and 15 – 50 nM of okadaic acid inhibits 50% of PP1 activity (Swingle et al., 2007). Additionally, okadaic acid inhibits protein phosphatase 4, protein phosphatase 5, and protein phosphatase 2B as well as PP2A under certain conditions (Louzauo et al., 2005).

Pharmacologic inhibition of PP2A by okadaic acid has been shown to induce tau hyperphosphorylation and increase the accumulation of paired helical filaments in several models of Alzheimer's disease. Increased tau phosphorylation was observed in human brain slices of the temporal lobe treated with okadaic acid (Harris et al., 1993). In a cell culture model of Alzheimer's disease, undifferentiated SH-SY5Y neuroblastoma cells treated with 0, 15, and 30 nM okadaic acid for 24 hours showed dose-dependent hyperphosphorylation and accumulation of neurofilament proteins localized to the cell body (Wang et al., 2001). Primary hippocampal cultures isolated

from rats at gestational day 18 develop strong SMI-3I immunoreactivity in the soma and dystrophic neurites, indicating neurofilament phosphorylation, when treated with 10 nM okadaic acid for 36 hours (Kim et al., 1999). Treatment of human neuronal NT2N cells differentiated with retinoic acid and subsequently treated with PP2A inhibitors, including okadaic acid, showed increased tau phosphorylation, decreased binding of tau to microtubules, depolymerization of Glu-microtubules, and degeneration of axons (Merrick et al., 1997). Furthermore, cultured neurons showed an increase in paired helical filament 1 (PHF-1) expression in response to 10 nM okadaic acid for 6 hours, 12 hours, and 24 hours compared to cells not treated with okadaic acid, weakly induced expression of the AT8 epitope of tau, and cleaved tau protein into a 45 kDa fragment after 24 hours (Kim et al., 1999). Okadaic acid treatment has been reported to specifically enhance phosphorylation at the following tau phosphorylation epitopes: Ser396/404, Ser202/205, Ser262, and Thr205 (Ekinici and Shea, 1999; Alvarez-de-la-Rosa et al., 2005; Zhang and Simpkins, 2008). Thus, treatment of cells with okadaic acid is a useful in vitro model of tau hyperphosphorylation and paired helical filament assembly and accumulation in Alzheimer's disease.

Methods

Cell Culture Growth and Differentiation

Human neuroblastoma SH-SY5Y cells were grown as monolayer cultures in T75 (Thermo Fisher Scientific) flasks in Dulbecco's Modified Eagle Medium (DMEM)/F12 (Gibco) supplemented with 10% fetal bovine serum, 100 U/ml penicillin, 100 µg/ml streptomycin, and 2 mM L-glutamine at 37°C incubator in a humid

environment (95% air, 5% CO^2) as previously described (Bihaqi et al., 2017). Viable cells were stained with the exclusion dye Trypan blue solution, 0.4% (Thermo Fisher Scientific) and counted with a hemocytometer before seeding the cells into 6-well and 96-well plates at cell densities of 1.0 x 10^5 cells/well and respectively. Twenty-four hours after subculturing the cells, the cells were differentiated with 10 µM all-*trans*-retinoic acid (Sigma-Aldrich) for six days as previously described (Bihaqi et al., 2017). Briefly, lyophilized retinoic acid (50 mg) was dissolved in 1.67 ml of dimethyl sulfoxide (DMSO) and aliquoted. Retinoic acid stock solution was diluted in 100% ethanol and subsequently added to complete DMEM culture medium to a final concentration of 10 µM. Retinoic acid causes morphological changes such as neurite outgrowth and activates expression of neuronal markers such as NeuN, NSE, and synaptophysin in SH-SY5Y cells (Cheung et al., 2009).

Okadaic Acid Treatment

Lyophilized okadaic acid sodium salt (Enzo Life Sciences) was reconstituted in 100% ethanol to yield a stock solution of 1 mM okadaic acid, which was diluted in 100% ethanol to a final working concentration of 0.1 mM okadaic acid. Okadaic acid solution was added to DMEM media to yield final concentrations of 10, 25, 50, and 100 nM okadaic acid.

Protein Extraction and Western Blotting

Cells were collected by centrifugation at 1000 x*g* for 5 minutes at 4°C. Cell pellets were washed twice with ice-cold phosphate-buffered saline solution and subsequently resuspended in Radio-Immunoprecipitation Assay (RIPA) Buffer

containing phosphatase inhibitors and protease inhibitors. The composition of RIPA buffer was: 50 mM Tris-Cl, pH 7.4, 1% Nonidet-P40, 0.25% sodium deoxycholate, 150 mM sodium chloride, 1 mM ethylene glycol tetraacetic acid, 1 mM phenylmethylsulfonyl fluoride, 1 mM sodium orthovanate, 1mM sodium fluoride, and 1 tablet of cOmplete™, mini protease inhibitor cocktail (Roche). For every 10^6 cells, 100 µL of RIPA buffer was used to lyse cells. Lysates were vortexed for 5-minute intervals for a total of 30 minutes. Lysates were then centrifuged at 10,000 x*g* for 20 minutes at 4°C. The BCA protein assay kit (Peirce) was used to determine total protein concentration in lysates. Samples were normalized and boiled in lithium dodecyl-sulfate (LDS) sample buffer (Thermo Fisher Scientific) for 5 minutes at 95°C. Proteins were separated by SDS-PAGE and transferred to nitrocellulose membranes. Nonspecific protein binding was blocked by incubating the blots in 2% nonfat milk in TBS-T buffer (Tris-Cl buffer saline pH 7.6 containing 0.5% Tween-20) for 2 hours at room temperature. Membranes were incubated in primary antibody solutions overnight at 4°C. Chaperone protein expression levels were determined using antibodies against Hsp90 (Thermo Fisher Scientific), Hsp110 (Enzo Life Sciences), Hsp90 (Thermo Fisher Scientific), and Hsp70 (Rockland Inc.). Total tau protein levels were found with anti-tau antibody against the human 46 kDa tau isoform (Sigma-Aldrich). Phosphorylated tau epitopes were detected using antibodies against Thr212 (Sigma-Aldrich), AT8 (Thermo Fisher Scientific), and Ser396 (Cell Signaling Technology). Blots were stripped with mild stripping buffer (15 g glycine, 1 g SDS, 0.1% SDS, 10 ml Tween-20; pH 2.2) for 10 minutes at room temperature and probed for housekeeping protein beta-actin (Abcam) or GAPDH (Thermo Fisher Scientific). Membranes were incubated in HRP-conjugated secondary antibody dilutions for 1 hour at room temperature before developing the blots with chemiluminescent West Pico Plus reagent (Thermo Fisher Scientific).

Cell Death and Cell Viability Assay

To determine the effects of okadaic acid on differentiated cell morphology, cells in 6-well plates were visualized with phase-contrast microscopy using EVOS FL Auto Cell Imaging System. Cell viability was determined using the CellTiter 96® Aq_{ueous} One Solution Cell Proliferation Assay (Promega). Briefly, CellTiter 96® Aq_{ueous} One Solution Cell Proliferation Reagent was thawed in a 37°C water bath and 20 µl of MTS reagent was added to each well of the 96-well containing 100 µl DMEM culture medium not containing serum. After incubation of the 96-well plates at 37°C for 3 hours, plates were gently shaken and the absorbance was read at 490 nm in a microplate reader. Absorbance values were background-corrected for DMEM culture medium containing MTS reagent alone in wells that did not contain cells. Cell viability is expressed as percentages of the control group, which was treated with 0.1% ethanol.

Statistical Analyses

Statistical analyses were conducted with Graphpad Prism version 6.0, GraphPad Software, La Jolla, California, USA (www.graphpad.com). Error bars represent mean +/- standard error mean (SEM). One-way analysis of variance (ANOVA) followed by Tukey's post hoc multiple comparisons test was used to analyze data sets containing more than two groups. P-values less than 0.05 were considered significant.

Results

Phosphatase inhibition by okadaic acid in undifferentiated neuronal cells

To monitor the effects of increased phosphorylation of tau on the physiology and chaperone protein expression of neuroblastoma cells, we first treated undifferentiated SH-SY5Y cells with okadaic acid, which inhibits PP2A phosphatase leading to tau hyperphosphorylation (schematic in Figure 1C) (Bialojan and Takai, 1988). As shown in Figure 2A, undifferentiated cells do not develop neurite extensions and are not post-mitotic, in contrast to differentiated neuroblastoma cells (Figure 2B). Undifferentiated SH-SY5Y cells were cultured at a density of 1.6×10^6 cells/ml and treated with 0 nM, 50 nM, and 100 nM of okadaic acid for 24 hours, doses of okadaic acid that have previously been used to study tau hyperphosphorylation in a cell culture model of Alzheimer's disease (Zhang and Simpkins, 2010; Choi et al., 2015). We probed cell lysates of undifferentiated cells treated with okadaic acid for Hsp70, Hsp90 and Hsp110 and observed that while levels of Hsp90 and Hsp110 do not change, Hsp70 appeared to be induced upon okadaic acid treatment. Previous reports of protein phosphatase 2A inhibition by okadaic acid treatment showed that in vitro levels of the tau phosphorylation epitope Thr212 increased in response to okadaic acid (Wu et al., 2017). Thus, we probed for phosphorylated tau using the phosphorylated Thr212 epitope to determine if undifferentiated SH-SY5Y treated with 50 nM and 100 nM okadaic acid have increased phosphorylated Tau levels compared to control cells that were not treated with okadaic acid. We observed a modest migration shift in phosphorylated tau (pTau) at Thr212 suggesting that in response to okadaic acid treatment, tau may accumulate additional modifications. However, phosphorylation intensity at Thr212 appears to be similar (Figure 2C). Together, undifferentiated SH-SY5Y cells appear to have only modest changes resulting from incubation with okadaic acid, although the increase in Hsp70 levels is consistent with an enhanced stress response.

Phosphatase PP2A inhibition by okadaic acid leads to reduced chaperone function and tau phosphorylation in differentiated neuronal cells

Next, we differentiated SH-SY5Y cells with retinoic acid to generate cells with neurite extensions and produce physiology that is more relevant to neurons (Figure 2B). Then we treated differentiated cells with okadaic acid to investigate cell viability, tau hyperphosphorylation and levels of chaperone proteins in response to treatment. After differentiation with retinoic acid, cells were treated with 0 nM, 25 nM, 50 nM, and 100 nM of okadaic acid (n = 4 per treatment group) for 3 hours (Figure 3A) and 8 hours (Figure 3B) and overall cell morphology was monitored by phase-contrast microscopy. After 3 hours of okadaic acid exposure, SH-SY5Y cells in the 0 nM and 25 nM okadaic acid treatment groups had apparent normal morphology defined as cells that had phase-bright soma and neuritic processes, as established by previous reports of SH-SY5Y healthy phenotype (Kim et al., 1999) (Figure 3A). However, treatment of cells with either 50 nM or 100 nM okadaic acid for 3 hours caused widespread cell death as evidenced by loss of neurite extensions, cell rounding, and cell detachment from the plate (Figure 3A). We observed similar results when cells were incubated with okadaic acid for 8 hours with high doses associated with cell detachment and death but normal physiology observed at the lower dose (Figure 3B). These results suggest that cytoxicity associated with okadaic acid is enhanced in differentiated cells compared to undifferentiated cells.

Next, we measured cell viability of differentiated SH-SY5Y cells after exposure to okadaic acid using the MTT colorimetric assay to detect metabolic activity. SH-SY5Y cells were seeded at a cell density of 5.0×10^4 cells/ml in a 96-well plate. Twenty-four hours post-seeding, cells were differentiated with retinoic acid and then

treated with 0 nM, 10 nM, and 25 nM for 3 hours, 6 hours, and 24 hours. The MTT assay conducted at the 3-hour and 6-hour exposures to 0 nM, 10 nM, and 25 nM okadaic acid did not show any significant differences in cell viability compared to cells treated with only vehicle (0.1% ethanol) (Figure 3C and 3D). However, the 10 nM and 25 nM doses of okadaic acid were associated with reduced metabolic function in the cells at the 24-hour time point suggesting reduced cell viability (Figure 3E and 3F). Consistent with this, we also observed that after 24 h exposure to low doses of okadaic acid cells, cells became rounded and detached (Supplemental Figure S1A). Viability continued to decrease across a range of okadaic acid concentrations during prolonged incubations (42 h) (Supplemental Figure S1B and S1C).

Since differentiated SH-SY5Y cells displayed phenotypically normal morphologies and no significant loss of viability after low-dose (10 nM and 25 nM) short-term (3 hr) treatment with okadaic acid (Figure 3A, 3C, 3G and S1A), we harvested cell lysates under these conditions to probe for changes in expression levels of Hsp70 and Hsp90 and to detect increased levels of phosphorylated tau using phospho-specific antibodies for the Ser396, Thr212, and Thr181 epitopes. Del Barrio and colleagues have shown that undifferentiated SH-SY5Y cells treated with 30 nM of okadaic acid for 16 hours show significant changes in tau phosphorylation at the Ser396/404 epitope (Del Barrio et al., 2011). After 3 hours of treatment with okadaic acid, we detected increased levels of Tau phosphorylated at Thr212 and, to a lesser extent, Ser396, most notably at the 25 nM dose (Figure 4A). However, we observed no increase in Tau phosphorylated at Thr181, indicating that not all sites are uniformly affected by okadaic acid. Interestingly, Hsp70 protein levels decrease dramatically after exposure to 25 nM okadaic acid for 3 h, and we also observed slightly less Hsp90 after treatment (Figure 4A).

Next, to determine if changes in protein levels that we detected get more pronounced with extended incubation with okadaic acid, we harvested cells at 6 h and probed lysates for Hsp70, Hsp90 and phosphorylated-tau (Thr212) (Figure 4B). We observed that levels of Hsp70 and Hsp90 continued to decrease over time, indicating that the reductions in levels were both dose-dependent and time-dependent. Moreover, we continued to observe elevated levels of tau phosphorylated at Thr212. Finally, long-term exposure to okadaic acid does not impact overall tau levels as detected by total tau antibody, which reacts with multiple tau isoforms (Supplemental Figure S2A and S2B). Together, these results demonstrate that inhibition of protein phosphatases leads to enhanced phosphorylation of tau and correlates with reduced function of ATP-dependent chaperones in differentiated SH-SY5Y cells.

Discussion

Protein aggregation is observed throughout several neurodegenerative diseases, such as Alzheimer's disease (AD), Parkinson's disease, and Huntington's disease (Pruisner, 2013). Proteins misfold into a biologically nonfunctional, insoluble state and proceed to form detergent-resistant aggregates that cannot be degraded by cellular degradation mechanisms, such as the ubiquitin proteasome pathway in humans (Jucker and Walker, 2013; Vashist et al., 2011). It is hypothesized that protein aggregates form in diseases as a result of inefficient protein quality control, possibly due to aging (Saez and Vilchez, 2014). Research provides evidence that amyloids and amyloid-like fibers interfere with neuronal functions, including cell communication, which may contribute to neuronal cell death in neurodegenerative diseases (Kakkar et al., 2014). In Alzheimer's disease, tau becomes hyperphosphorylated and both mouse and human hyperphosphorylated tau have

been shown to aggregate in vitro (Alonso et al., 2001; Chohan et al., 2005). Tau hyperphosphorylation is not exclusive to Alzheimer's disease; aberrant phosphorylation of tau and formation of tau-positive inclusions occurs in several human neurodegenerative diseases, including Pick's disease, progressive supranuclear palsy, corticobasal degeneration, and frontotemporal dementia and Parkinsonism linked to chromosome-17 (Goedert et al., 2010).

Cells have robust protein quality control networks that resolubilize misfolded proteins and degrade aggregated proteins. Within this network, molecular chaperones function to stabilize properly folded proteins, refold misfolded or partially unfolded proteins, and degrade misfolded proteins that are unamenable to refolding mechanisms (Bukau and Horwich, 1998). There is evidence that molecular chaperones may be involved in the progression of Alzheimer's disease pathology. Research shows that expression levels of ATP-dependent molecular chaperones, Hsp90 and Hsp70, decrease during the course of aging and neurodegenerative diseases (Salminen et al., 2011; Brehme et al., 2014). Normally, cellular stress triggers the upregulation of heat shock proteins, which regulate the folding of unfolded or misfolded proteins and degrade irreversibly misfolded proteins (Morimoto and Santoro, 1998). Studies have shown that increasing the expression of heat shock proteins in animal models of neurodegenerative diseases can be neuroprotective. The overexpression of Hsp70 mitigates pathological phenotypes in transgenic mouse models of spinal and bulbar muscular atrophy (Adachi et al., 2003; Katsuno et al., 2005).

In this study we sought to determine if okadaic acid, a known inhibitor of PP2A, alters chaperone protein levels in differentiated human neuroblastoma SH-SY5Y cells. It is thought that inhibition of PP2A may have a role in Alzheimer's

disease pathogenesis. In the brains of patients with Alzheimer's disease there is an increase in both the levels of mRNA and expression of inhibitor 1 of PP2A ($I1^{PP2A}$) and in vitro expression of $I1^{PP2A}$ hyperphosphorylates tau in NIH3T3 cells (Wang et al., 2015). Here, we found that long-term exposure to okadaic acid significantly impairs the viability of differentiated SH-SY5Y cells treated with 10 nM, 30 nM, and 50 nM okadaic acid for 24 and 42 hours. However, cells tolerated short-term exposure to 10 nM and 25 nM okadaic acid (3 h) without significant loss of viability. These observations suggest that 24-hour exposure of okadaic acid to differentiated SH-SY5Y cells is toxic. Future experiments that measure caspase-3 activation in response to 24-hour exposure of 10 nM and 25 nM okadaic acid to differentiated SH-SY5Y cells could investigate this further.

Reduced chaperone function could exacerbate defects in overall cell viability and neurodegeneration. Notably, both Hsp70 and Hsp90 chaperone protein levels decreased in response to increasing doses of okadaic acid at the 3-hour and 6-hour exposures of okadaic acid to SH-SY5Y cells. Although after 24 hours, we did observe a surprising increase in Hsp70 levels (data not shown), but the cells had become rounded and detached with widespread cell death. Together, increasing doses of okadaic acid seemed to correlate with decreased levels of Hsp70 and Hsp90 in differentiated cells. It is possible that Hsp70 is downregulated or degraded in response to phosphatase inhibition. Further research that investigates the mRNA levels, localization and protein turnover of of Hsp70 and Hsp90 are warranted. Hsp70 and Hsp90 are both also known to be phosphorylated, and phosphorylation states regulate binding to co-chaperones and substrate selection (Muller, et al., Oncogene, 2013).

Okadaic acid has been widely used to inhibit protein phosphatases and model tau hyperphosphorylation and dissociation of tau from microtubules in cultured human neuroblastoma cells (Caillet-Boudin et al., 1996; Shea et al., 1996). Furthermore, okadaic acid has been shown to inhibit PP2A and PP1 in vivo. Rat brains injected with okadaic acid have shown decreased expression of PP2A and PP1 (Arendt et al., 1998). However, the use of okadaic acid and other small molecule inhibitors commonly used to inhibit protein phosphatases, such as calyculin A, tautomycin, nodularin, microcystin-LR, and fostriecin, have several limitations (Swingle et al., 2007). Calyculin A, nodularin, and microcystin-LR are the most potent phosphatase inhibitors; nanomolar concentrations of these compounds inhibit PP2A, PP1, PP4, and PP5 (Swingle et al., 2007). A drawback to using small molecule inhibitors to inhibit phosphatases is their ability to effectively enter the cell and selectively inhibit a given phosphatase. For example, cell membranes are permeable to calyculin A and okadaic acid, but the hydrophobicity of calyculin A and, to a lesser extent, okadaic acid limit their solubility in cell culture media (Swingle et al., 2007). This study assumed that okadaic acid effectively entered cells and sought to determine which doses of okadaic acid could alter tau phosphorylation in vitro. However, it is possible that okadaic acid did not efficiently inhibit PP2A using the doses 10 nM and 25 nM and exposure times of 6 and 24 hours. Living cells contain concentrations of PP2A and PP1 between 0.1 – 1.0 μM depending on the cell line (Cohen et al., 1990). For future experiments, it is possible to inhibit phosphatases more efficiently by adding a protein phosphatase inhibitor, such as microcystin or nodularin, directly to cell extracts and immunoblotting lysates to determine possible alterations in the expression of tau phospho-epitopes and chaperone protein expression (Swingle et al., 2007).

Phase-contrast microscopy clearly showed neuronal degeneration in response to short exposures (3 hours, 8 hours) of 50 nM and 100 nM okadaic acid but it is difficult to determine the extent of phosphorylation inhibition due to widespread cell death and low protein yield in cell extracts. Okadaic acid toxicity could be due in part to impaired cytoskeletal architecture and loss of cell-cell contact (Opsahl et al., 2013). The toxin has previously been shown to impair cell adhesion and reorganize filamentous actin, resulting in morphological rearrangement (Vale and Botana, 2008; Franchini et al., 2010). Previous reports demonstrated that okadaic acid within the range of 100 – 500 nM alters cytoskeletal structure and induces apoptotic cell death in human neuroblastoma cells (Kahn et al., 2012, Valdiglesias et al., 2011). Stable isotope labeling of amino acids in undifferentiated SH-SY5Y cells treated with 400 nM okadaic acid followed by isolation of lipid rafts and mass spectroscopy analysis identified 167 phosphoepitopes of 67 proteins associated with the actin cytoskeleton, mictrotubules, and cell adhesion structures that are affected by okadaic acid (Opsahl et al., 2013). Thus, okadaic acid may exert cytotoxicity by promoting the breakdown of the cytoskeleton and inducing cell detachment.

Furthermore, okadaic acid causes oxidative damage, genotoxicity, and activation of apoptosis in various cell lines. Treatment of leukocytes, HepG-2 cells, and SH-SY5Y cells with okadaic acid resulted in altered cell morphology in all cell lines tested and changes in the cell cycle of leukocytes and SH-SY5Y cells with the greatest impairment observed in SH-SY5Y cells (Valdiglesias et al., 2011). Moreover, treatment of the cell lines with okadaic acid both increased the rate of apoptosis and caspase-3 activation in leukocytes, HepG-2 cells, and SH-SY5Y cells (Valdiglesias et al., 2011). Okadaic acid treatment has also been shown to induce both direct and indirect oxidative damage to SH-SY5Y cells in culture (Valdiglesias et al., 2011).

Additionally, DOK cells treated with 10 nM okadaic acid showed evidence of cytotoxicity based on LDH release and the same dose of okadaic acid induced caspase-3-dependent apoptosis and DNA damage in HepG-2 hepatic cells (Souid-Mensi et al., 2008).

The most selective phosphatase inhibitors are tautomycin/tautomycetin, okadaic acid, and fostriecin (Swingle et al., 2007). Of these, fostriecin, a phosphate ester, has the most selectivity, inhibiting PP2A/PP4 compared to PP1/PP5 with selectivity $\geq 10^4$, whereas the selectivity of okadaic acid to inhibit PP2A/PP4 compared to PP1/PP5 is $<10^2$ (Swingle et al., 2007). Furthermore, fostricein is water soluble and readily enters living cells via the reduced folate transporter (Fry et al., 1984). Therefore, fostriecin has advantages over okadaic acid in models of in vitro and in vivo phosphorylation. A drawback of using fostriecin is the instability of the compound due to its lactone ring compared to okadaic acid, which is stable in organic solvents (Swingle et al., 2007). However, fostriecin can be stored in buffered solution containing ascorbate with a pH range of 5.5 – 7.5 to prevent oxidation and exposure to light (Swingle et al., 2007). The use of fostriecin to inhibit PP2A in human neuroblastoma SH-SY5Y cells is a more selective, and possibly less toxic, experimental approach compared to okadaic acid. Moreover, it is possible to model the phosphorylation of tau by mutating Ser/Thr residues to Glu, or pseudophosphorylate tau to determine which phosphoepitopes of tau are directly involved in Alzheimer's disease pathogenesis (Alonso et al., 2010).

Here, we used okadaic acid as it has previously been reported to alter tau phosphorylation (Harris et al., 1993). Phase-contrast microscopy clearly showed neuronal degeneration in response to short exposures (3 hours, 8 hours) of 50 nM and 100 nM okadaic acid (Figure 3), but it is difficult to determine the extent of

phosphorylation inhibition due to widespread cell death and low protein yield in cell extracts. Okadaic acid toxicity could be due in part to impaired cytoskeletal architecture and loss of cell-cell contact (Opsahl et al., 2013). The toxin has previously been shown to impair cell adhesion and reorganize filamentous actin, resulting in morphological rearrangement (Vale and Botana, 2008; Franchini et al., 2010). Previous reports demonstrated that okadaic acid within the range of 100 – 500 nM alters cytoskeletal structure and induces apoptotic cell death in human neuroblastoma cells (Kahn et al., 2012, Valdiglesias et al., 2011). Stable isotope labeling of amino acids in undifferentiated SH-SY5Y cells treated with 400 nM okadaic acid followed by isolation of lipid rafts and mass spectroscopy analysis identified 167 phosphoepitopes of 67 proteins associated with the actin cytoskeleton, mictrotubules, and cell adhesion structures that are affected by okadaic acid (Opsahl et al., 2013). Thus, okadaic acid may exert cytotoxicity by promoting the breakdown of the cytoskeleton and inducing cell detachment under high exposure conditions. Furthermore, okadaic acid causes oxidative damage, genotoxicity, and activation of apoptosis in various cell lines. Treatment of leukocytes, HepG-2 cells, and SH-SY5Y cells with okadaic acid resulted in altered cell morphology in all cell lines tested and changes in the cell cycle of leukocytes and SH-SY5Y cells with the greatest impairment observed in SH-SY5Y cells (Valdiglesias et al., 2011b). Moreover, treatment of the cell lines with okadaic acid both increased the rate of apoptosis and caspase-3 activation in leukocytes, HepG-2 cells, and SH-SY5Y cells (Valdiglesias et al., 2011b). Okadaic acid treatment has also been shown to induce both direct and indirect oxidative damage to SH-SY5Y cells in culture (Valdiglesias et al., 2011c).

Based on our results, chaperone protein expression of Hsp70 decrease in response to increasing exposure and dosage of okadaic acid. However, Hsp90

expression increases in response to increasing exposure and concentration of okadaic acid. It is possible that Hsp70 destabilize fibrils and aggregates of hyperphosphorylated tau and the levels of these chaperones may decrease in correlation to increasing aggregate load (Figure 5). By contrast, Hsp90 may stabilize aberrantly phosphorylated tau protein and could be involved in the assembly of tau fibrils into neurofibrillary tangles. Our results show that Hsp70 levels consistently decrease in response to increasing concentration of okadaic acid over 3 hours and 6 hours of exposure. However, differentiated SH-SY5Y cells treated with okadaic acid for 24 hours show a two-fold increase in Hsp70 levels compared to vehicle-treated cells (Supplemental Figure S3). We could not probe for changes in Hsp70 expression in cells treated with 25 nM okadaic acid for 24 hours due to widespread cell death and low protein concentration. Thus, further research should be done to investigate long-term effects of okadaic acid on cultured human neuroblastoma cells differentiated with retinoic acid to investigate changes in chaperone levels over chronic exposure. Treating differentiated neuroblastoma cells with low doses of okadaic acid, such as 5 nM and 10 nM okadaic acid for 24 hours and 48 hours would provide more information to compare to the findings discussed here. Moreover, future experiments should be carried out that expose differentiated SH-SY5Y cells to okadaic acid for 24 hours, remove the cell culture medium containing okadaic acid, replace with growth medium containing fetal bovine serum, and monitor cells over time for changes in Hsp90, Hsp70, and Hsp110 chaperone protein levels.

A caveat of the okadaic acid model of hyperphosphorylated tau is that inhibition of PP2A and to a lesser extent, PP1, could phosphorylate the chaperone proteins Hsp70 and Hsp90. Phosphorylation of Hsp90 and Hsp70 in eukaryotes may change the functional activities and interactions of these chaperone proteins with co-

chaperone proteins. Post-translational modifications that regulate Hsp90 conformation and binding to co-chaperone proteins include phosphorylation, methylation, acetylation, ubiquitylation, nitrosylation, and sumoylation (Kargöz and Rüdiger, 2015; Wandinger et al., 2008). Therefore, excessive phosphorylation of chaperone proteins could alter their accessibility for nucleotides and substrate proteins. It is interesting to note that the proline-directed kinase Gsk3β, which regulates tau phosphorylation, is a client of Hsp90 (Lochhead et al., 2006; Tortosa et al., 2009; Banz et al., 2009). It is possible that Hsp90 may contribute to Alzheimer's disease by facilitating the phosphorylation activity of the tau kinase Gsk3β. Overall, it is clear that ATP-dependent chaperone proteins are involved in Alzheimer's disease tau pathology and it remains to be understood how molecular chaperone proteins are affected by the aggregation and accumulation of hyperphosphorylated tau protein.

Funding

This work was funded by an Institutional Development Award (IDeA) from the National Institute of General Medical Sciences of the National Institutes of Health (#P20GM103430 to J. Camberg). S.E.M was supported by the George and Anne Ryan Institute for Neuroscience Graduate Student Fellowship. The funders had no role in study design, data collection and interpretation, or the decision to submit the work for publication.

Acknowledgements

This material is based upon work conducted at a Rhode Island NSF EPSCoR research facility, the Genomics and Sequencing Center, supported in part by the NSF

EPSCoR Cooperative Agreement #EPS-1004057. Research reported in this work was made possible by the use of equipment and services available through the Institutional Development Award (IDeA) Network for Biomedical Research Excellence from the National Institute of General Medical Sciences of the National Institute of Health under the grant number P20GM103430. We thank Aseel Eid, Jaunetta Hill, Allison Leso, Catherine Trebino, and Syed Bihaqi for helpful discussions.

References

1. Adachi H, Katsuno M, Minamiyama M, Sang C, Pagoulatos G, Angelidis C, Kusakabe M, Yoshiki A, Kobayashi Y, Doyu M, and Sobue G. Heat shock protein 70 chaperone overexpression ameliorates phenotypes of the spinal and bulbar muscular atrophy transgenic mouse model by reducing nuclear-localized mutant androgen receptor protein. *J Neurosci*. 2003; 23: 2203 – 2211.
2. Alonso AD, Di Clerico J, Li B, Corbo CP, Alaniz ME, Grundke-Iqbal I, and Iqbal K. Phosphorylation of tau at Thr212, Thr231, and Ser262 combined causes neurodegeneration. *J Biol Chem*. 2010; 285(40): 30851 – 3060.
3. Alonso A et al. Hyperphosphorylation induces self-assembly of tau into tangles of paired helical filaments/straight filaments. *Proc Natl Acad Sci USA*. 2001; 98: 6923 – 6928.
4. Alonso AC, Grundke-Iqbal I, and Iqbal K. Alzheimer's disease hyperphosphorylated tau sequesters normal tau into tangles of filaments and disassembles microtubules. *Nature Medicine*. 1996. 2(7): 783 – 787.
5. Alonso AC, Zaidi T, Grundke-Iqbal I, Iqbal K. Role of abnormally phosphorylated tau in the breakdown of microtubules in Alzheimer disease. *Proc Natl Acad Sci USA.* 1994; 91(12): 5562 – 5566.

6. Alvarez-de-la-Rosa M, Silva I, Nilsen J, Pérez MM, García-Segura LM, Avila J, and Naftolin F. Estradiol prevents neural tau phosphorylation characteristic of Alzheimer's disease. *Ann NY Acad Sci*. 2005; 1052: 210 – 224.
7. Arif M, Wei J, Zhang Q, Liu F, Basturo-Islas G, Grundke-Iqbal I, and Iqbal K. Cytoplasmic retention of protein phosphatase 2A inhibitor 2 (I_2^{PPA2}) induces Alzheimer-like abnormal hyperphosphorylation of tau. *Journal Biological Chemistry*. 2014; 289(40): 27677 – 27691.
8. Arioka M, Tsukamoto M, Ishiguro K, Kato R, Sato K, Imahori K, and Uchida T. Tau protein kinase II is involved in the regulation of the normal phosphorylation state of tau protein. *J Neurochem*. 1993; 60(2): 461 – 468.
9. Augustinack JC, Schneider A, Mandelkow EM, and Hymann BT. Specific tau phosphorylation sites correlate with severity of neuronal cytopathology in Alzheimer's disease. *Acta Neuropathol*. 2002; 103: 26 – 35.
10. Balch WE, Morimoto RI, Dillin A, and Kelly JW. Adapting proteostasis for disease intervention. *Science*. 2008; 319(5865): 916 – 919.
11. Banz VM, Medova M, Keogh A, Furer C, Zimmer Y, Candinas D, and Stroka D. Hsp90 transcriptionally and post-translationally regulates the expression of NDRG1 and maintains the stability of its modifying kinase GSK3β. *Biochim Biophys Acta*. 2009; 1793 (10): 1597 – 1603.
12. Bialogan C and Takai A. Inhibitory effect of a marine-sponge toxin, okadaic acid, on protein phosphatases. Specificity and kinetics. *Biochem J*. 1988; 256: 283 – 290.
13. Binder LI, Guillozet-Bongaarts AL, Garcia-Sierra F, and Berry RW. Tau, tangles, and Alzheimer's disease. *Biochimica et Biophysica Acta*. 2005; 1739(2-3): 216 – 223.

14. Blair LJ, Nordhues BA, Hill SE, Scaglione KM, O'Leary JC 3rd, Fontaine SN, Breydo L, Zhang B, Li P, Wang L, Cotman C, Paulson HL, Muschol M, Uversky VN, Klengel T, Binder EB, Kayed R, Golde TE, Berchtold N, and Dickey CA. Accelerated neurodegeneration through chaperone-mediated oligomerization of tau. *J Clin Invest*. 2013; 123(10): 41558 – 4169.
15. Braak H, Thal DR, Ghebremedhin E, Del Tredici K. Stages of the pathologic process in Alzheimer disease: age categories from 1 to 100 years. *J Neuropathol Exp Neurol*. 2011; 70: 960 – 969.
16. Braak H and Braak E. Demonstration of amyloid deposits and neurofibrillary changes in whole brain sections*. Brain Pathol*. 1991; 1: 213 – 216.
17. Braithwaite SP, Stock JB, Lombroso PJ, and Nairn AC. Protein phosphatases and Alzheimer's disease. *Prog Mol Biol Transl Sci*. 2012; 106: 343 – 379.
18. Brehme M, Voisine C, Rolland T, Wachi S, Soper JH, Zhu Y, Orton K, Villella A, Garza D, Vidal M, Ge H, and Morimoto RI. A chaperome subnetwork safeguards proteostasis in aging and neurodegenerative disease. *Cell Reports*. 2014; 9(3): 1135-1150.
19. Bukau B and Horwich AL (1998). The Hsp70 and Hsp60 chaperone machines. *Cell*. 92, 351-366.
20. Carmichael J, DeGraff WG, Gazdar AF, Minna, JD, and Mitchell JB. Evaluation of tetrazolium-based semiautomated colorimetric assay: assessment of chemosensitivity testing. *Cancer Res*. 1987; 47(4): 936 – 942.
21. Cembella A. Occurrence of okadaic acid, a major diarrheic shellfish toxin, in natural populations of *Dinophysis* spp. From the eastern coast of North America. *J Appl Phycol.* 1990; 1: 307 – 310.

22. Chételat G, La Joie R, Villain N, Perrotin A, De La Sayette V, Eustache F, et al. Amyloid imagining in cognitively normal individuals, at-risk populations and preclinical Alzheimer's disease. *Neuroimage Clin*. 2013; 2: 356 – 365.
23. Choi S, Oh JH, Kim H, Nam SH, Shin J, and Park JS. Protective effect of Tat PTD-Hsp27 fusion protein on tau hyperphosphorylation induced by okadaic acid in the human neuroblastoma cell line SH-SY5Y. *Cell Mol Neurobiol*. 2015; 35(7): 1049 – 1059.
24. Cohen P, Homles CF, and Tsukitani Y. Okadaic acid: a new probe for the study of cellular regulation. *Trends Biochem Sci*. 1990; 15: 98 – 102.
25. Cuchillo-Ibanez I, Seereeram A, Byers HL, Leung KY, Ward MA, Anderton BH, and Hanger DP. Phosphorylation of tau regulates its axonal transport by controlling its binding to kinesin. *FASEB J*. 2008; 22(9): 3186 – 3195.
26. Davis DG, Schmitt FA, Wekstein DR, and Markesbery WR. Alzheimer neuropathologic alterations in aged cognitively normal subjects. *J Neuropathol Exp Neurol*. 1999; 58: 376 – 388.
27. Del Barrio L, Martín-de-Saavedra MD, Romero A, Parada E, Egea J, Avila J, McIntosh JM, Wonnacott S, and López MG. Neurotoxicity induced by okadaic acid in the human neuroblastoma SH-SY5Y cell line can be differentially prevent by α7 and β2* nicotinic stimulation. *Toxicol Sci*. 2011; 123(1): 193 – 205.
28. Di J, Cohen LS, Corbo CP, Phillips GR, El Idrissi A, and Alonso AD. Abnormal tau induces cognitive impairment through two different mechanisms: synaptic dysfunction and neuronal loss. *Sci Rep*. 2016; 6 (20833).
29. Dickey CA, Kamal A, Lundgren K, Klosak N, Bailery RM, Dunmore J, Ash P, Shoraka S, Zlatkovic J, Eckman CB, Patterson C, Dickson DW, Nahman Jr. NS, Hutton M, Burrows F, and Petrucelli L. The high-affinity Hsp90-CHIP complex

recognizes and selectively degrades phosphorylated tau client proteins. *J Clin Invest*. 2007; 117(3): 648 – 658.

30. Dickey RW, Bobzin SC, Faulkner FA, and Andrzejewski D. Identification of okadaic acid from a Caribbean dinoflagellate, *Prorocentrum concavum*. *Toxicon*. 1990; 28(4): 371 – 7.
31. Drewes G, Lichtenberg-Kraag B, Döring F, Mandelkow EM, Biernat J, Goris J, Dorée M, and Mandelkow E. Mitogen activated protein (MAP) kinase transforms tau protein into an Alzheimer-like state. *EMBO Journal*. 1992; 11(6): 2131 – 2138.
32. Drubin DG and Kirschner MW. Tau protein function in living cells. *The Journal of Cell Biology*. 1986; 103(6): 2739 – 2746.
33. Dubey J, Ratnakaran N, and Koushika SP. Neurodegeneration and microtubule dynamics: death by a thousand cuts. *Frontiers in Cellular Neuroscience*. 2015; 9(343).
34. Duo F, Netzer WJ, Tanemura K, Li F, Hartl U, Takashima A, Gouras GK, Greengard P, and Xu H. Chaperones increase association of tau protein with microtubules. *Proc Natl Acad Sci USA*. 2003; 100(2): 721 – 726.
35. Edebo L, Lange S, Li XP, and Allenmark S. Toxic mussels and okadaic acid induce rapid hypersecretion in the rat small intestine. *APMIS*. 1988; 96(11): 1029 – 1035.
36. Edison P, Archer Ha, Hinz R, Hammers A, Pavese N, Tai YF, et al. Amyloid, hypometabolism, and cognition in Alzheimer disease: An [11C]PIB and [18F]FDG PET study. *Neurol*. 2007; 68: 501 – 508.
37. Ehlers A, Scholz J, These A, Hessel S, Preiss-Weigert A, and Lampen A. Analysis of the passage of the marine biotoxin okadaic acid through an in vitro human gut barrier. *Toxicology*. 2011; 279(1 – 3): 196 – 202.

38. Ekinici FJ, Ortiz D, and Shea TB. Okadaic acid mediates tau phosphorylation via sustained activation of the L-voltage-sensitive calcium channel. *Molecular Brain Research.* 2003; 117(2): 145 – 157.
39. Eroglu B, Moskophidis D, and Mivechi NF. Loss of Hsp110 leads to age-dependent tau hyperphosphorylation and early accumulation of insoluble amyloid beta. *Mol Cell Biol*. 2010; 30(19): 4626 – 4643.
40. Fagan AM, Mintun MA, Shah AR, Aldea P, Roe CM, Mach RH, et al. Cerebrospinal fluid tau and ptau(181) increase with cortical amyloid deposition in cognitively normal individuals: implications for future clinical trials of Alzheimer's disease. *EMBO Mol Med*. 2009; 1: 371 – 380.
41. Franchini A, Malagoli D, and Ottaviani E. Targets and effects of yessotoxin, okadaic acid and palytoxin: a differential review. *Mar Drugs*. 2010; 8: 658 – 677.
42. Fry DW, Besserer JA, and Boritzki TJ. Transport of the antitumor antibiotic Cl-920 into L1210 leukemia cells by the reduced folate carrier system. *Cancer Res*. 1984; 44: 3366 – 3370.
43. Fujiki H and Suganama M. Carcinogenic aspects of protein phosphatase 1 and 2A inhibitors. *Prog Mol Subcell Biol*. 2009; 46: 221 – 54.
44. Gidalevitz T, Ben-Zvi A, Ho KH, Brignull HR, and Morimoto RI. Progressive disruption of cellular protein folding in models of polyglutamine diseases. *Science*. 2006; 311(5766): 1471 – 1474.
45. Gong CX, Liu F, Grundke-Iqbal I, and Iqbal K. Post-translational modifications of tau protein in Alzheimer's disease. *J Neural Transm (Vienna*). 2005; 112(6): 813 – 838.
46. Grundke-Iqbal I, Iqbal K, Tung YC, Quinlan M, Wisniewski HM, and Binder LI. Abnormal phosphorylation of the microtubule-associated protein tau in Alzheimer cytoskeletal pathology. *Proc Natl Acad Sci USA*. 1986; 83(13): 4913 – 4917.

47. Guo T, Noble W, and Hanger DP. Roles of tau protein in health and disease. *Acta Neuropathol.* 2017; 133(5): 665 – 704.
48. Hanger DP, Hughes K, Woodgett JR, Brion J, and Anderton BH. Glycogen synthase kinase-3 induces Alzheimer's disease-like phosphorylation of tau: Generation of paired helical filament epitopes and neuronal localisation of the kinase. *Neuroscience Letters.* 1992; 147(1): 58 – 62.
49. Harris KA, Oyler GA, Dolittle GM, Vincent I, Lehman RAW, Kincaid RL, and Billingsley ML. Okadaic acid induces hyperphosphorylated forms of tau protein in human brain slices. *Annals of Neurology*. 1993; 33(1): 77 – 87.
50. Hasegawa M et al. Protein sequences and mass spectrometric analyses of tau in the Alzheimer's disease brain. *J Biol Chem*. 1992; 267: 17047 – 17054.
51. Hoshino T, Murao N, Namba T, Takehara M, Adachi H, Katsuno M, Sobue G, Matsushima T, Suzuki T, and Mizushima T. Suppression of Alzheimer's disease-related phenotypes by expression of heat shock protein 70 in mice. *J Neurosci*. 2011; 31(14): 5225 – 5234.
52. Hurtado DE, Molina-Porcel L, Iba M, Aboagye AK, Paul SM, Trojanowski JQ, and Lee V M-Y. Aβ accelerates the spatiotemporal progression of tau pathology and augments tau amyloidosis in an Alzheimer mouse model. *American Journal of Pathology*. 2010; 177(4): 1977 – 1988.
53. Ihara Y, Nukina N, Miura R, and Ogawara M. Phosphorylated tau protein is integrated into paired helical filaments in Alzheimer's disease. *J Biochem*. 1986; 99(6): 1807 – 1810.
54. Iqbal K, Alonso AC, Chen S, Chohan MO, El-Akkad E, Gong CX, Khatoon S, Li B, Liu F, Rahman A, Tanimukai H, and Grundke-Iqbal I. Tau pathology in Alzheimer disease and other tauopathies. *Biochim Biophys Acta*. 2005; 1739: 198 – 210.

55. Ito E and Terao K. Injury and recovery process of intestine caused by okadaic acid and related compounds. *Nat Toxins*. 1994; 2(6): 371 – 377.
56. Johnson GV and Stoothoff WH. Tau phosphorylation in neuronal cell function and dysfunction. *Journal of Cell Science*. 2004; 117(Pt 24): 5721 – 5729.
57. Kahn S, Lykkebo S, Jakobsen LD, Nielsen MS, and Jensen PH. Caspase-mediated parkin cleavage in apoptotic cell death. *J Biol Chem*. 2012; 277(18): 15303 – 15308.
58. Kametani F and Hasegawa M. Reconsideration of amyloid hypothesis and tau hypothesis in Alzheimer's disease. *Frontiers in Neuroscience*. 2018; 12(25): 1 – 11.
59. Kargöz GE and Rüdiger SG. Hsp90 interaction with clients. *Trends Biochem Sci*. 2015; 40(2): 117 – 25.
60. Katsuno M, Sang C, Adachi H, Minamiyama M, Waza M, Tanaka F, Doyu M, and Sobue G. Pharmacological induction of heat-shock proteins alleviates polyglutamine-mediated motor neuron disease. *Proc Natl Acad Sci USA*. 2005; 102: 16801 – 16806.
61. Kim D, Su J, and Cotman CW. Sequence of neurodegeneration and accumulation of phosphorylated tau in cultured neurons after okadaic acid treatment. *Brain Research*. 1999; 839(2): 253 – 262.
62. Kim J, Chakrabarty P, Hanna A, Marcha A, Dickson DW, Borchelt DR, et al. Normal cognition in transgenic BRI2-Abeta mice. *Mol Neurodegener*. 2013; 8(15).
63. Kim J, Onstead L, Randle S, Price R, Smithson L, Zwizinski C, et al. Abeta40 inhibits amyloid deposition in vivo*. J Neurosci*. 2007; 27: 627 – 633.
64. Köpke E, Tung YC, Shaikh S, Alonso AC, Iqbal K, and Grundke-Iqbal I. Microtubule-associated protein tau: abnormal phosphorylation of a non-paired

helical filament pool in Alzheimer disease. *J Biol Chem*. 1993; 268: 24374 – 24384.

65. Kosik KS, Joachim CL, Selkoe DJ. Microtubule-associated protein tau is a major antigenic component of paired helical filaments in Alzheimer disease. *Proc Natl Acad Sci USA*. 1986; 83(11): 4044 – 4048.
66. Ksiezak-Reding H et al. Phosphate analysis and dephosphorylation of modified tau associated with paired helical filaments. *Brain Res*. 1992; 597: 209 – 219.
67. Ledesma MD, Correas I, Avila J, and Diaz-Nido J. Implications of brain cdc2 and MAP2 kinases in the phosphorylation of tau protein in Alzheimer's disease. *FEBS Letters*. 1992; 308(2): 218 – 224.
68. Lee G and Leugers CJ. Tau and tauopathies. *Prog Mol Biol Transl Sci*. 2012; 2:a006247.
69. LeCorre S, Klafki HW, Plesnila N, Hubinger G, Obermeier A, Sahagun H, et al. An inhibitor of tau hyperphosphorylation prevents serious motor impairments in tau transgenic mice*. Proc Natl Acad Sci USA.* 2006; 103: 9673 – 9678.
70. Lindwall G and Cole RD. Phosphorylation affects the ability of tau protein to promote microtubule assembly*. J Biol Chem*. 1984; 259: 5301 – 5305.
71. Lochhead PA, Kinstrie R, Sibbet G, Rawjee T, Morrice N, and Cleghon V. A chaperone-dependent GSK3β transitional intermediate mediates activation-loop autophosphorylation. *Mol Cell*. 2006; 24(4): 627 – 633.
72. Louzauo MC, Vieytes MR, and Botano LM. Effect of okadaic acid on glucose regulation. *Mini Rev Med Chem.* 2005; 5(2): 207 – 215.
73. Luo W, Dou F, Rodina A, Chip S, Kim J, Zhao Q, Moulick K, Aguirre J, Wu N, Greendard P, and Chiosis G. Roles of the heat-shock protein 90 in maintaining and facilitating the neurodegenerative phenotype in tauopathies. *Proc Natl Acad Sci USA*. 2007; 104(22): 9511 – 9516.

74. Magrané, Smith RC, Walsh K, and Querfurth HW. Heat shock protein 70 participated in the neuroprotective response to intracellularly expressed beta-amyloid in neurons. *J Neurosci*. 2004; 24(7): 1700 – 1706.
75. Mandelkow EM and Mandelkow E. Biochemistry and cell biology of tau protein in neurofibrillary degeneration. *Cold Spring Harb Perspect Med*. 2012; 2(7): a006247.
76. Merick S, Trojanowski JQ, and Lee VM-Y. Selective destruction of stable microtubules and axons by inhibition of protein serine/threonine phosphatases in cultured human neurons (NT2N cells). *Journal of Neuroscience*. 1997; 17(15): 5726 – 5737.
77. Miyata Y, Koren J, Kiray J, Dickey CA, and Gestwicki JE. Molecular chaperones and regulation of tau quality control: strategies for drug discovery in tauopathies. *Future Med Chem.* 2011; 3(12): 1523 – 1537.
78. Morimoto RI. Proteotoxic stress and inducible chaperone networks in neurodegenerative disease and aging. *Genes Dev*. 2008; 22(11): 1427 – 1438.
79. Morimoto RI and Santoro MG. Stress-inducible responses and heat shock proteins: new pharmacologic targets for cytoprotection. *Nat Biotechnol.* 1998; 16: 833 – 838.
80. Morris M, Maeda S, Vossel K, and Mucke L. The many faces of tau. *Neuron*. 2011; 70: 410 – 426.
81. Nagel F, Falkenburger BH, Tönges L, Kowsky S, Pöppelmeyer C, Schulz JB, Bähr M, and Dietz GP. Tat-Hsp70 protects dopaminergic neurons in midbrain cultures and in the substantia nigra in models of Parkinson's disease. *J Neurochem*. 2008; 105(3): 853 – 864.

82. Noble W, Hanger DP, Miller CCH, and Lovestone S. The importance of tau phosphorylation for neurodegenerative diseases. *Frontiers in Neurology*. 2013; 4(83): 1 – 11.

83. Noble W, Planel E, Zehr C, Olm V, Meyerson J, Suleman F, et al. Inhibition of glycogen synthase kinase-3 by lithium correlated with reduced tauopathy and degeneration in vivo. *Proc Natl Acad Sci USA*. 2005; 102(19): 6990 – 6995.

84. Novoselova EG, Glushkova OV, Cherenkov DA, Chudnovsky VM, and Fesenko EE. Treatment with extracellular Hsp70/Hsc70 protein can reduce polyglutamine toxicity and aggregation. *J Neurochem*. 2005; 94(3): 597 – 606.

85. Patterson KR, Ward SM, Combs B, Voss K, Kanaan NM, Morfini G, Brady ST, Gamblin TC, and Binder LI. Heat shock protein 70 prevents both tau aggregation and the inhibitory effects of preexisting tau aggregates on fast axonal transport. *Biochemistry*. 2011; 50(47): 10300 – 10310.

86. Powers ET and Balch WE. Diversity in the origins of proteostasis networks—a driver for protein function in evolution. *Nat Rev Mol Cell Biol*. 2013; 14(4): 237 – 248.

87. Price JL, Mckeel DW Jr, Buckles VD, Roe CM, Xiong C, Grundman M, et al. Neuropathology of nondemented aging: presumptive evidence for preclinical Alzheimer disease. *Neurobiol Aging*. 2009; 30: 1026 – 1036.

88. Rampelt H, Kirstein-Miles J, Nillegoda NB, Chi K. Scholz SR, Morimoto RI, and Bukau B. Metazoan Hsp70 machines use Hsp110 to power protein disaggregation. *EMBO J*. 2012; 31(21): 4221 – 4235.

89. Robertson ED, Scearce-Levie K, Palop JJ, Yan F, Cheng IH, Wu T, Gerstein H, Yu GQ, and Mucke L. Reducing endogenous tau ameliorates amyloid beta-induced deficits in an Alzheimer's disease mouse model. *Science.* 2007; 316(5825): 750 – 754.

90. Sadlish H, Rampelt H, Shorter J, Wegrzyn RD, Andreasson C, Lindquist S, et al. Hsp110 chaperones regulate prion formation and propagation in S. cerevisiae by two discrete activities. *PloS One*. 2008; 3(3): e1763.

91. Salminen A, Ojala J, Kaarniranta K, Hiltunen M, and Soininen H. Hsp90 regulates tau pathology through co-chaperone complexes in Alzheimer's disease. *Progress in Neurobiology*. 2011; 93(1): 99 – 110.

92. Santacruz K, Lewis J, Spires T, Paulson J, Kotilinek L, Ingelsson M, Guimaraes A, DeTure M, Ramsden M, McGowan E, Forster C, Yue M, Orne J, Janus C, Mariash A, Kuskoski M, Hyman B, Hutton M, and Ashe KH. Tau suppression in neurodegenerative mouse model improves memory function. *Science*. 2005; 309(5733): 476 – 481.

93. Schneider A, Biernat J, von Bergen M, Mandelkow E, and Mandelkow EM. Phosphorylation that detaches tau protein from microtubules (Ser262, Ser214) also protects it against aggregation into Alzheimer paired helical filaments. *Biochemistry*. 1999; 38(12): 3549 – 3558.

94. Shelton LB, Baker JD, Zheng D, Sullivan LE, Solanki PK, Webster JM, Sun Z, Sabbagh JJ, Nordhus BA, Koren J 3rd, Ghosh S, Blagg BSJ, Blair LJ, and Dickey CA. Hsp90 activator Aha1 drives production of pathological tau aggregates. *Proc Natl Acad Sci USA*. 2017; 114(36): 9707 – 9712.

95. Shorter J. The mammalian disaggregase machinery: Hsp110 synergizes with Hsp70 and Hsp40 to catalyze protein disaggregation and reactivation in a cell-free system. *PLoS One*. 2011; 6(10): e26319.

96. Sontag JM and Sontag E. Regulation of cell adhesion by PP2A and SV40 small tumor antigen: an important link to cell transformation. *Cell Mol Life Sci*. 2006; 63(24): 2979 – 91.

97. Souid-Mensi G, Moukha S, Mobio TA, Maaroufi K, and Creppy EE. The cytotoxicity and genotoxicity of okadaic acid are cell-line-dependent. *Toxicon*. 2008; 51(8): 1338 – 1344.

98. Suganama M, Fujiki H, Suguri H, Yoshizawa S, Hirota M, Nakayasu M, Ojika M, Wakamatsu K, Yamada K, and Sugimara T. Okadaic acid: an additional non-phorbitol-12-tetradecanoate-13-acetate-type tumor promoter. *Proc Natl Acad Sci USA*. 1988; 85(6): 1768 – 1771.

Medina M, Avila J, and Villaneuva N. Use of okadaic acid to identify relevant phosphoepitopes in pathology: a focus on neurodegeneration. *Mar Drugs*. 2013; 11(5): 1656 – 1668.

99. Sundaram JR, Poore CP, Sulaimee NH, Pareek T, Asad AB, Rajkumar R, et al. Specific inhibiton of p25/Cdk5 activity by the Cdk5 inhibitory peptide reduces neurodegeneration in vivo. *J Neurosci*. 2013; 33: 334 – 343.

100. Swingle M, Ni L, and Honkanen RE. Small-molecule inhibitors of ser/thr protein phosphatases: specificity, use and common forms of abuse. *Methods Mol Biol*. 2007; 365: 23 – 38.

101. Taylor RC and Dillin A. Aging as an event of proteostasis collapse*. Cold Spring Harbor Perspectives in Biology*. 2011; 3: a004440.

102. Thompson AD, Scaglione KM, Prensner J, Gillies AT, Chinnaiyan A, Paulson HL, Jinwal UK, Dickey CA, and Gestwicki JE. Analysis of the tau-associated proteome reveals that exchange of Hsp70 for Hsp90 is involved in tau degradation. *ACS Chem Biol*. 2012; 7(10): 1677 – 1686.

103. Tortosa E, Santa-Maria I, Moreno F, Lim F, Perez M, and Avila J. Binding of Hsp90 to tau promotes a conformational change and aggregation of tau protein. *J Alzheimers Dis*. 2009; 17(2): 319 – 325.

104. Vale C and Botana LM. Marine toxins and the cytoskeleton: okadaic acid and dinophysistoxins. *FEBS J*. 2008; 275: 6060 – 6066.

105. Valdiglesias V, Laffon B, Pásaro E, and Méndez J. Evaluation of okadaic acid-induced genotoxicity in human cells using the micronucleus test and γH2AX analysis. *J Toxicol Environ Health A*. 2011; 74(15 – 16): 980 – 982.

106. Valdiglesias V, Laggon B, Pásaro E, and Méndez J. Okadaic acid induces morphological changes, apoptosis, and cell cycle alteration in different human cell types. *J Environ Monit.* 2011; 13(6): 1831 – 1840.

107. Valdiglesias V, Laffon B, Pásaro E, Cemeli E, Anderson D, and Méndez J. Induction of DNA damage by the marine toxin okadaic acid depend on human cell type. *Toxicon*. 2011; 57(6): 882 – 888.

108. Valdiglesias V, Prego-Faraldo MV, Pásaro E, Méndez J, and Laffon B. Okadaic acid: more than a diarrheic toxin. *Marine Drugs*. 2013; 11(11): 4328 – 4349.

109. Voss K, Combs B, Patterson KR, Binder LI, and Gamblin TC. Hsp90 alters tau function and aggregation in an isoform specific manner. *Biochemistry*. 2012; 51(4): 888 – 898.

110. Wandinger SK, Richter K, and Buchner J, The Hsp90 chaperone machinery. *J Biol Chem.* 2008; 283: 18472 – 18477.

111. Wang J, Tung YC, Wang Y, Li XT, Iqbal K, Grundke-Iqbal I. Hyperphosphorylation and accumulation of neurofilament proteins in Alzheimer disease brain and in okadaic acid-treated SY5Y cells. *FEBS Letters*. 2001; 507(1): 81 – 87.

112. Wang X, Blanchard J, Tung YC, Grundke-Iqbal I, and Iqbal K. Inhibition of protein phosphatase-2A (PP2A) by I1PP2A leads to hyperphosphorylation of tau,

neurodegeneration, and cognitive impairment in rats. *J Alzheimer's Disease*. 2015; 45(2): 423 – 435.

113. Wu X, Kosaraju J, and Tam KY. SLM, a novel carbozole-based fluorophore attenuates okadaic acid-induced tau hyperphosphorylation via downregulating GSK-3β activity in SH-SY5Y cells. *European Journal of Pharmaceutical Sciences*; 2017. 110: 101 – 108.

114. Zhang Z and Simpkins JW. Okadaic acid induces tau phosphorylation in SH-SY5Y cells in an estrogen-preventable manner. *Brain Res*. 2010; 1345: 176 – 181.

Figure 1. Tau protein hyperphosphorylation and chaperone proteins.

A.) Human tau phosphorylation in Alzheimer's disease. Exon 2 and 3 are located near the N-terminus of tau protein.

B.) Chaperone protein structures. Hsp110: crystal structure of Sse1, yeast Hsp110 as a complex with ATP, PDB 2QXL (Liu Q and Henderson WA, 2007). Full-length Hsp90 crystal structure of HtpG from E. coli is shown bound to ADP (PDB 2IOP; Shiau AK, et al., 2006). The crystal structure of human Hsp70 nucleotide binding domain with the mutation R272K is shown bound to ADP (PDB 5BN9; Narayanan D, et al., to be published).

C.) Experimental setup for okadaic acid treatment of undifferentiated (1) and differentiated (2) SH-SY5Y cells.

A

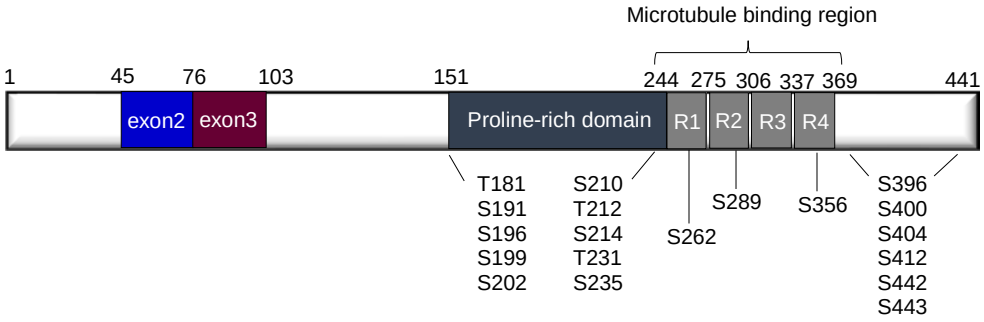

B

Hsp110
PDB 2QXL
S. cerevisiae

Hsp90
PDB 2IOP
E. coli

Hsp70 NBD
PDB 5BN9
Hs

C

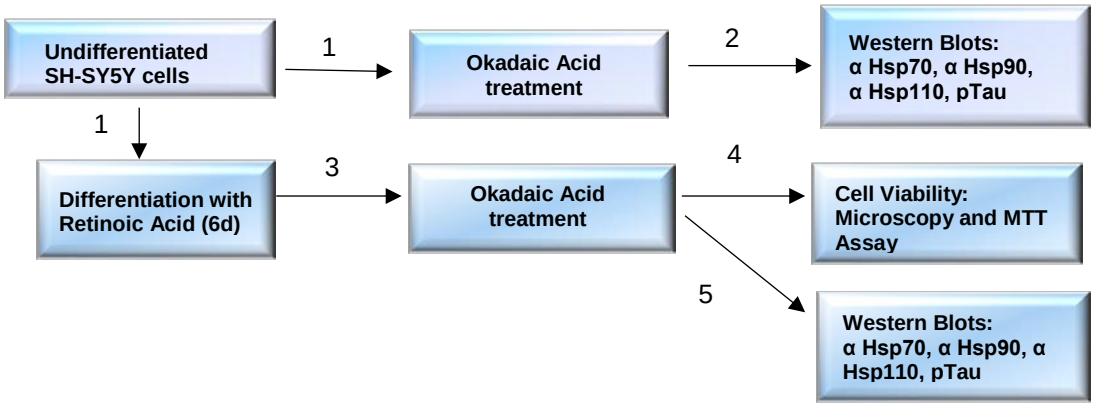

Figure 2. Undifferentiated SH-SY5Y cell response to okadaic acid treatment.

A.) Undifferentiated SH-SY5Y morphology. Scale bar indicates 100 μm.

B.) Morphology of SH-SY5Y cells after retinoic acid-induced differentiation. SH-SY5Y cells were treated with retinoic acid (10μM) for six days to induce morphological changes such as neurite extension. Scale bar indicates 100 μm.

C.) Western blots of undifferentiated SH-SY5Y cells. Cells were treated with 0 nM, 50 nM, and 100 nM okadaic acid for 24 hours in culture media. Antibodies were used to determine protein levels of Hsp90, Hsp70, Hsp110, and the phosphorylated tau protein epitope Thr212.

A

Undifferentiated SH-SY5Y cells

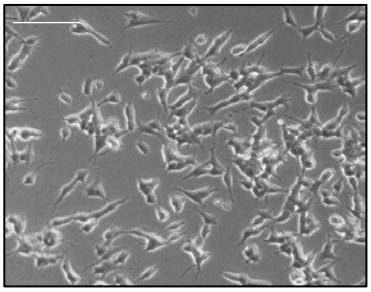

B

Differentiated SH-SY5Y cells

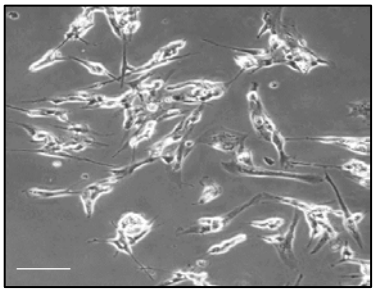

C

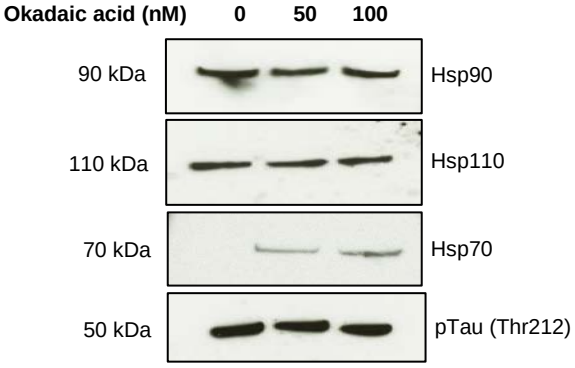

Figure 3. Differentiated cell response to okadaic acid. A.) Cells treated with 0 nM, 25 nM, 50 nM, and 100 nM okadaic acid for 3 hours. Microscopy of the cells shows that the 50 nM dose of okadaic acid at 3 hours is lethal to cells (40x objective). Cells are rounded and floating when treated with 100 nM okadaic acid for 3 hours (20x objective). The 50 nM dose of okadaic acid at 8 hours causes cells to lose morphology (40x objective). The 100 nM dose of okadaic acid at 8 hours causes widespread cell death (20x objective). After 3 hours of okadaic acid exposure, cells treated with 10 and 25 nM okadaic acid do not show changes in morphology or viability compared to vehicle-treated cells. **B.)** Cells do not show changes in cell viability after 8 hours of exposure to 10 nM and 25 nM okadaic acid. **C.)** Cells treated with 10 nM and 25 nM okadaic acid for 3 hours do not have significantly different percent cell viability compared to vehicle-treated cells. **D.)** Cells exposed to 10 nM and 25 nM okadaic acid for 6 hours show reduced cell viability compared to vehicle-treated cells. **E.)** Cells treated with 10 nM and 25 nM okadaic acid show a significant decrease in viability after 24 hours of treatment. **F.)** Absorbance values at 490 nm over 3, 6, and 24 hours of okadaic acid treatment of differentiated SH-SY5Y cells. Cell viability decreases over time and levels off at 24 hours of okadaic acid treatment. **G.)** Morphology of differentiated SH-SY5Y cells treated with 10 nM okadaic acid for 3 hours. For all microscopy images, scale bar indicates 100 µm.

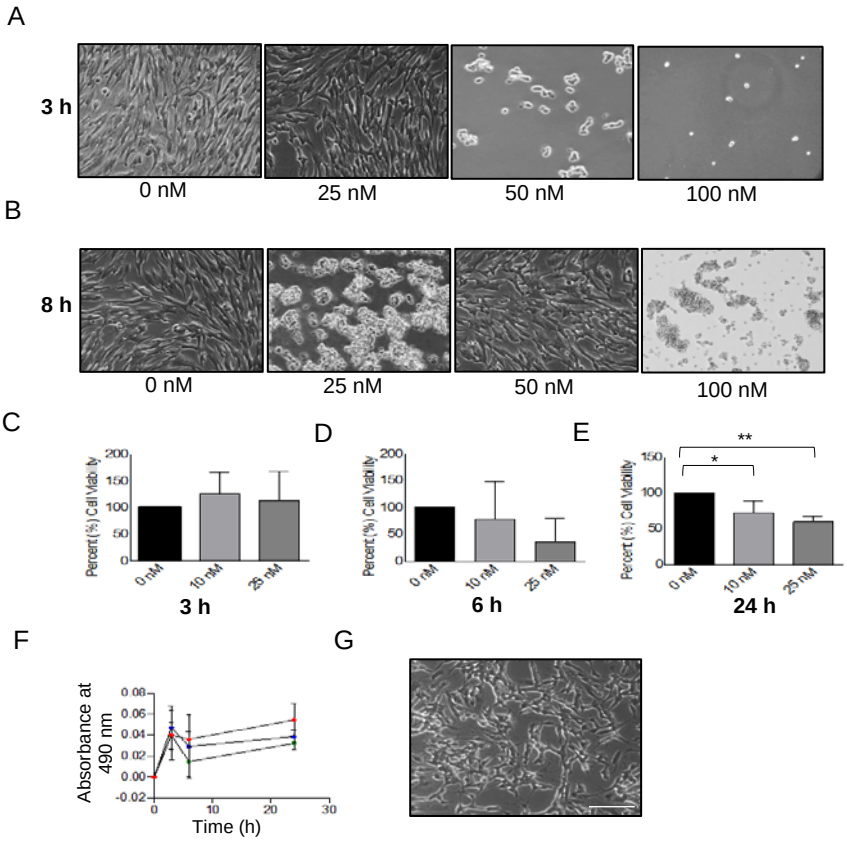
A
3 h
0 nM
25 nM
50 nM
100 nM
B
8 h
0 nM
25 nM
50 nM
100 nM
C
Percent (%) Cell Viability
0 nM
10 nM
25 nM
3 h
D
Percent (%) Cell Viability
0 nM
10 nM
25 nM
6 h
E
**
*
Percent (%) Cell Viability
0 nM
10 nM
25 nM
24 h
F
Absorbance at 490 nm
Time (h)
G

Figure 4. Chaperone protein expression levels in okadaic acid-treated differentiated SH-SY5Y cells over time.

A.) SH-SY5Y cells were exposed to okadaic acid for 3 hours and 25 µg of cell lysate was run on SDS-PAGE and immunoblotted.

B.) SH-SY5Y cells were exposed to okadaic acid for 6 hours and 15 µg of cell lysate was run on SDS-PAGE and immunoblotted.

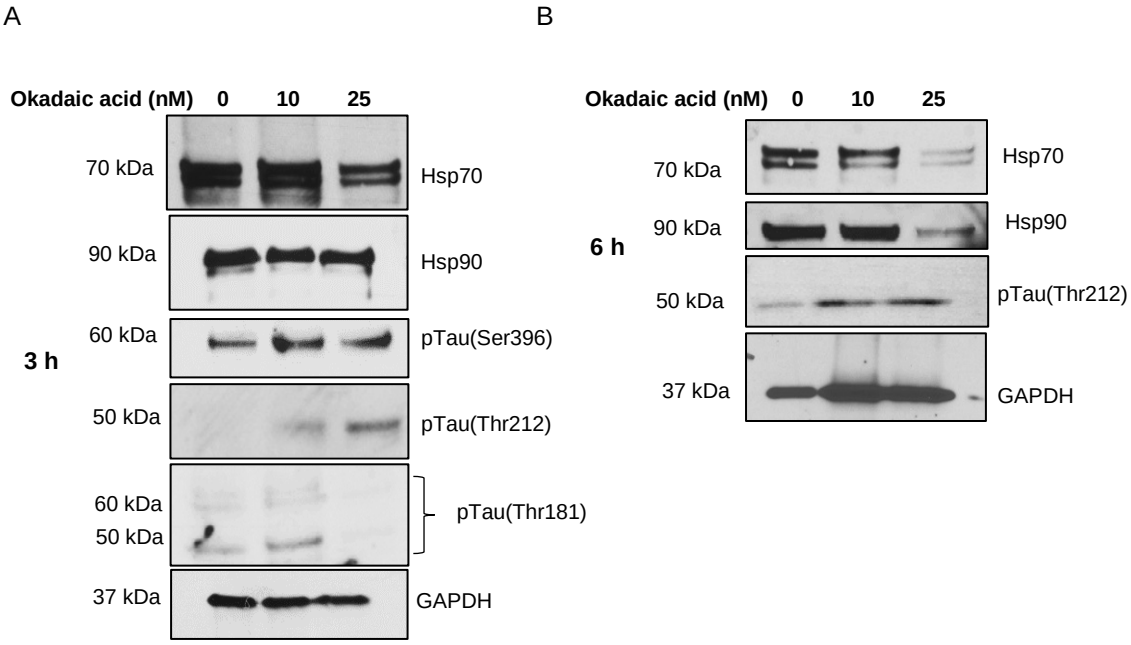
A
B
Okadaic acid (nM) 0 10 25
3 h
70 kDa
Hsp70
90 kDa
Hsp90
60 kDa
pTau(Ser396)
50 kDa
pTau(Thr212)
60 kDa
50 kDa
pTau(Thr181)
37 kDa
GAPDH
Okadaic acid (nM) 0 10 25
6 h
70 kDa
Hsp70
90 kDa
Hsp90
50 kDa
pTau(Thr212)
37 kDa
GAPDH

Figure 5. Model of chaperone-mediated tau assembly into neurofibrillary tangles. Hsp70 and Hsp110 destabilize fibrils and aggregates of tau. By contrast, Hsp90 stabilizes misfolded tau and facilitates the assembly of tau into fibrils and ordered aggregates.

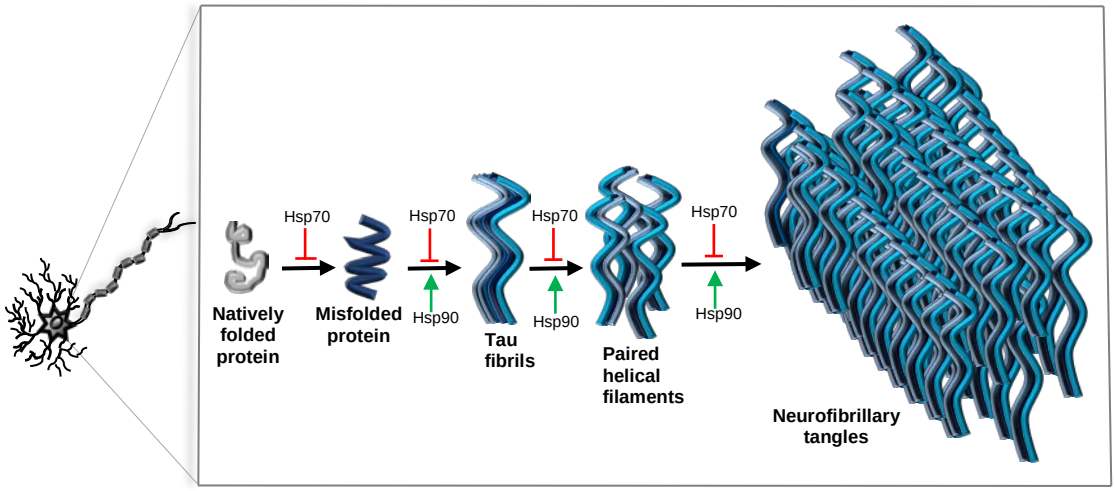
Hsp70
Hsp70
Hsp70
Hsp70
Hsp90
Hsp90
Hsp90
Natively folded protein
Misfolded protein
Tau fibrils
Paired helical filaments
Neurofibrillary tangles

Figure S1. Time-course viability of differentiated SH-SY5Y cells in response to okadaic acid treatment.

A.) SH-SY5Y cells were treated with retinoic acid (10 μM) for 6 days and subsequently treated with 0, 10, and 25 nM okadaic acid for 3, 6, and 24 hours. Phase-contrast microscopy. Scale bar indicated 100 μm.

B.) Percentage of viable cells decreases in response to increasing doses of okadaic acid after 24 hours of exposure. Cells treated with vehicle only, 0.1% ethanol, had 100% viability.

C.) Cell viability in response to treatment with 0, 10, and SH-SY5Y cells treated with 0, 10, 25, 30, and 50 nM okadaic acid for 42 hours.

A

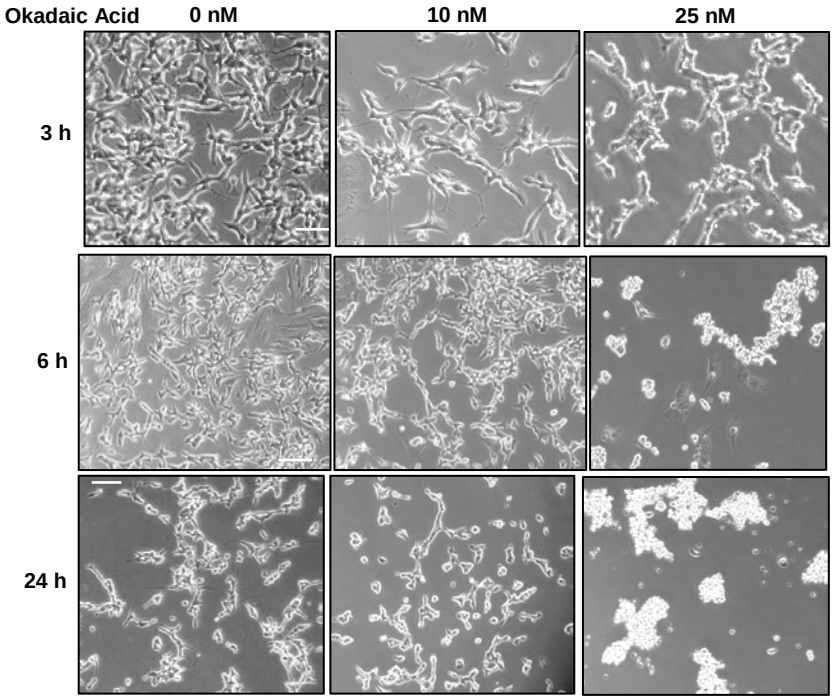
Okadaic Acid
0 nM
10 nM
25 nM
3 h
6 h
24 h

B

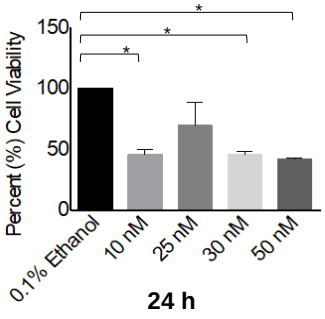
Percent (%) Cell Viability
150
100
50
0
*
*
*
0.1% Ethanol
10 nM
25 nM
30 nM
50 nM
24 h

C

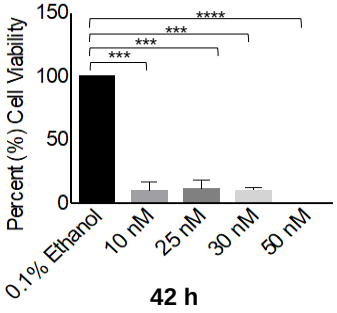
Percent (%) Cell Viability
150
100
50
0
****
***
***
***
0.1% Ethanol
10 nM
25 nM
30 nM
50 nM
42 h

Figure S2. Differentiated SH-SY5Y morphology and chaperone protein expression in response to okadaic acid.

A.) Microscopy of differentiated SH-SY5Y were treated with 0 nM okadaic acid and 25 nM of okadaic acid for 24 hours and with 50 nM okadaic acid for 3 hours.

B.) Cells were treated with 50 nM okadaic acid for 3 hours and 25 nM okadaic acid for 24 hours. Tau protein levels after okadaic acid treatment. Total tau levels do not change, but the phospho-Tau epitope Thr212 is reactive to okadaic acid-induced tau hyperphosphorylation.

C.) ATP-dependent chaperone protein levels after okadaic acid treatment. Cells were treated with 50 nM okadaic acid for 3 hours and 25 nM okadaic acid for 24 hours. Hsp70 levels decrease in response to prolonged OA exposure. Hsp90 shifted in migration in response okadaic acid induced PP2A inhibition.

A

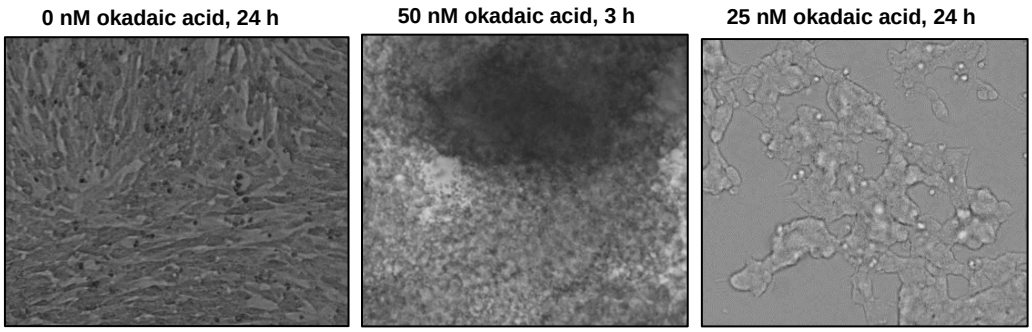
0 nM okadaic acid, 24 h
50 nM okadaic acid, 3 h
25 nM okadaic acid, 24 h

B

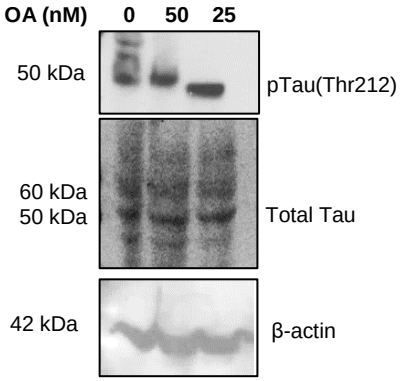
OA (nM) 0 50 25
50 kDa
pTau(Thr212)
60 kDa
50 kDa
Total Tau
42 kDa
β-actin

C

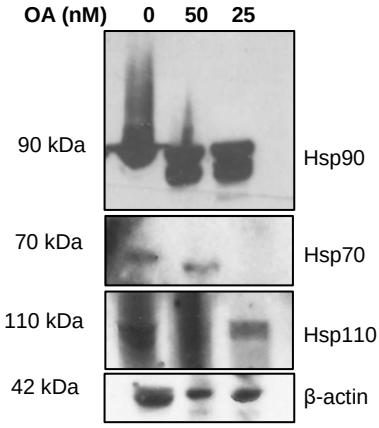
OA (nM) 0 50 25
90 kDa
Hsp90
70 kDa
Hsp70
110 kDa
Hsp110
42 kDa
β-actin

Figure S3. Expression of Hsp70 in SH-SY5Y cells treated with okadaic acid for 24 hours. Cells treated with 10 nM okadaic acid show an increase in Hsp70 levels compared to vehicle-treated cells.

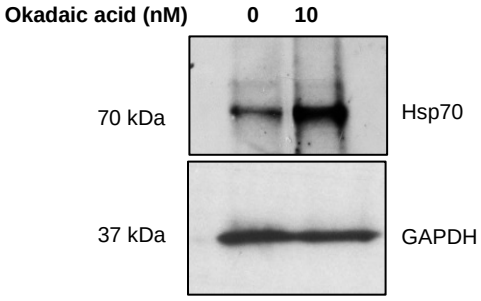
Okadaic acid (nM)
0
10
70 kDa
Hsp70
37 kDa
GAPDH

Table S1. Okadaic acid doses required to observe in vitro changes in tau phosphorylation levels.

Okadaic Acid Dose	Length of Exposure	Phospho-Tau Epitope	Reference
40 nM	8 hours	Ser404	Ma XH, et al. *Brain Res*. 2018; 1690: 1 – 11.
30 nM	36 hours	Ser202/Thr205 Thr212 Thr231 Ser262	Wu X, et al. *European Journal of Pharmaceutical Sciences.* 2017; 110: 101 – 108.
100 nM	3 hours	Thr205	Zhang Z and Simpkins JW. *Brain Res*. 2010; 1345: 176 – 181.
50 nM and 100 nM	2 hours	Ser202/Thr205	Choi S, et al. *Cell Mol Neurobiol*. 2015; 35: 1049 – 1059.

Appendix A

Publication status: formatted for submission as a short communication to *Journal of Molecular Biology*

Title: Engineering AAA+ Chaperone Proteases with Enhanced Substrate Specificity for Amyloid Protein Aggregates

Authors: Shannon E. May[1,2] and Jodi L. Camberg[1,2,3]

Author Affiliations:

[1] Interdisciplinary Neurosciences Program, University of Rhode Island, Kingston, RI 02881

[2] George and Anne Ryan Institute for Neuroscience, University of Rhode Island, Kingston, RI 02881

[3] Department of Cell and Molecular Biology, College of the Environment and Life Sciences, University of Rhode Island, Kingston, RI 02881

Author Contributions: S.E.M. designed experiments, performed experiments, interpreted data and wrote paper; J.L.C. designed experiments, interpreted data, and wrote paper.

Address correspondence to: Jodi L. Camberg, 120 Flagg Road, CBLS, Room 470, University of Rhode Island, Kingston, RI 02881

Keywords: chaperone protein, ClpXP, AAA+ protein, aggregates

Abstract

Protein aggregates are thought to be the end result of derailed protein quality control pathways, which are impaired during aging (1). The protein quality control system involves different pathways that manage and regulate protein folding and aggregation. Misfolded proteins such as Aβ peptide, tau, alpha-synuclein, and yeast prion proteins (insoluble Sup35 protein) share the motif of stacked, in-register beta sheets; thus, these misfolded proteins represent different types of amyloid protein (2). Amyloid proteins have stable, low-energy conformations that are resistant to protein degradation (3). Important components of the protein quality control network are molecular chaperones. Restoring protein homeostasis by modulating chaperone proteins may provide disease-modifying therapeutic strategies for managing neurodegenerative diseases (4). We hypothesize that *E. coli* ClpX and ClpXP expressed in *S.cerevisiae* will not recognize Sup35 amyloid fibers. Decreasing the substrate specificity of the chaperone protein complex ClpXP may result in a novel chaperone tool with enhanced specificity for amyloid aggregates that can both bind and degrade amyloids. Thus, we constructed and expressed a novel chimeric protein in the [PSI^{+}] yeast prion system, an extensively utilized model of amyloid assembly, to determine if non-native chaperone proteins affect prion propagation and amyloid assembly.

In the cell, protein homeostasis is regulated by chaperone proteins that can remodel and degrade misfolded, unfolded, and aggregate proteins. ClpXP and Hsp104 are chaperone proteins that belong to the AAA+ superfamily of ATPases (5). The AAA+ (ATPases associated with diverse cellular activities) superfamily of ATP-dependent enzymes have highly conserved domains and function as chaperones and/or proteases to manage protein folding and multiprotein complexes (5). The Clp/Hsp100 family of ATP-dependent enzymes within the AAA+ protein superfamily includes the cytosolic proteins ClpX, ClpA, and Hsp104. Members of the Clp/Hsp100 family refold or degrade protein assemblies, misfolded proteins, and aggregated proteins (6). Within the Clp/Hsp100 family, ATPases (ClpX) partner with a peptidase (ClpP) to form stacked, barrel-like structures that functions as chaperone proteases (6). The chaperone ATPase component of this complex threads polypeptides through the central axial channel of the chaperone protease complex into the peptidase chamber for degradation (7).

ClpXP is an ATP-dependent chaperone protease that binds to and degrades an estimated 50 substrate proteins based on proteomic analysis (8). ClpX forms a hexameric ring that binds to ClpP, which forms stacked heptameric rings; thus, there is asymmetrical binding between ClpX and ClpP (9, 10). ClpX contains an N-domain, a large nucleotide-binding domain (AAA+ domain), and a small AAA+ domain (11). The N-domain of ClpX forms dimers that are connected to the large AAA+ domain by a flexible linker region and functions to bind adaptors, client proteins, and stabilize the hexameric structure of ClpX (12). Substrate recognition by ClpX requires the presence of short peptide sequences, or degradation tags, on client proteins, on the C-terminus or N-terminus of client proteins (5, 83). An example of a C-terminal degradation tag recognized by ClpX is the ssrA tag, an 11-amino acid peptide

signaling sequence on substrate proteins (8, 13, 14, 15). The ClpX N-domain is required for recognition of several client proteins, such as the λO protein and the UmuD subunit of UmuD·D' DNA polymerase (11).

The chaperone ATPase ClpXP couples ATP binding and hydrolysis to mechanical force, which is required for translocation of polypeptides through the axial channel of ClpX into the cavity of ClpP, a serine protease (16). The pore loops (GYVG) in the axial channel of ClpX grip and processively thread unfolded polypeptides through the narrow central channel of ClpX into the ClpP barrel (11, 13, 17). ClpX also functions independently of ClpP as a chaperone protein to remodel misfolded proteins in vitro and in vivo and disassemble protein complexes, notably the MuA transposase tetramer (19 – 21). Biochemical studies have shown that ClpX functions at small step sizes to perform mechanical work, which allows the enzyme to generate substantial force to remodel diverse sets of substrate proteins (21).

Lon is a chaperone protease that belongs to the AAA+ superfamily of ATPases. Unlike ClpX, Lon can bind to a wider range of substrates and recognizes surface-exposed hydrophobic residues on misfolded or unfolded proteins (22). Both ClpXP and Lon bind to proteins via the recognition of degradation signals on the C-terminus or N-terminus of substrate proteins (5, 8). The N-domain of Lon contains three amino acid residues that bind to the degradation signal of the substrate SulA (23). ClpX and Lon associate with aggregates in bacteria, but it is currently unknown if Lon can disassemble aggregates in vivo (24, 25).

The only member of the Clp/Hsp100 proteins within the AAA+ protein superfamily that can disaggregate proteins is the chaperone protein Hsp104 (26). In *Saccharomyces cerevisiae*, deletion and overexpression of Hsp104 modulate prion propagation and thus alter the [PSI^+] prion phenotype in yeast; thus, changes in the

basal levels of Hsp104 “cures” yeast of the [PSI$^+$] prion phenotype (27, 28). The N-domain of Hsp104 (amino acid residues 1 – 147) is required for [PSI$^+$] prion curing in *S. cerevisiae*, but is not required for thermotolerance or [PSI$^+$] prion propagation (Hung and Masison, 2006). Overexpression of Hsp104 is neuroprotective in models of Parkinson’s disease, suggesting that Hsp104 can also bind to human prion proteins, such as alpha-synuclein (30).

Engineered chimeric AAA+ chaperone proteases can refold aggregates and degrade misfolded proteins. The ClpB variant referred to as BAP associates with the ClpP peptidase and functions to both disaggregate and degrade aggregates in cooperation with the co-chaperone bacterial protein DnaK (31). Moreover, an Hsp104 variant called HAP was engineered to display both disaggregation and proteolytic activity; HAP consists of Hsp104 in association with ClpP (32). Replacing the helix-loop-helix region of Hsp104 and ClpB with the helix-loop-helix from ClpA containing the IGL/F motif required for ClpP association allows both ClpB and Hsp104 to translocate segments of polypeptides extracted from misfolded proteins into the ClpP protease barrel (31, 32). Therefore, we hypothesized that engineering a novel chaperone protease containing the N-domain of Hsp104 and the ClpXΔNTD sequence in association with ClpP could bind to and proteolytically degrade amyloid proteins.

Before testing this hypothesis, we first tested if AAA+ chaperone proteins could affect prion propagation in the [PSI$^+$] yeast prion model of amyloid assembly. We utilized two approaches to answering this research question. First, we screened domain-specific mutations Lon in the *S. cerevisiae* [PSI$^+$] model of amyloid assembly to identify variants with enhanced amyloid substrate recognition. Next, we engineered a novel chaperone protease and expressed the construct in the [PSI$^+$] yeast amyloid

model to determine if the chimeric protein had enhanced recognition of amyloid. We hypothesized that the chimeric protein would resolubilize amyloid protein, thereby abrogating prion propagation.

Results

Random mutations in the N-domain of Lon (amino acid residues 1 – 307) were generated with an error-prone DNA polymerase with the goal of decreasing substrate specificity of Lon. Decreasing the substrate specificity of Lon could result in substrate recognition of fibrillar amyloid proteins. We hypothesized that wild-type Lon would not recognize Sup35 amyloid fibers in yeast. After cloning wild-type *lon* into the double expression vector pYES2 and transforming this construct in [PSI$^+$] yeast, we observed that the phenotype of the colonies was the same as [PSI$^+$] yeast cells containing the empty vector pYES2 (Figure S1). This suggests that prion propagation was not altered by the expression of the *E. coli* chaperone protease Lon in *S. cerevisiae*. Next, we investigated if the expression of *E. coli* ClpXP affects prion propagation and amyloid assembly in [PSI$^+$] yeast by transforming the construct pESC-URA + ClpXP (Marissa Viola) into yeast. We observed expression of ClpXP in [PSI$^+$] yeast did not change the prion phenotype; yeast colonies were white, which is associated with a [PSI$^+$] prion phenotype (Figure S2A). We analyzed the phenotype of yeast lysates containing ClpXP using a novel spectrophotometric liquid assay to detect the red pigment from *ade2-1* yeast mutants that accumulates in [psi$^-$] yeast cells. Extraction of protein from yeast cells using Y-PER (Thermo Fisher Scientific), normalization of yeast lysates, and excitation of lysates at 488 nm showed that yeast expressing ClpXP has a similar emission profile as [PSI$^+$] yeast containing empty pYES2 vector (Figure SB). Thus, wild-type Lon and ClpXP do not recognize Sup35 prion in the

[PSI$^+$] amyloid model system in vivo and do not modulate prion propagation or curing of [PSI$^+$] prion in yeast.

Mutations were randomly generated at a low frequency in the Lon N-domain and transformed into XL Gold *E. coli* cells. Clonal isolate plasmid DNA was recovered and transformed into [PSI$^+$] *S. cerevisiae.* In total, 116 clonal isolates derived from the random mutagenesis of the N-domain of Lon were screened in [PSI$^+$] yeast. Of these mutations, no hits in the [PSI$^+$] colorimetric screen were found. A hit in the screen was defined as a mutation in *lon* that was associated with a uniform pink or red phenotype in [PSI$^+$] *S. cerevisiae.* Hits in the screen were sequenced to classify the mutation(s) in *lon*. Sequencing results showed that a hit in the screen had multiple mutations (> 5 mutations) and a frameshift mutation at nucleotide base pair 157. Therefore, we did not identify any residues in Lon associated with altered substrate recognition by domain-specific point mutations. Thus, we did not discover mutant gene copies of *lon* that modified the interaction between Lon and Sup35 amyloid to improve amyloid recognition.

Next, we investigated if engineered chaperone proteases could recognize and disassemble Sup35 prion fibrils in vivo. The AAA+ protein superfamily consists of a diverse set of ATP-dependent chaperone proteins that have highly conserved domains (Figure 1A). Within the AAA+ superfamily, distinct families of chaperone proteins are grouped together based on their domain architecture (67). We cloned the N-domain of Hsp104 and the ClpXΔNTD sequence into pESC-URA+ClpXP. First, *clpX* was constructed and expressed in the double expression vector pYES2 (Invitrogen). Primers were designed to insert a HindII restriction enzyme site upstream of the *clpX* sequence and insert an XhoI restriction enzyme site downstream of the *clpX* sequence (Table 1). Site-directed mutagenesis was carried

out using the QuikChange II XL Site-directed Mutagenesis kit. To express the ClpX sequence without the N-terminal domain (ClpXΔNTD), both pYES2 and pYES2+ClpX were double digested using the restriction enzymes SacI and NotI (New England Biolabs), resulting in linearized DNA that was subsequently ligated overnight at 16°C. The ligation products were heat inactivated at 65°C and ligation products were transformed into XL Blue chemically competent *Escherichia coli* cells (Agilent). Sanger sequencing of the construct confirmed that the ClpXΔNTD sequence (1092 base pairs) was successfully cloned into the pYES2 vector.

In order to express the Hsp104 N-terminal domain (amino acid residues 1 – 161) in the pYES2+ClpXΔNTD construct, restriction enzyme sites flanking the Hsp104 N-domain sequence were cloned into the pYS104 vector using the polymerase chain reaction (PCR). Upstream of the Hsp104 N-domain, a KpnI site, 5' GGTACC 3', was inserted and downstream of the Hsp104 N-domain a SacI site was inserted. The pYS104 construct containing SacI and KpnI sites and the vector pYES2 were double digested with KpnI and SacI. Ligation was carried out with 80 ng of pYES2 vector. Subsequently, a NotI restriction enzyme site, 5' GCGGCCGC 3', was inserted at the beginning of the N-domain of ClpX and a SacI site was inserted at the end of the ClpX sequence in the vector pYES2.

Sanger sequencing of the vector pYES2 + Hsp104 N-domain + ClpXΔNTD showed that a spontaneous mutation arose; a transition substitution occurred at nucleotide base pair 928 of the ClpXΔNTD sequence. To correct this, primers were designed to mutate thymine to cytosine at base pair 928 of ClpXΔNTD. In order to express the Hsp104 N-domain + ClpXΔNTD construct in the vector pESC-ura+ClpP (constructed by Marissa Viola), the pYES2 + Hsp104 N-domain + ClpXΔNTD construct and the pESC-URA + ClpP construct were double digested using the

restriction enzymes NotI and SacI (New England Biolabs). Subsequently, ligation reactions were carried out with 100 ng of pESC-URA + ClpP vector (9000 base pairs) per reaction. Ligation products were heat inactivated and transformed into XL Blue chemically competent *E. coli* cells.

The chimeric protein Hsp104 + ClpXΔNTD + ClpP has an N-terminal domain from Hsp104, and ATPase domain from ClpX, and the ClpP full-length sequence (Figure 1B). The chimeric protein Hsp104 + ClpXΔNTD + ClpP was transformed into [PSI^+] yeast and grown on SD-URA plates for five days at 30°C. The chimeric protein did not alter [PSI^+] phenotype in yeast (Figure 1C). To determine if ClpX and ClpP protein were expressed in yeast, lysates were extracted, normalized, and immunoblotted. We found that yeast containing the chimeric protein did express ClpX and ClpP (Figure 2A). Moreover, spectrophotometric analysis of yeast lysates using a novel [PSI^+] assay that we developed showed that level of red pigmentation, which accumulates in [psi^-] yeast, is reduced in yeast expressing the chimeric proteins Hsp104 NTD + ClpXΔN and Hsp104 NTD + ClpXΔN + ClpP compared to yeast overexpressing Hsp104 from the plasmid PYS104 and yeast expressing the Walker B NBD1 mutation Hsp104(E285Q) (Figure 2B).

Based on our findings, the chimeric protein Hsp104 NTD + ClpXΔN + ClpP does not cure [PSI^+] yeast of Sup35 prion. However, it is possible that the novel chaperone protease could enhance prion propagation by severing amyloid fibrils and generating amyloid seeds for nucleated polymerization of Sup35 protein, thereby facilitating the amyloid assembly of Sup35 (Figure 3). The chimeric protein Hsp104 NTD + ClpXΔN + ClpP hypothetically could recognize all targets of Hsp104. Future biochemical assays with this protein should be done to determine if the protein has enhanced binding of amyloid compared to Hsp104 wild-type protein. Degradation

assays would determine whether the chimeric protein is degrading amyloid fibrils into small peptides and thereby functioning as a chaperone protease.

References:

1. Saez I and Vilchez D. The mechanistic links between proteasome activity, aging, and age-related diseases*. Curr Genomics*. 2014; 15(1): 38 – 51.
2. Cobb NJ, Sonnichsen FD, McHaourab H, and Surewicz WK. *Proc Natl Acad Sci USA*. 2007; 104(48): 18946 – 18951.
3. Vashist S, Cushman M, and Shorter J. Applying misfolded Hsp104 to protein-misfolding disorders. *Biochem Cell Biol*. 2010; 88(1): 1 – 13.
4. Voisine C, Pedersen JS, and Morimoto RI. Chaperone networks: tipping the balance in protein folding diseases. *Neurobiol Dis*. 2010; 40(1): 12 – 20.
5. Sauer RT and Baker TA. AAA+ Proteases: ATP-fueled machines of protein destruction. *Annu Rev Biochem*. 2011; 80: 587 – 612.
6. Burton BM and Baker TA. Remodeling protein complexes: Insights from the AAA+ unfoldase ClpX and Mu transposase. *Protein Science*. 2005; 14(8): 1945 – 1954.
7. Ishikawa T, Beuron F, Kessel M, Wickner S, Maurizi MR, and Steven AC. Translocation pathway of protein substrates in ClpAP protease. *Proc Natl Acad Sci USA*. 2001; 98(8): 4328 – 4333.
8. Flynn JM, Neher SB, Kim YI, Sauer RT, and Baker TA. Proteomic discovery of cellular substrates of the ClpXP protease reveals five classes of ClpX-recognition signals. *Mol Cell*. 2003; 11(3): 671 – 683.
9. Sauer RT, et al. Sculpting the proteome with AAA+ proteases and disassembly machines. *Cell*. 2004; 119: 9 – 18.

10. Wang J, Hartling JA, and Flanagan JM. The structure of ClpP at 2.3 A resolution suggest a model for ATP-dependent proteolysis. *Cell*. 1997; 91: 447 – 456.
11. Baker TA and Sauer RT. ClpXP, an ATP-powered unfolding and protein-degradation machine. *Biochimica et Biophysica Acta*. 2012; 1823: 15 – 28.
12. Wojtyra UA, Thibault G, Tuite A, and Houry WA. The N-terminal zinc binding domain of ClpX is a dimerization domain that modulates the chaperone function. *J Biol Chem*. 2003; 278: 489981 – 48990.
13. Gottesman S, Roche E, Zhou YN, and Sauer RT. The ClpXP and ClpAP proteases degrade proteins with C-terminal peptide tails added by the SsrA tagging system. *Genes Dev*. 1998; 12(9): 1338 – 1347.
14. Flynn JM, Levchenko I, Seidel M, Wickner SH, Sauer RT, and Baker TA. Overlapping recognition determinants within the ssrA degradation tag allow modulation of proteolysis. *Proc Natl Acad Sci USA*. 2001; 98(19): 10584 – 10589.
15. Kim YI, Burton, RE, Burton BM, Sauer RT, and Baker TA. Dynamics of substrate denaturation and translocation by the ClpXP degradation machine. *Mol Cell*. 2000; 5(4): 639 – 648.
16. Glynn SE, Martin A, Nager AR, Baker TA, and Sauer RT. Structures of asymmetric ClpX hexamers reveal nucleotide-dependent motions in a AAA+ protein-unfolding machine. *Cell*. 2009; 139: 744 – 745.
17. Maillard RA, Chistol G, Sen M, Righini M, Jiongyi T, Kaiser CM, Hodges C, Martin A, and Bustamante C. ClpXP generates mechanical force to unfold and translocate its protein substrates. *Cell*. 2011; 145(3): 459 – 469.
18. LaBreck CJ*, May S*, Viola MG*, Conti J, and Camberg JL. The ATP-dependent chaperone ClpX targets native and non-native aggregated substrates for remodeling, disassembly, reactivation and degradation. *Front Mol Biosci*. 2017; 12(1): e0170505.

19. Levchenko I, Luo L, and Baker TA. Disassembly of the Mu transposase tetramer by the ClpX chaperone. *Genes Dev*. 1995; 9: 2399 – 2408.
20. Kruklitis R, Welty DJ, and Nakai H. ClpX protein of *Escherichia coli* activates bacteriophage Mu transposase in the strand transfer complex for initiation of Mu DNA synthesis. *EMBO J*. 1996; 15(4): 935 – 944.
21. Aubin-Tam ME, Olivares AO, Sauer RT, Baker TA, and Lang MJ. Single-molecule protein unfolding and translocation by an ATP-fueled proteolytic machine. *Cell*. 2011; 145: 257 – 267.
22. Gur E and Sauer RT. Recognition of misfolded proteins by Lon, a AAA(+) protease. *Genes Dev*. 2008; 22(16): 2267 – 2277.
23. Wohlever ML, Baker TA, and Sauer RT. Roles of the N domain of the AAA+ Lon protease in substrate recognition, allosteric regulation and chaperone activity. *Molecular microbiology*. 2014; 9(1): 66 – 78.
24. Vera A, Aris A, Carrio M, Gonzalez-Montalban N, and Villaverde A. Lon and ClpP proteases participate in the physiological disintegration of bacterial inclusion bodies. *J Biotechnol*. 2005; 119(2): 163 – 171.
25. Winkler J, Seybert A, Konig L, Pruggnaller S, Haselmann U, Sourjik V, Weiss M, Frangakis AS, Mogk A, and Bukau B. Quantitative and spatio-temporal features of protein aggregation in *Escherichia coli* and consequences on protein quality control and cellular ageing. *The EMBO Journal*. 2010; 29(5): 910 – 923.
26. Sanchez Y and Lindquist SL. Hsp104 required for induced thermotolerance. *Science*. 1990; 248(4959): 1112 – 1115.
27. Chernoff YO, Lindquist SL, Ono B, Inge-Vechtomov SG, Liebman SW. Role of the chaperone protein Hsp104 in propagation of the yeast prion-like factor [psi+]. *Science*. 1995; 268: 880 – 884.

28. Patino MM, Liu JJ, Glover JR, and Lindquist S. Support for the prion hypothesis for inheritance of a phenotypic trait in yeast. *Science*. 1996; 273(5275): 622 – 626.
29. Hung GC and Masison DC. N-terminal domain of yeast Hsp104 chaperone is dispensable for thermotolerance and prion propagation but necessary for curing prions by Hsp104 overexpression. *Genetics*. 2006; 173(2): 611 – 622.
30. Lo Bianco C, Shorter J, Régulier E, Lashuel H, Iwatsubo T, Lindquist S, and Aebischer P. Hsp104 antagonizes alpha-synuclein aggregation and reduces dopaminergic degeneration in a rat model of Parkinson disease. *J Clin Invest*. 2008; 118: 3087 – 3097.
31. Weibezahn J, Tessarz P, Schlieker C, Zahn S, Zentgraf H, Weber-Ban EU, Dougan DA, Tsai FTF, Mogk A, and Bukau B. Thermotolerance requires refolding of aggregated proteins by substrate translocation through the central pore of ClpB. *Cell*. 2004; 119: 653 – 665.
32. Tessarz P, Mogk A, and Bukau B. Substrate threading through the central pore of the Hsp104 chaperone as a common mechanism for protein disaggregation and prion propagation. Molecular Microbiology. 2008; 68(1): 87 – 97.

Table 1. Primers Used for Cloning

Primer	DNA Sequence (5' to 3')
pYES2 ClpX HindIII Forward	GTACATAAGCTTATGACAGATAAACGCAAACGCAAA
pYES2 ClpX XhoI Reverse	TGAAATGAGCTCTTATTCACCAGATGCCTG
Hsp104 NTD KpnI Forward	TTCACAGGTACCATGAACGACCAAACGCAATTT
Hsp104 NTD SacI Reverse	TCGGATGAGCTCTTAAGGTGTGTTCGTATCAGC
ClpXΔNTD NotI Forward	GAAGCGCAACAGGCATCTGGTGAATAAGCGGCCGCGAGCTCTTAATTAAC
ClpXΔNTD SacI Reverse	GTCGGTAGCGCACTGAGCTCGCGTTCACGATGC
pYES2+Hsp104 + ClpXΔNTD bp 928 FWD	CGACGTCTTCCATGGACGGCAGATCGTACAT
pYES2+Hsp104 + ClpXΔNTD bp 928 FWD	ATGTACGATCTGCCGTCCATGGAAGACGTCG

Figure 1. Domain organization and phenotype of chimeric protein.

A.) Domain architecture of ClpX and Hsp104. ClpX contains an N-domain that dimerizes, a large nucleotide-binding domain, and a small nucleotide-binding domain. Hsp104 contains an N-domain, two nucleotide-binding domains, and a unique coiled-coil middle domain.

B.) Proposed surface structure of chimeric chaperone protease Hsp104 NTD + ClpXΔNTD + ClpP. Hsp104 N-domain structure (PDB 6AMN; Lee et al., 2017). ClpXΔNTD structure (PDB 3HWS; Glynn et al., 2009). ClpP structure (PDB 1TYF; Wang et al., 1997).

C.) [PSI^{+}] yeast containing the chimeric protein Hsp104 NTD + ClpXΔN + ClpP has white colony color and thus carry a [PSI^{+}] phenotype. [PSI^{+}] yeast containing the plasmid pYS104 overexpress Hsp104, which resolubilizes insoluble Sup35 protein and is associated with a [psi^{-}] phenotype.

A

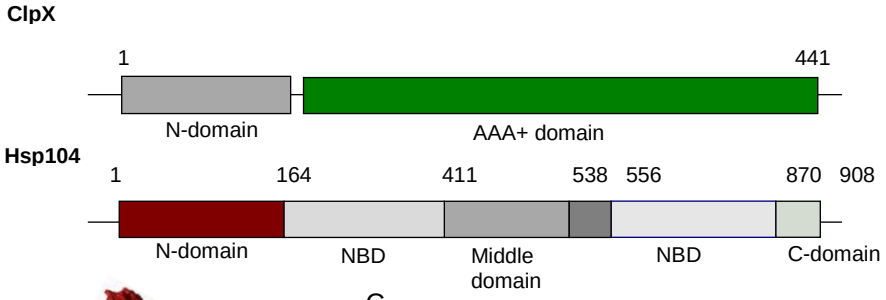

B

Hsp104 NTD + ClpXΔNTD + ClpP

C

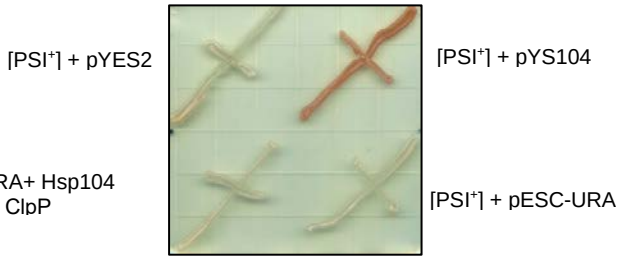

Figure 2. Expression of chimeric protein in *S. cerevisiae* and functional analysis.

A.) Western blots shows bands reactive to ClpX and ClpP for lysate extracted from yeast cells transformed with Hsp104 NTD + ClpXΔN + ClpP.

B.) Functional analysis of Hsp104 NTD + ClpXΔN + ClpP shows that the level of red pigmentation, which correlates to soluble Sup35 levels, is decreased in yeast expressing the chimeric proteins Hsp104 NTD + ClpXΔN and Hsp104 NTD + ClpXΔN + ClpP compared to yeast overexpressing Hsp104 and the Hsp104 Walker B mutation E285Q. Day 5 lysates, induced by galactose on solid SD-URA media.

A

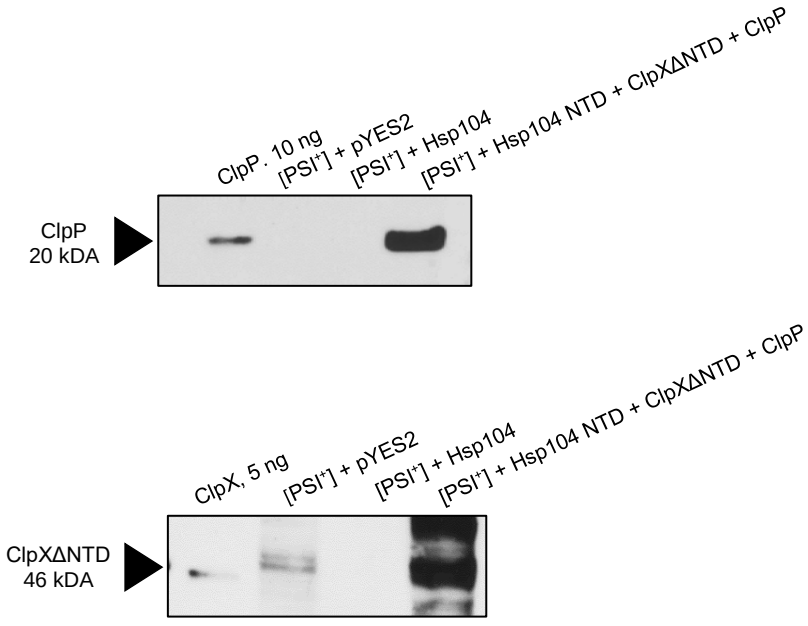
ClpP. 10 ng
[PSI+] + pYES2
[PSI+] + Hsp104
[PSI+] + Hsp104 NTD + ClpXΔNTD + ClpP
ClpP
20 kDA
ClpX, 5 ng
[PSI+] + pYES2
[PSI+] + Hsp104
[PSI+] + Hsp104 NTD + ClpXΔNTD + ClpP
ClpXΔNTD
46 kDA

B

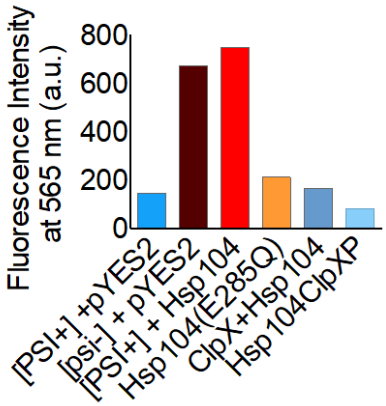
Fluorescence Intensity at 565 nm (a.u.)
800
600
400
200
0
[PSI+] +pYES2
[psi-] + pYES2
[PSI+] + Hsp104
Hsp104(E285Q)
ClpX+Hsp104
Hsp104ClpXP

Figure 3. Model of Sup35 amyloid fibril severing by Hsp104 NTD + ClpXΔNTD + ClpP. Polypeptide segments of amyloid aggregate is threaded through the central channel of Hsp104 and substrate is translocated into the ClpX central channel where it is threaded into the ClpP proteolytic barrel. The degradation products, short polypeptide segments, may serve as amyloid seeds to propagate Sup35 prion in yeast. Both substrate translocation and degradation of polypeptide require ATP binding and hydrolysis.

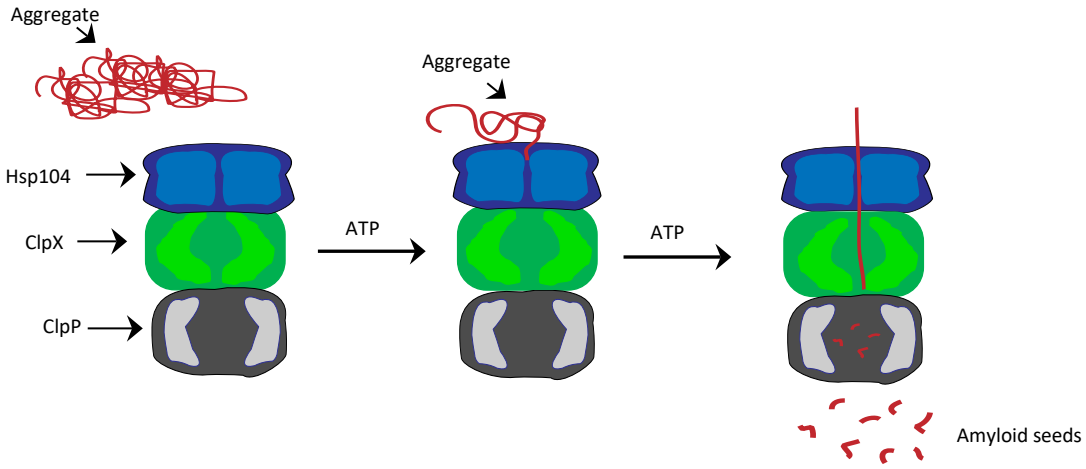
Aggregate
Hsp104
ClpX
ClpP
ATP
Aggregate
ATP
Amyloid seeds

Supplemental Figure S1. **Phenotype of [PSI$^+$] yeast carrying pyes2 + Lon wild-type construct.** Yeast expressing the full-length *lon* sequence in the vector pYES2 have [PSI$^+$] phenotype, which is associated with the presence of insoluble Sup35 fibrils.

[PSI^{+}] + pYES2

[PSI^{+}] + Hsp104

[PSI^{+}] + pYES2+ Lon

[psi^{-}] + pYES2